University of Southampton

Faculty of Engineering and The Physical Sciences

Bioengineering Science Research Group

Liposomes Encapsulating Model Drugs and Silver Nanoparticles for Illumination Based Drug Release

by

Fatih Yanar

Thesis for the degree of Doctor of Philosophy

December 2020

University of Southampton

Abstract

Faculty of Engineering and The Physical Sciences

Bioengineering Science Research Group

Doctor of Philosophy

Liposomes Encapsulating Model Drugs and Silver Nanoparticles for Illumination Based Drug Release

by

Fatih Yanar

Drug delivery systems include the delivery of the drug within the nanocarriers targeted to the diseased site, thereby the side effects caused by the interaction of the drugs with the untargeted regions are limited. One of the common nanocarriers employed is the liposomes, which are polymolecular aggregates of certain amphipathic molecules, formed in aqueous solution. The unique architecture of liposomes provides a useful platform for incorporation of hydrophilic and/or hydrophobic molecules within the core and/or the bilayer, which has opened the way for the usage of liposomes as nanocarrier systems in pharmaceutical applications. However, this type of therapy still needs improvement because of limitations in stability, encapsulation efficiency, the interaction between the nanocarrier and the cell, and also problems related to rapid clearance by reticuloendothelial system, which has lead researchers to produce novel ways. Photothermal-triggered drug release is one of the novel drug delivery systems which has the potential in delivering higher amounts of drugs to the diseased site, aiming to deliver the encapsulated compound effectively while minimizing the toxicity. This type of therapy based on the phase transition of liposome layers as a result of local temperature increase following the exposure of light, and consequently the release of the encapsulated content.

In this study, to develop a system that can serve the release of payload upon light exposure, the silver nanoparticles (AgNPs) which have remarkable optical features, were encapsulated within the liposomes, and the drug release was tested upon illumination. The synthesis of thermosensitive liposomes loaded with model drugs (i.e. rhodamine) and AgNPs, as a novel photothermal drug delivery system was performed successfully in a continuous flow millireactor. Analytical techniques including dynamic light scattering (DLS), UV-Vis spectrophotometry or transmission electron microscopy (TEM) were employed to characterize the efficiency of the production, the encapsulation of the AgNPs and the drug release performance. Results showed that liposomes can be produced with the intended size in a controllable manner by changing millifluidic conditions. Also, the encapsulation of AgNPs in liposomes was confirmed with DLS results and TEM images. The association between liposomes and AgNPs revealed that it can be regarded as a mixture of incorporation and encapsulation. Drug release profiles characterized by fluorescence intensity in a plate reader or under a fluorescence microscope showed promising results. However, the system needed further modification to demonstrate the drug release assisted by the photothermal effect of AgNPs, such as to have the ability to release drugs on demand by operating as an opening and closing mechanism, or to function as a therapeutic system capable of real-time monitoring in addition to drug release on demand.

Table of Contents

Table of Tables

Table of Figures

Table of Figures

Table of Figures

Table of Figures

Table of Figures

Research Thesis: Declaration of Authorship

Print name: Fatih Yanar

Title of thesis: Liposomes Encapsulating Model Drugs and Silver Nanoparticles for Illumination Based Drug Release

I declare that this thesis and the work presented in it are my own and has been generated by me as the result of my own original research.

I confirm that:

1. This work was done wholly or mainly while in candidature for a research degree at this University;
2. Where any part of this thesis has previously been submitted for a degree or any other qualification at this University or any other institution, this has been clearly stated;
3. Where I have consulted the published work of others, this is always clearly attributed;
4. Where I have quoted from the work of others, the source is always given. With the exception of such quotations, this thesis is entirely my own work;
5. I have acknowledged all main sources of help;
6. Where the thesis is based on work done by myself jointly with others, I have made clear exactly what was done by others and what I have contributed myself;
7. Parts of this work have been published as:

Article

- **Yanar, F**., Mosayyebi, A., Nastruzzi, C., Carugo, D., & Zhang, X. (2020). *Continuous-Flow Production of Liposomes with a Millireactor under Varying Fluidic Conditions*. Pharmaceutics, 12(11), 1001.
- Cristaldi, D. A., **Yanar, F.,** Mosayyebi, A., García-Manrique, P., Stulz, E., Carugo, D., & Zhang, X. (2018). *Easy-to-perform and cost-effective fabrication of continuous-flow reactors and their application for nanomaterials synthesis.* New biotechnology, 47, 1-7.

Conference

- **F. Yanar**, A. Cristaldi, A. Mosayyebi, D. Carugo, X. Zhang, "*Dual encapsulation of silver nanoparticles and model drugs in liposomes: a microfluidic-based approach*", BioMedEng19 Conference | 5 – 6 September 2019, Imperial College London
- **F. Yanar**, A. Cristaldi, A. Mosayyebi, D. Carugo, X. Zhang "*Imaging of liposomes encapsulating silver nanoparticles*", BioMedEng19 Conference | 5 – 6 September 2019, Imperial College London

Signature: Date:

Acknowledgements

First and foremost, I would like to express my deep gratitude to my supervisors Prof Xunli Zhang and Dr Dario Carugo for their priceless support throughout my project. I am grateful to them for their precious guidance, endless patience and valuable help. I am very proud to complete this project under their excellent supervision.

I thank my colleagues, who are Dr Ali Mosayyebi, Dr D. Andrea Cristaldi, Dr Harriet Kimpton and Dr Thomas Mabey. I am thankful to them for their valuable contributions especially to experimental aspect of this project. Additionally, I am pleased to meet Dr Sharon Coleman, who was our chief technician in the bio-lab. I thank her for all her support.

I also thank all members of Biomedical Imaging Unit in Southampton General Hospital for their help. Besides, I am grateful to Dr Jonathan May and Dr Mark Willett for their valuable recommendations and support.

I would like to express my special thanks to my wonderful and lovely family. I do not experience these days without their paramount support and tremendous compassion.

Finally, I am thankful to Ministry of Education of Republic of Turkey for the financial support throughout my PhD studies.

Definitions and Abbreviations

ABC..... Accelerated blood clearance

AgNPs..... Silver nanoparticles

AuNCs/Dox-liposome..... Gold nanoclusters and doxorubicin dual-loaded liposomes

CFD..... Computational fluid dynamics

Chol..... Cholesterol

Cryo-TEM ..... Cryogenic electron microscopy

De..... Dean number

DLS ..... Dynamic light scattering

Dox..... Doxorubicin

DPPC ..... Dipalmitoylphosphatidylcholine

EE% ..... Encapsulation Efficiency

EPR..... Enhanced permeability and retention

FDA..... (Food and Drug Administration)

FRR..... Flow rate ratio

IPA..... Isopropyl alcohol

Lipo/AgNPs ..... Liposomes encapsulating silver nanoparticles

Lipo/Rho ..... Liposomes encapsulating rhodamine

Lipo/Rho/SNPs..... Liposomes encapsulating rhodamine and silver nanoprisms

Lipo/SNPs..... Liposomes encapsulating silver nanoprisms

Lipo/SNSs..... Liposomes encapsulating silver nanospheres

mM..... Millimolar

mL ..... Millilitre

nm..... Nanometre

NP ..... Nanoparticle

ODA..... Octadecylamine, stearylamine

PC..... Phosphatidylcholine

PDMS..... Polydimethylsiloxane

PEG..... Polyethylene glycol

PEG-40..... Polyoxyethylene (40) stearate

Re ..... Reynolds number

RES ..... Reticuloendothelial system

Rho ..... Rhodamine

RT ..... Room temperature

SNPs ..... Silver nanoprisms

SNSs ..... Silver nanospheres

SPR ..... Surface plasmon resonance

TEM ..... Transmission electron microscopy

TFR ..... Total flow rate

VR..... Volume ratio

The Outline of the Thesis

Chapter 1 describes firstly a general introduction with aim and objectives section, and is followed with a literature review focusing on the scope of drug delivery systems followed by the production of liposomal drug delivery systems and the properties of silver nanoparticles (AgNPs).

The experimental work was divided into three chapters and explained in the second, third and fourth chapters. Each of these chapters was written as separate sections so that they include a specific introduction, materials and methods, results and discussion, and conclusions sections. Part of the information given in these chapters (e.g. the materials and methods section), includes parallel information for each chapter. Also, part of the data was reused in separate sections or be referred to as a part of the discussion in separate chapters.

Chapter 2 describes the controllable liposome synthesis in different lipid compositions and varied fluidic conditions, using conventional methods (i.e. ethanol injection) and a continuous-flow millireactor. **Chapter 3** describes the liposomal encapsulation of AgNPs, focusing on the purification of liposomal dispersions and the characterization of the encapsulation. As the final section of the experimental work, the synthesis of thermosensitive liposomes dual loaded with model drugs and AgNPs and the performance of the drug release assisted by photothermal effect from thermosensitive liposomes was experimentally demonstrated in **Chapter 4**, and the involving mechanisms were discussed and explained.

Chapter 5 comprises a conclusion presenting the key findings and possible future works. Also, **Chapter 6** includes the supporting information and consists mainly of experimental data that is considered a side-work of the project and which was referred to in the experimental chapters.

Chapter 1 Introduction and Literature Review

1.1 Introduction

A disease can be defined as an abnormal condition or a disorder of functionality in a particular site, tissue or system in the body. The condition can affect only a site or the whole body, and considered as a medical condition accompanied by symptoms [1]. Based on the symptoms, a diagnosis is made and the therapy is administered in order to re-establish the function of the diseased tissue, potentially via different treatment options including forms of traditional medicine (i.e., systemic free drugs) or alternative therapies (i.e., targeted or stimuli-responsive agents) [2].

Although many of the diseases including cardiovascular and cancerous ones, can be treated pharmacologically, conventional therapeutics suffer from many limitations such as drug clearance, low tolerability, low efficacy, high toxicity and narrow therapeutic index [2]. It is aimed to develop drugs, which ideally have only a therapeutic effect, to eradicate the abnormal condition completely, without causing adverse effects or toxicity on healthy tissues, however, the therapies may cause severe side effects even when the most commonly used and preferred drugs are employed [3].

Drug delivery is a process that involves enhancing therapeutic efficacy and reducing toxicity by the targeted release of pharmaceutic agents [4]. The approach here is that not only curing the disease but also to prevent any toxicity that might occur in healthy tissues. Considering the cancer disease, unacceptable side effects may occur, especially when the drug intended to affect cancer cells interacts with healthy tissues. It is important to note that the delivery route of the medication may play an important role in this process along with the way the body responds. For instance, administering the drug locally rather than systemically is a common way to decrease side effects, as the interaction of the drugs with remaining sites other than intended regions is limited. In this respect, drug delivery technologies have great importance in delivering pharmaceutical molecules to the diseased site.

In recent years, pharmaceutical sciences have made phenomenal progress especially employing novel drug delivery technologies as controlled or targeted drug delivery in curing cancer diseases, including the application of nanotechnology with the aim of reducing toxicity and adverse effects [4, 5]. The novel approaches for developing drug delivery systems employs nanoscale carriers that aim to deliver the pharmaceutical active to the diseased site, in cancer treatment [6-8].

Liposomes, which are lipid-based vesicular systems and can be loaded with anti-cancer drugs either within the lipid bilayer or within the aqueous core, are the most commonly used nanoscale carriers for drug delivery, especially in cancer disease. Liposomes typically consist of an aqueous core

enclosed within one or more bilayers of natural or synthetic amphipathic molecules. This unique architecture provides a useful platform for incorporation of hydrophilic and/or hydrophobic molecules within the core and/or the bilayer, which has opened the way for the usage of liposomes as nanocarrier systems in pharmaceutical applications. Liposomes have demonstrated potential for delivering pharmaceutical actives to pathological sites within the body, with high efficacy and minimal toxicity, thereby reducing undesired side effects. It has been demonstrated that a nanotechnological medicine called Liposomal Doxorubicin®, also called by the brand names with different formulations, Caelyx, Myocet or Doxil, enhanced drug delivery efficiency and therapeutic efficacy in animal models [9], comparing to use of free Doxorubicin which is one of the powerful drugs for treating solid tumours. However, other adverse effects have been reported in clinical trials in addition to reduced toxicity [10]. Also, that type of therapy needs improvement because of limitations in stability, encapsulation efficiency, interaction between the nanocarrier and the cell, and also problems related to rapid clearance by the reticuloendothelial system (RES), which has lead researchers to produce novel ways. Photothermal-triggered drug release [11], theranostic liposomes [12] or ultrasound triggered liposomes [13] are some of examples of novel drug delivery systems which can be more effective in delivering drugs to the diseased site, aiming to deliver the encapsulated compound effectively while minimizing the toxicity. The combined use of drug-loaded liposomes and photothermal drug release, which presents triggering thermosensitive liposomes by light to release the payload, has been shown to increase the treatment efficiency compared to free drug or drug-loaded liposomes alone in vitro [14].

AgNPs are one of the most attractive nanomaterials due to their remarkable optical and antibacterial properties. These properties have led AgNPs to be used in various fields including electrochemistry, catalysis industry, food industry, pharmaceutical industry and nanomedicine [15]. In the field of medicine, AgNPs are used as imaging probes, plasmonic antennas and nanoprobes due to their ability to destroy cancer cells [16-18]. Among these nanoparticles, triangular silver nanoprisms (SNPs) attract attention due to their remarkable features relying on SPR and sharp tip morphology [19, 20], in addition to their antibacterial effects. The optical properties of SNPs are remarkable due to the strong plasmonic interaction between silver and light. The unique optical properties of SNPs also make them a potential tool for noninvasive tracking and imaging in cancer therapy, besides, the SNPs can be used as anticancer agents.

The aforementioned features make SNPs potential tools that can be used in controlled drug release studies. In addition to their ability to kill cancer cells [16-18], when SNPs are encapsulated in liposomes they can cause a phase change in the lipid layer by increasing the local temperature

thanks to the photothermal effect [21]. In this study, this effect was thought to be a mechanism that can be used in controlled drug release.

Considering that SNPs and drugs could be simultaneously encapsulated in liposomes, it was thought that SNPs could convert light energy to heat energy under illumination and cause a phase change of the lipid layer from gel to liquid crystalline, thereby releasing the encapsulated drugs. This is the underlying rationale at the basis of the design of the nanocarrier system and controlled drug release mechanism in this study.

On the other hand, the industrial production of the aforementioned technologies is limited due to difficulties in achieving repeatability [22]. More recently, microfluidic-based devices have been employed as an alternative technique for the production of aforementioned systems in a continuous-flow format. Compared to traditional batch methods, microfluidic approaches have shown advantages in many aspects, including precise control over the transport of fluids, chemical species and heat, and the potential for tuning vesicle properties on-demand [23]. However, there are still significant limitations that hinder industrial translation of this technology; these can be mostly attributed to the small dimensional scale of the microfluidic architectures, and include high manufacturing costs, complexity of device's operation, low particle production rates and low device's lifetime [24-26]. To address these challenges, millimetre-scale flow reactors (referred to as 'millifluidic reactors' or 'millireactors') have been recently developed and employed for controllable production of both inorganic and organic nanomaterials, at volumetric flow rates up to 18 mL/min [25, 27-33]. Notably, scaling-up in these earlier studies enabled increased particle production capacity, while still retaining the fluidic controllability over particle's properties. Moreover, given their larger dimensions, devices could be manufactured using cost-effective and user-friendly techniques compared to conventional microfabrication methods [27, 28, 34].

1.2 Aim and Objectives

Considering the advantages and limitations in liposomal drug delivery, with the purpose of introducing a new approach, this project aims; (i) to develop a novel drug delivery system in which AgNPs and model drugs are loaded into liposomes simultaneously; (ii) to evaluate drug release from nanocarriers induced by illumination, which relies on the plasmon resonance effect of AgNPs in order to provide more effective ways of increasing local concentration of drugs in real-time.

The main objectives are:

(i) To produce liposomes with traditional batch and continuous-flow reactors with an intended size and dispersity in a controllable manner.

(ii) Encapsulating AgNPs in liposomes; that will be designed and synthesized by using initially conventional batch reactors and then, more advanced continuous-flow reactors.

(iii) Encapsulating both AgNPs and model drugs (e.g. rhodamine) in a thermosensitive liposome; that will be synthesized using advanced continuous-flow reactors.

(iv) To investigate the drug release profile of developed thermosensitive liposome via a photothermal drug release mechanism assisted by plasmon resonance effect of AgNPs encapsulated in a designed platform.

1.3 Literature Review

Considering cancer disease, there are different types of treatments including surgery, radiation therapy or chemotherapy [35]. However, none of these therapies can cure the disease effectively without causing a side effect. Enormous effort has been made to develop new ways to treat cancer by combining knowledge from different disciplines including nanotechnology, medicine and engineering. Studies showed that using developed nanoparticle formulations could enable the process of delivering the pharmaceutical compound to the targeted area. However, this type of therapy still needs improvement to be more effective in delivering high concentration of drugs to cancer cells because of some limitations such as rapid clearance by RES and low encapsulation efficiency (EE%), or due to the fact that cancer cells resist treatment by developing new ways such as DNA mutations to overcome the therapy [14]; that led researchers to develop novel drug delivery systems to improve the therapeutic efficacy. In view of developing a new drug delivery system, investigating effective ways to address the limitations of nanomedical treatments for cancer, the state-of-the-art of the research field must be understood, including the advantages and disadvantages of relevant techniques.

1.3.1 Cancer disease

Cancer can be defined as a large family of diseases that are associated with abnormal cell growth, which has the potential to invade other regions of the body (**Figure 1**) [36]. Development of cancer – referred to as carcinogenesis, oncogenesis or tumorigenesis - is a process of transformation of normal cells to cancer cells because of mutations and epimutations in DNA which results in uncontrolled cell division and disrupted balance between cell proliferation and cell death leading to the formation of a tumour [37].

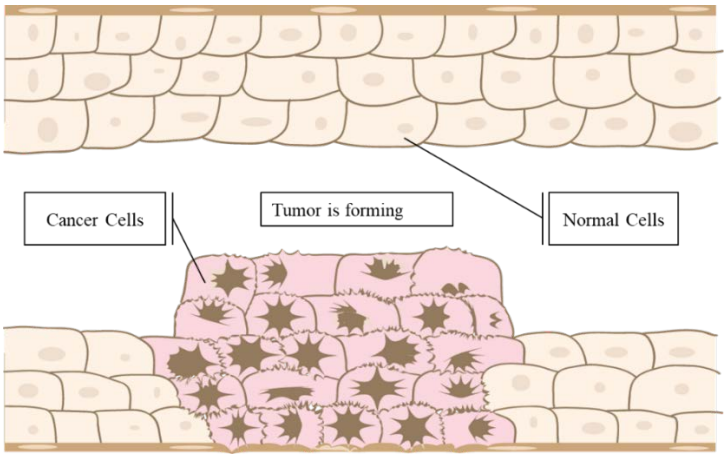

Figure 1 Tumour formation, showing normal cells and cancer cells in a tumour formation [36].

Treatment of cancer is commonly carried out by killing cells in the relevant region using radiotherapy or chemotherapy or by complete removal of affected tissue which can be accomplished by surgery [38]. These therapies are not fully effective since the invasion of cancer to adjacent tissue by metastasis is possible after surgery. Additionally, healthy cell death can take place along with cancer cells in chemotherapy or radiotherapy, which can lead the patients to experience severe side effects [39]. Drug delivery systems are built up for targeting the drug to a specific area of the body to only give the damage to cancer cells to reduce the side effects of the chemotherapeutics [40]. It was shown that drug-encapsulating liposomes improve targeting the drug and the treatment efficiency compared to its free form in pharmacological therapy [41].

It should be noted that even though cancer is mentioned in this literature review as the main focus, drug delivery technologies gain success in treating infectious diseases [42], respiratory diseases [43], hypertension [44], diabetes mellitus [45] and in targeting brain in terms of enabling drug transport at the Blood-Brain Barrier (BBB) [46].

1.3.2 Drug delivery technology

Drug delivery technologies are designed for the targeted site storage of the pharmaceutical actives in order to increase therapeutic efficacy. Comparing to exploring new drugs, improving controlled drug release technologies enables researchers to use of available drugs without undesirable toxicity and to overcome problems arising from high-cost expense in exploring new drugs [14]. Other than targeted therapy, controlled drug release and slow delivery are other approaches to drug delivery as conventional methods.

The history of drug delivery systems can be divided into three stages. First-generation systems were developed between the 1950s and 1980s and mainly focused on sustained drug release via oral and transdermal administration. Dextroamphetamine (Dexedrine) was the first controlled release

system, which provides 12-hour delivery, presented in 1952 [47]. The mechanisms employed with this approach included dissolution, diffusion, osmosis, ion exchange [48]. The development of second-generation systems (the 1980s – 2010s) focused on developing zero-release systems, depot formulations, self-regulated systems and nanotechnology-based delivery systems. It was initially thought that zero-release systems would keep the drug concentration constant in the blood. It was later realized that it was not necessary to keep concentration constant because the effectiveness stayed the same even if the drug concentration was higher than the minimum. That was followed by the development of "smart" drugs [48]. Polymers and hydrogels were the products of this group, which can be triggered by environmental factor such as pH, temperature or glucose [49]. Third-generation systems (present) can be termed as modulated systems since the carrier can be targetable and operate like a controllable on-off system. At present, this is still being progressed with the contributions from engineering, pharmacology and genetics.

The common approach in targeted drug delivery is to encapsulate or to associate the pharmaceutical active with the nanoparticle and then deliver the nanoparticle via passive or active targeting to the relevant zone [14]. Liposomes, metal nanoparticles, mesoporous silica systems, polymeric micelles, dendrimers, and carbon nanotubes are examples of nanomaterials used in drug delivery systems [50].

It has been observed that the concentration of the drug accumulated at the targeted site has increased by 100-400% when using nanoparticle-based systems compared to conventional formulations in terms of drug delivery efficacy [49]. This shows that the concentration of the accumulated drug in the diseased site has increased from 1% to 5% when nanoparticle-based formulations were used. (**Figure 2**).

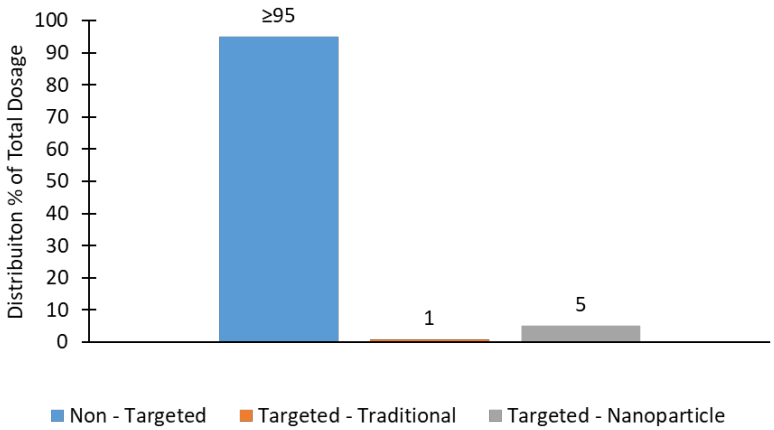

Figure 2 Distribution of drugs in terms of efficiency at the targeted site based on using nanoparticle formulations and conventional formulations [49].

However, more than 95% of the administered formulation still reaches the sites that are not targeted. It should also be noted that not only the nanoparticle formulations increase the delivered drug concentration, but also the amount of drug used in the nanoparticle formulation significantly affects the accumulated drug concentration in the targeted area [51]. It is therefore understood that by increasing the amount of drug loaded to the nanoparticles, the concentration of the drug at the targeted area would increase. Thus, nanoparticles have a great importance in drug delivery technology.

1.3.3 Nanotechnology

According to the National Nanotechnology Initiative, nanotechnology is generally regarded as the manipulation of matter with at least one dimension from 1 to 100 nanometres in size [52]. Nanotechnology can also be defined as the design, synthesis, characterization and application of materials at the nanometre scale (i.e., one billionth of a metre in size). At these scales, the behaviour of the single molecules or groups of molecules becomes more important in contrast to bulk macroscopic structures which can be incorporated into designing novel approaches for treating diseases related to subcellular structures with a size at ~10-100nm [53]. Living organisms are formed of cells, which are typically at ~10 µm, and subcellular structures have a typical size at ~10 nm such as proteins [54]. These dimensions make it possible to use man-made nanoparticles as small vehicles in investigating cell mechanisms and hopefully to treat diseases. In that aspect, nanotechnology can provide significant advances when applied in various disciplines including medicine, biology or chemistry.

The journey from traditional therapy to the use of nano-drugs in drug delivery started around a half-century ago by using colloidal nanostructures in membrane related researches [55], which then led to investigating nanoparticles in drug delivery [56]. Nano-sized phospholipid-based vesicles, which has later be called liposomes, have gained momentous attention, and the implantation of nanotechnology into medicine has been developed with the application of anthracycline encapsulated in liposomes in order to reduce the cardiotoxicity caused by doxorubicin [57]. Many liposome-based nanomedicine products (**Table 1**) are in clinical use in the field of drug delivery in terms of therapy [58]. Doxil® is the first nanomedicine product that can be called an FDA (U.S. Food and Drug Administration) approved drug delivery system which has been used in the cancer treatment field [59].

Considering the achievements made depending on the liposomal products, it appears possible to solve the difficulties, such as delivering poorly water-soluble drugs, delivering drugs across tight epithelial barrier, delivering large molecules to intracellular sites or co-delivery of two or more

drugs by using nanotechnology [60]. There are also other applications that have been built up with nanotechnology and are in use for various purposes such as detection of protein, tissue engineering, tumour detection, purification of molecules and cells, and also drug delivery [61].

Table 1 A summary of clinically available liposome-based drugs [10].

Clinical Products (Approval Year)	Administration	Active Agent	Indication	Company
Doxil® (1995)	Intravenous	Doxorubicin	Ovarian, breast cancer, Kaposi's sarcoma	Sequus Pharmaceuticals
DaunoXome® (1996)	Intravenous	Daunorubicin	AIDS-related Kaposi's sarcoma	NeXstar Pharmaceuticals
Depocyt® (1999)	Spinal	Cytarabine/Ara-C	Neoplastic meningitis	SkyPharma Inc.
Myocet® (2000)	Intravenous	Doxorubicin	Combination therapy with cyclophosphamide in metastatic breast cancer	Elan Pharmaceuticals
Mepact® (2004)	Intravenous	Mifamurtide	High-grade, resectable, non-metastatic osteosarcoma	Takeda Pharmaceutical Limited
Marqibo® (2012)	Intravenous	Vincristine	Acute lymphoblastic leukaemia	Talon Therapeutics, Inc.
Onivyde™ (2015)	Intravenous	Irinotecan	Combination therapy with fluorouracil and leucovorin in metastatic adenocarcinoma of the pancreas	Merrimack Pharmaceuticals Inc.
Abelcet® (1995)	Intravenous	Amphotericin B	Invasive severe fungal infections	Sigma-Tau Pharmaceuticals
Ambisome® (1997)	Intravenous	Amphotericin B	Presumed fungal infections	Astellas Pharma
Amphotec® (1996)	Intravenous	Amphotericin B	Severe fungal infections	Ben Venue Laboratories Inc.
Visudyne® (2000)	Intravenous	Verteporphin	Choroidal neovascularisation	Novartis
DepoDur™ (2004)	Epidural	Morphine sulfate	Pain management	SkyPharma Inc.
Exparel® (2011)	Intravenous	Bupivacaine	Pain management	Pacira Pharmaceuticals, Inc.
Epaxal® (1993)	Intramuscular	Inactivated hepatitis A virus (strain RGSB)	Hepatitis A	Crucell, Berna Biotech
Inflexal® V (1997)	Intramuscular	Inactivated hemaglutinine of Influenza virus strains A and B	Influenza	Crucell, Berna Biotech

1.3.4 Liposomal drug delivery systems

Liposomes were first discovered in the 1960s by Alec D Bangham at the University of Cambridge [55]. Liposomes composed of natural or synthetic lipids (typically glycerophospholipids, i.e. lipids that contain a glycerol-3-phosphate unit) consisting of bilayers alternating with aqueous compartments and have characteristics of biocompatibility, biodegradability, low toxicity, increased biologic half-life and capable of encapsulating hydrophilic and hydrophobic molecules [62-64]. All of those features make them attractive as vehicles for drug delivery applications.

Liposomes can be classified as multilamellar and unilamellar vesicles. Unilamellar vesicles can be further classified as large with a typical size range from 100nm to a few micrometres, or small unilamellar vesicles ranging up to 100nm (**Figure 3**) [65]. Unilamellar liposomes have a single phospholipid bilayer surrounding the aqueous area while multilamellar liposomes have like an onion structure formed by several unilamellar vesicles [66]. Liposome size can be roughly 25nm to 2500nm in diameter and the number of liposome layer can be variable depending on the production method [67]. The size of the lipid vehicles applied to medical use ranges between 50 and 450 nm [68]. Size of liposomes along with a number of layers has great importance in drug delivery, because these are very important parameters determining the circulation half-life and the encapsulation efficiency, especially when considering extravasation of liposomes into the tumour, the enhanced permeability and retention (EPR) effect and the recognition by macrophages [69]. The pore size in terms of gaps in tumour tissues varies between 100nm to 780nm, while it is lower than 6nm for vascular endothelium in most tissues. [70]. Therefore, the optimum vesicle size that can extravasate into the tumour tissue while avoiding heathy tissue should be at ~100nm, because the larger liposomes can go into faster clearance [71]. In terms of production, liposomes became producible in different range sizes and new systems were developed to perform large-scale production [72]. It is possible to produce even very small size liposomes 30-50nm with different techniques including microfluidics and sonication [73, 74].

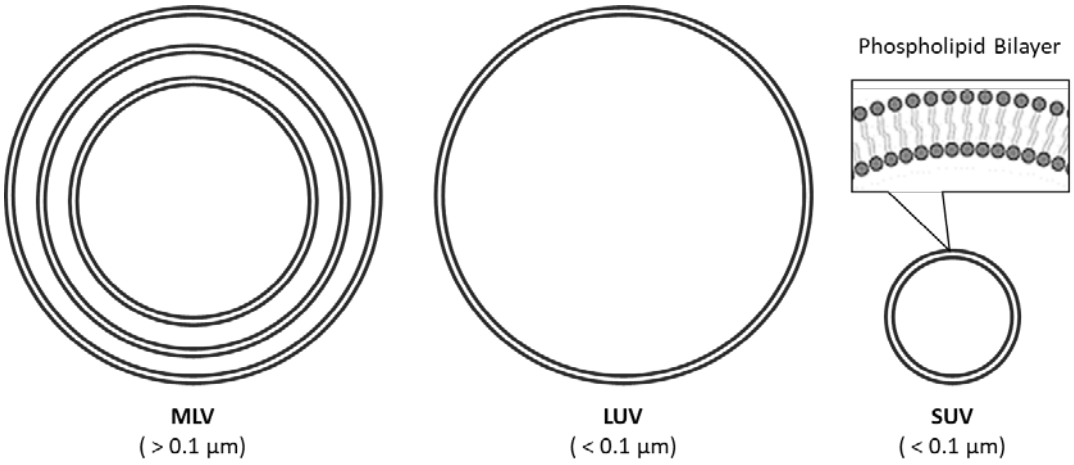

Figure 3 Types of liposomes depending on size and number of lamellae**.** Multilamellar vesicles (MLV), large unilamellar vesicles (LUV) and small unilamellar vesicles are depicted in the figure [65].

Liposomes play an important role in drug delivery systems since they can encapsulate a wide range of molecules including biopharmaceutical agents. Liposomal products can deliver the drug to a

specific site while minimizing the negative side effects since pharmaceutical agent, which can be any chemotherapeutic drug, is confined by the membrane of liposome so that healthy tissues are not directly exposed to the cytotoxic agent. Gregory Gregoriadis suggested for the first time that liposomes can encapsulate drugs and can be used as drug delivery systems [75, 76]. The first liposomal drug delivery systems which include anti-cancer drugs showed significant survival times in mice bearing leukaemia [77] and then these studies extended to clinical trials employing liposomal doxorubicin [41] (**Figure 4**) and liposomal amphotericin B [78].

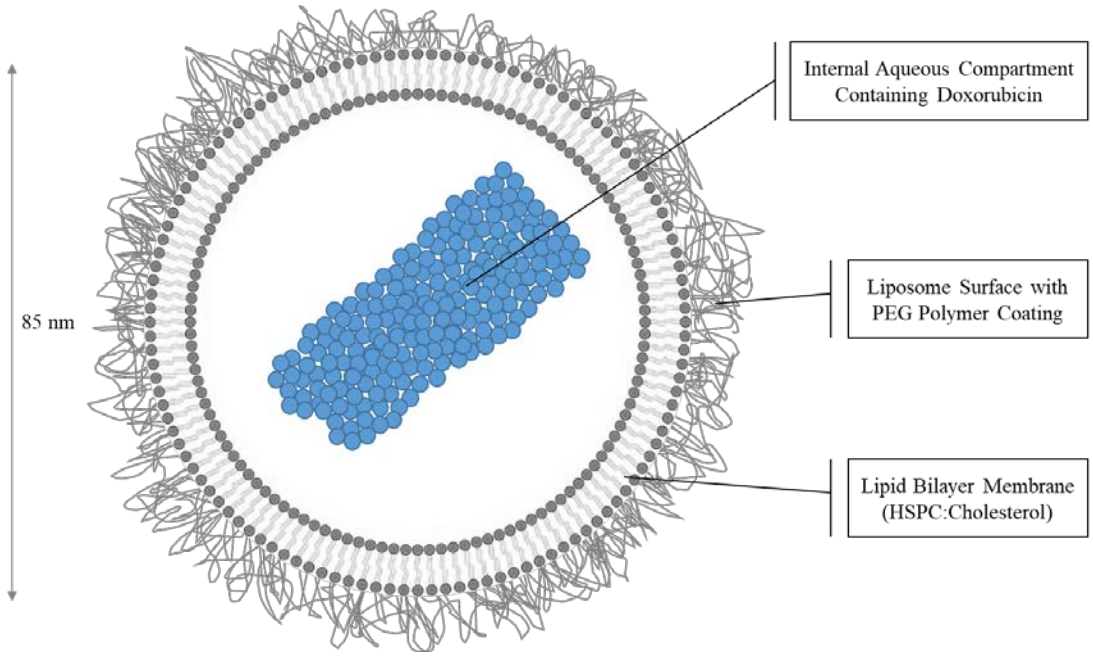

Figure 4 The illustration shows a cross-sectional view of a Doxil® Liposome. Doxorubicin is encapsulated in the internal aqueous area that is separated from the external medium via lipid bilayer. The liposome layer is PEG attached, and diameter is at ~85 nm. HSPC: Hydrogenated soy phosphatidylcholine [41].

Although liposomes minimize the side effects of chemotherapeutics compared to free form, there are still major factors to be considered like stability, circulation times, clearance, loading capacity and drug release. Liposomes can be exposed to rapid clearance due to opsonisation by serum proteins which means specific recognition of liposomes by cellular receptors that leads to digestion by macrophages of the RES [79], especially in the liver and spleen which results in a decrease in therapeutic efficacy. To overcome this problem, a hydrophilic polymer, polyethylene glycol (PEG) was introduced for coating liposomes to improve the stability and circulation times [80]. This barrier provides accumulation at the disease site and improves the efficacy of drugs by reducing opsonisation and recognition by macrophages and also it causes a decrease in side effects [81, 82]. In addition to opsonisation, there is another challenge called accelerated blood clearance (ABC)

phenomenon that liposomes have to overcome. Repeated injection of PEGylated liposomes followed by the loss of long-circulating properties, which leads to exposure and ends up with clearance from the blood; that is a process thought to be associated with ABC. Underlying mechanism of ABC is not fully understood and this is a major issue especially in multiple dosing regimens in clinics [83].

Liposomes can deliver drugs by active or passive targeting. Active targeting includes some modifications on liposome surface e.g., using charged lipids or attachment of ligands that can make the liposome to cross the biologic membranes through molecular processes [84]. Active targeting strongly reduces the undesired effects of drugs while providing high therapeutic efficacy by allowing high dosing on the diseased site. That is mainly due to the attached ligands such as antibodies, folates or peptides on the liposome surface, that give the ability of addressing the liposome to the receptors of the cancer cell (**Figure 5**) [85].

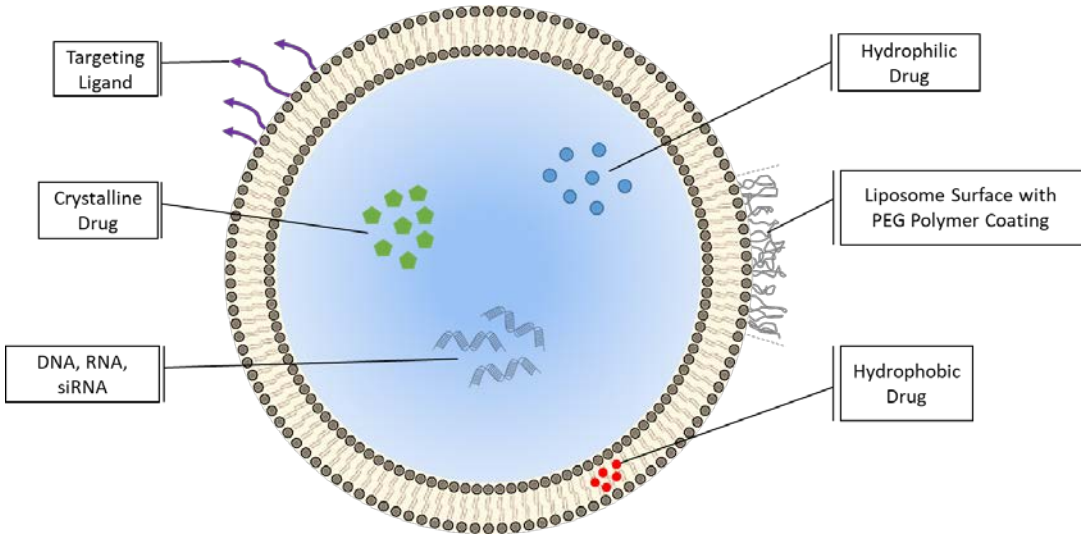

Figure 5 Liposome surface can be attached by PEG, antibodies or peptides. Drugs can be encapsulated in the aqueous area, incorporated into the liposome layer or attached to the surface of the liposome [86]. DNA: Deoxyribonucleic acid. RNA: Ribonucleic acid siRNA: Small interfering RNA.

Passive targeting includes the accumulation of liposomes to pathological sites as a result of EPR effect, where the increased permeability of vessels allows better supply of drugs to pathological sites. The width of junctions of regions between cells increases about 1 µm after exposed to inflammatory mediators and that helps liposomes to accumulate in tumour sites easily much more than they can in normal tissues [87]. This helps accumulation and extravasation of liposomes in pathological sites such as tumours [14] (**Figure 6**). The delivery of the active compound to the cell occurs via the interaction of the liposome and cell membrane. Depending on the attractive and repulsive forces between the surface and cell membrane event of simple adsorption happens, which is highly related to the liposome surface properties. Endocytosis is the entering of liposome

indirectly into the cytoplasm, which results in delivery of the content. Liposome lipids can merge with the cell membrane and the content is delivered directly, via the process named fusion. Another interaction between liposome and cell membrane is the lipid exchange, which includes the exchange of bilayer materials. These interactions happen with triggering the immune system at the same time. On this occasion, it is so important to develop the liposome surface to have the ability of being non-recognizable [8, 88]

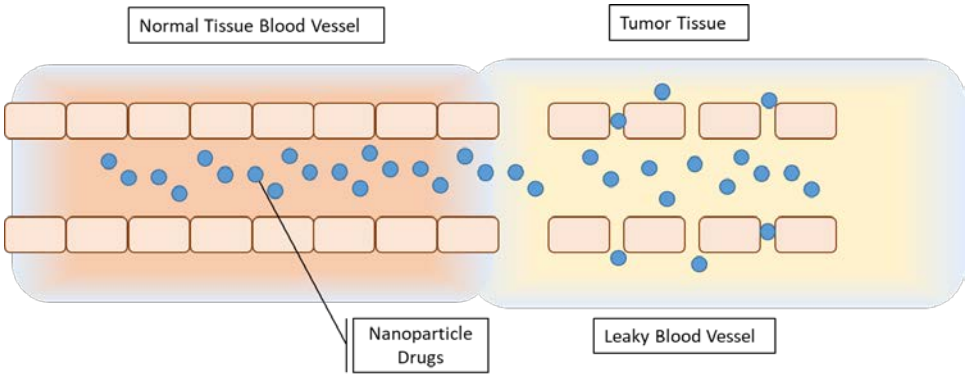

Figure 6 Passive targeting via the enhanced permeability and retention effect [89], Nanoparticle accumulation in tumour tissue via EPR effect. Normal tissue vasculature does not let nanoparticle pass while tumour tissue vasculature is leaky and allowing accumulation of nanoparticle in the interstitial space.

The use of liposomes had a great impact in cancer treatment due to the possibility of increasing low therapeutic index while reducing toxicity in healthy cells [8]. Various liposomal formulation moved preclinical stage as they served less toxicity compared to free drug in cancer treatment [90]. Even though there are some limitations with the liposomal drug delivery, liposomal nanoformulations are the most established nanomedicine products among others. There are many approved liposomal drug delivery systems for cancer treatment in clinical use (**Table 1**). The first FDA approved lipid-based drug, Liposomal Doxorubicin®, was designed as PEGylated [91].

Doxorubicin, daunorubicin, cytarabine for are some examples of pharmaceutical anticancer agents used in liposomal formulations for treating ovarian cancer, leukaemia, AIDS-related Kaposi's sarcoma, multiple myeloma and lymphomas. Doxil® is a liposomal formulation containing Doxorubicin HCl used against ovarian cancer. These liposomal drug delivery vehicles have a size at ~80-100 nm and comprise of 2000PEG-distearoylphosphatidylethanolamine, hydrogenated soybean phosphatidylcholine (PC) and Cholesterol (Chol) [92]. Circulation of Doxil® in the body can last for several days due to PEG attached layers, which increase the chance of extravasation into pathologic sites. Initial studies of liposomal doxorubicin showed increased distribution half-life of

approximately 2 days, besides almost the entire drug measured in plasma is encapsulated in liposome.

It was reported that the clinical activity was significantly modified after PEGylation and the clearance of Doxil was reduced; a comparison between the first generation (without PEG(L-DOX)) and the second generation (with PEG (Stealth-DOX)) liposomal doxorubicin formulations can be seen in **Table 2** [93]. Xing et al also demonstrated the improved efficacy by comparing clinical outcomes of the liposomal doxorubicin with the conventional doxorubicin with meta-analysis. Data provided from 2,889 patients suffering from advanced breast cancer were included in this report in terms of efficacy of the liposomal doxorubicin. Statistical calculations demonstrated that liposomal doxorubicin resulted in a significant reduction in the risk of cardiotoxicity ($p = 0.03$) and also a significant improvement in the overall response rate ($p = 0.03$) compared to conventional doxorubicin. However, there was no statistical difference between groups in terms of overall survival ($p = 0.93$). Overall, the study showed that liposomal doxorubicin was effective in improving the overall response rate and reducing cardiotoxicity risk [94]. Many other lipid-based PEGylated liposomes are FDA approved and are being used in clinical trials [14].

Table 2 Comparison of Dox Liposomes [93].

Liposome type	L-DOX	Stealth-DOX
	RES-directed, Short Circulated time	Sterically-stabilized, Long circulation time
Lipid composition	PC:PG:Chol	HPC:PEG-DSPE:Chol
(approximate molar ratio)	50:20:30	55:05:40
Surface charge in: Low ionic strength	Strongly negative	Negative
High ionic strength	Negative	Almost no charge
Size (diameter in nm)	200-500	< 100
Number of lamellae	Oligolamellar	Mostly unilamellar
Location of drug	Membrane-associated	Aqueous interior phase
Drug/phospholipid molar ratio	0.05-0.07	0.l -0.25
Release of drug upon dilution	Fast and KP dependent	None
Storage form	Liquid, lyophilized	Liquid, frozen
Plasma pharmacokinetics:		
1_{st} $t_{1/2}$	5 min	3 h
2_{st} $t_{1/2}$	12 h	45 h

Idoxuridine loaded liposomes used against herpes simplex infected corneal lesions in rabbits [95], is one of the applications used for drug delivery other than cancer disease treatment. Use of liposomes in treating asthma or cystic fibrosis also shows that liposomes can be used in pulmonary applications [8].

Due to relatively simple preparation of liposomes using basic equipment in a laboratory and effectiveness in encapsulating various drugs or genes, they have a major role in the mainstream of clinical application in treating various diseases. However, liposomes are still recognized as foreign materials by the body and need improvement. The limitations in stability, clearance, active targeting, drug loading and production at large scale have led researchers to discover various liposome formulations can be called as new generation liposomes. Archaesomes, niosomes, vesesomes, are some of the examples of these formulations, which are in research [8].

Additionally, many novel systems are being in research such as ultrasound-assisted drug delivery [96] or nanoparticles loaded liposomes [97] to enhance the efficacy of drug delivery via extravasation or triggered drug release besides providing imaging in real-time. As an example, Spring et al. have introduced a photoactivatable multi-inhibitor nanoliposome system, as a new approach to nanoparticle-based medicine. It consists of a liposome doped with a photoactivable chromophore in the membrane, and poly (lactic-co-glycolic acid) nanoparticles containing cabozantinib (an anticancer drug) in the aqueous compartment. The mechanism of this approach for drug delivery is that the near-infrared tumour irradiation triggers photodynamic damage of cancer cells and initiates the release of cabozantinib. Mouse models demonstrated that the treatment using the mentioned system achieved prolonged tumour induction and moreover this model offered control of drug release while minimizing the toxicity [11]. This study demonstrates the applicability of plasmonic nanoparticles in drug delivery applications.

1.3.5 The role of plasmonic nanoparticles in drug delivery

Plasmonic nanoparticles are metallic particles in nanosized range. They have attracted great attention in industry and technology because of their remarkable optical properties such as surface plasmon resonance (SPR) which refers to the excitation of electrons at the interface between the conductor and insulator part of the material, triggered by light [98]. Conduction electrons on the surface of metal undergo a collective oscillation when excited by light at specific wavelengths. Light is absorbed by the electrons in the metal nanoparticles causing them to resonate, which can arise as local heat. Metal nanoparticles in that way can be used in controlled drug delivery systems and also for tracking in real-time to detect cancer tissues [99].

Silver nanoprisms (SNPs) or silver nanospheres (SNSs), which have the SPR effect, have attracted considerable interest because of their simple synthesis and unique optical properties [100]. They are being used in molecular diagnostic, photonics, conductive inks, antimicrobial coating, textiles, biomedical devices due to their high efficiency at absorbing and scattering light [101, 102]. Optical

properties of these nanoparticles are mainly shape and size dependent, and accordingly the SPR depends on the composition, shape and size of the AgNPs [103-105]. AgNPs can be synthesised by adding certain amounts of silver nitrate, trisodium citrate, hydrogen peroxide, sodium borohydride and water followed by mixing. Depending on the mixing time SNPs or SNSs can be formed as well as the optical properties can be tuned (**Figure 7**) [106]. Spectral properties of AgNPs have been determined in previous studies [98, 107] but size dependent optical information about nanoparticles are also available through industrial suppliers (e.g., NanoComposix) [108].

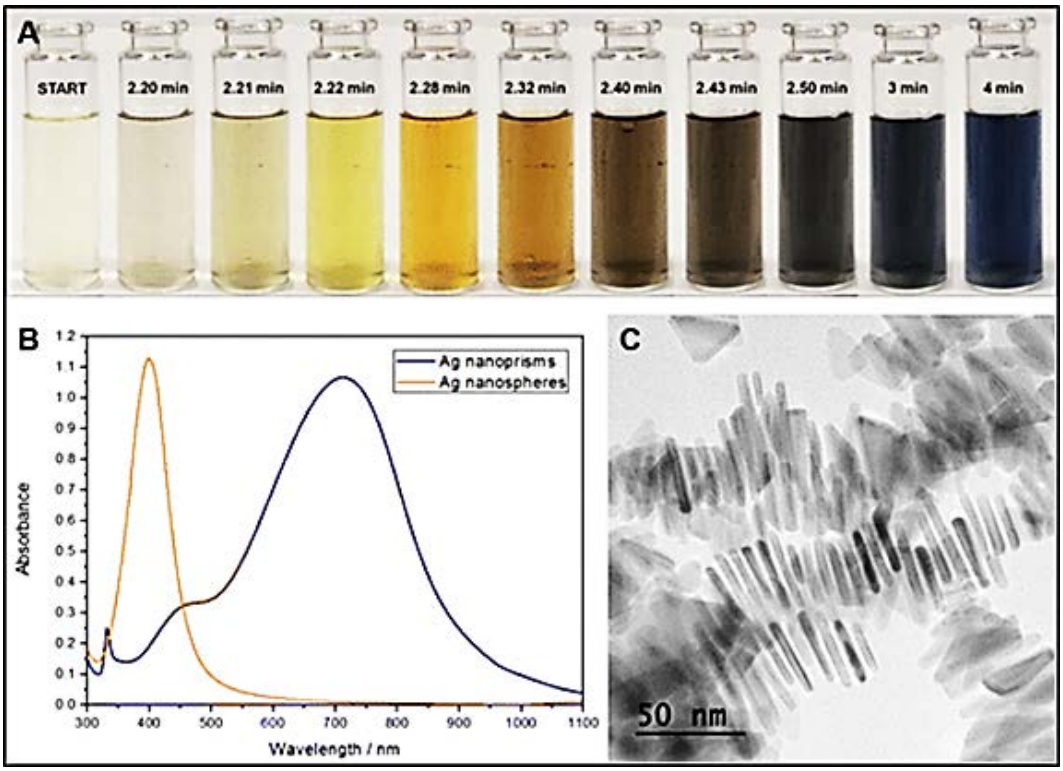

Figure 7 Optical and dimensional properties of AgNPs. A) The colour change during the formation of SNPs. B) The UV–vis absorption spectrum of SNPs and SNSs. C) TEM image of SNPs standing vertically upon their edges. Reprinted with permission from [106]. Copyright (2015) American Chemical Society.

Plasmonic nanoparticles are attractive for drug delivery since they can be employed to build a system having the ability to release the drug in a controllable manner. In principle, when plasmonic nanoparticles, such as gold or silver, are encapsulated inside the liposome they can trigger the liposomes layer to phase transition when they subject to light irradiation [97] since these metal nanoparticles can convert the optical energy into local heat energy [21, 109].

The use of plasmonic nanoparticles in pharmaceutical applications has been demonstrated by employing gold nanoclusters for photothermal therapy. Gui et al. have developed fluorescent gold nanoclusters and doxorubicin dual-loaded liposomes (AuNCs/Dox-liposome), which provides intracellular fluorescent thermometry, photothermal drug release and tumour therapy. The system

demonstrated here operates as a light-triggered nanoswitch for controlled drug release. When the temperature is above the phase transition the membrane of the liposome undergo a phase change from gel to liquid crystalline state and release the drug, while the membrane has reversed to a gel state when the temperature is under the phase transition temperature and the drug retains in the liposome (transition temperature of 42℃). In vitro studies demonstrated that upon irradiation of liver hepatocellular carcinoma cells for 180s, samples with free Dox showed decreased viability compared to the samples of AuNCs-Dox-Liposome. Continuous irradiation for 250s showed higher cell viability in samples of free-Dox comparing to AuNCs-Dox-Liposome; which demonstrates the delivery of Dox starts when the media temperature reaches the phase transition temperature. The release of the drug has stopped when the irradiation stops, which shows the drug delivery vehicle here works like triggered nanoswitch [97].

1.3.6 Production of liposome-based drug delivery systems

Fabrication of drug delivery systems especially the liposomes is mainly focussed in batch and well described in the literature [4, 84]. Production of liposomes with traditional methods includes thin-film hydration, detergent dialysis, reverse-phase evaporation and solvent injection [110]. Briefly, lipids are dissolved in a transfer medium following removal of the medium. Lipids are spontaneously self-assembled in bulk phase by hydration of a thin film. Self-assembly of lipids occurs in the dimension of millimetres with the lack of complete control over the physical properties in a batch reactor, which means poor control over liposome size that results in prepared vesicles being multilamellar and heterogeneous. Therefore, conventional methods need post-processing steps such as freeze-thaw, sonication, extrusion or high-pressure homogenization to obtain homogeneous or unilamellar vesicles [110]. On the other hand, the emerging technology of continuous-flow production has demonstrated the capability to provide particular size and size distributions by changing flow conditions in channels [33], in recent years.

1.3.6.1 Batch methods for liposome production

The features of the liposomes are directly related to the manufacturing method employed. Therefore, some key parameters must be considered in manufacturing phase, such as concentration and the potential toxicity of lipid type used to manufacture liposomes, the medium which lipids are dissolved in, the concentration and the potential toxicity of the material that will be encapsulated, size of liposomes, dispersity, intended use, stability, possibility of large-scale production or additional processes such as administration type [22, 33]. Some of the commonly used manufacturing methods of liposomes are reviewed, below, in more detail.

1.3.6.1.1 Solvent evaporation

This method begins with the solubilisation of the lipid in an organic solvent. It is important to have an absolute and homogeneous mixing of lipids. The next step is to evaporate the solvent using a rotary evaporator to obtain a thin lipid film on the walls of a round bottom flask. It is followed by the hydration step, which is the addition of the aqueous medium with a temperature above the phase transition temperature of the lipids used. This method gives multilamellar liposomes with a heterogeneous size, which is not suitable for many applications. Ultra-sonication or extrusion are some of the methods that can be employed to obtain small unilamellar liposomes. Also, freeze-thaw or freeze-drying can be implemented to increase the entrapment volume or reducing the lamellarity [111].

1.3.6.1.2 Mechanical agitation

This method includes the use of probe sonication to yield unilamellar liposomes with homogeneous size. Mechanical agitation of the solution following solubilisation of lipids in water gives liposomes easily but it has some drawbacks due to the risk of degradation of lipids caused by increased temperature arising from hot probe contacted with the solution. The advantage of this method is providing easy production and no need to remove organic solvents [112].

1.3.6.1.3 Solvent Injection

Lipids are first dissolved in an organic solvent such as Ethanol or Ether. The addition of ethanol with a fine needle into an aqueous solution or excess saline yields a solution containing small unilamellar liposomes. The advantage of this method is its simplicity and low risk of degradation of lipids. On the other hand, the amount of ethanol that can be introduced to the aqueous part, and the lipid amount can be dissolved in the ethanol, are limited, in which results in with low EE% for the hydrophilic materials; besides, removal of the ethanol from the dispersion is another problem for this method [8, 113].

Ether injection involves injecting the solvent very slowly into the aqueous solution with a narrow needle. The process occurs at a temperature where the solvent can evaporate, leading to the formation of bilayer sheets, which results in the form of sealed vesicles. This method has a low risk of oxidative degeneration; besides, since the solvent is being brought into contact with the aqueous solution and evaporated simultaneously, there is no limit for the lipid can be introduced to the system. This enables high proportion of aqueous medium for the liposomes to have high amount of encapsulated material. The disadvantage of this method is that, it needs to be paid attention when introducing the lipid solution, and also it can take long time to produce in large scale [114].

1.3.6.1.4 Drug loading and Purification

Drug entrapment or drug encapsulation is dependent on the properties like “hydrophilicity" of the molecules that will be loaded to the liposomes. After the contact of the aqueous phase containing hydrophilic materials with the lipids, bilayer formation is carried out by self-assembly and some of the hydrophilic materials are encapsulated in the aqueous area of the liposomes. Unencapsulated hydrophilic materials stay in the bulk solution; which then has to be separated from the solution since only the encapsulated materials are of interest. Therefore, an additional process is needed for the purification. Separation of the unencapsulated materials can be performed via gel filtration column chromatography or centrifugation or dialysis; which is based on the properties of the material and differences in size between the liposome and the unencapsulated material. Centrifugation is a common method to separate materials like proteins or DNA or materials that may form aggregates. Densities of the liposomes and materials that will be separated, have importance in this method since only a difference between the vesicle and the material may give separate phase belonged to free materials and liposome encapsulating materials [115].

Active loading is a method commonly used to have hydrophilic drugs encapsulated with high efficiency. In this technique, the internal part of the liposome is ionized so that the drug to be entrapped enters the liposome passively, and then retained inside the liposomes thanks to the ionization. This feature can be gained by employing charged lipids incorporated into the membrane of the liposome or buffers with suitable pH values as the aqueous medium [116]. Should the materials that will be encapsulated into the liposomes are hydrophobic, they are entrapped in the bilayer membrane because they have a very low affinity to transit to the aqueous phase inside or outside the liposomes. In this method, the materials are solubilised with the lipids in the same solvent; following the hydration step, materials stay within the hydrophobic parts, which are the inner membranes of the liposomes [117].

1.3.6.2 Microfluidics and millifluidics-based liposome production

Microfluidics refers to flow and manipulation of small amount of fluids with at least dimension < 1000 µm [118]. Microfluidics technology enables precise control, mixing of fluid streams where liposome size can be controlled as opposed to batch production.

Production with microfluidics tools comes into prominence with much more potential in recent years. Interest in using microfluidics method mainly depends on micro dimensions where the behaviour of the fluid, in terms of surface tension, energy dissipation or fluidic resistance is different than macroscale [119]; also there are many advantages that microfluidics provide such as

lower amount of reagents, lower cost, improved mass and heat transfer, precise control over the flow regime, reduced mixing time, lower power consumption, potential for tuning vesicle properties on demand, rapid screening of nanoparticles [23]. The liposome synthesis occurs within the microreactors having channels with microscale architectures with cross-sectional dimensions in the order of tens to hundreds of micrometres.

The fabrication of microreactors or chips is performed typically via microfabrication techniques, in which a set of microchannels is either etched or moulded into a material like glass or polymer (typically Polydimethylsiloxane (PDMS)). Fabrication of microfluidic chips normally starts with designing the microfluidic channels with a software such as Solidworks, Autocad or ANSYS. The fabrication of the microfluidic chip can be carried out by employing various processes such as micro-milling, lithography or mould replication (**Figure 8**). Microchannels are entrapped within the chip and connected with the outer environment via inlets/outlets using tubing. Depending on the intended application, the injection of the fluids or the materials through the inlets of the microfluidic chip by using equipment such as syringe pumps or peristaltic pumps results with the generation of the product in the microchannel, and the resultant particles can be obtained from outlets of the microfluidic chip via tubing [120].

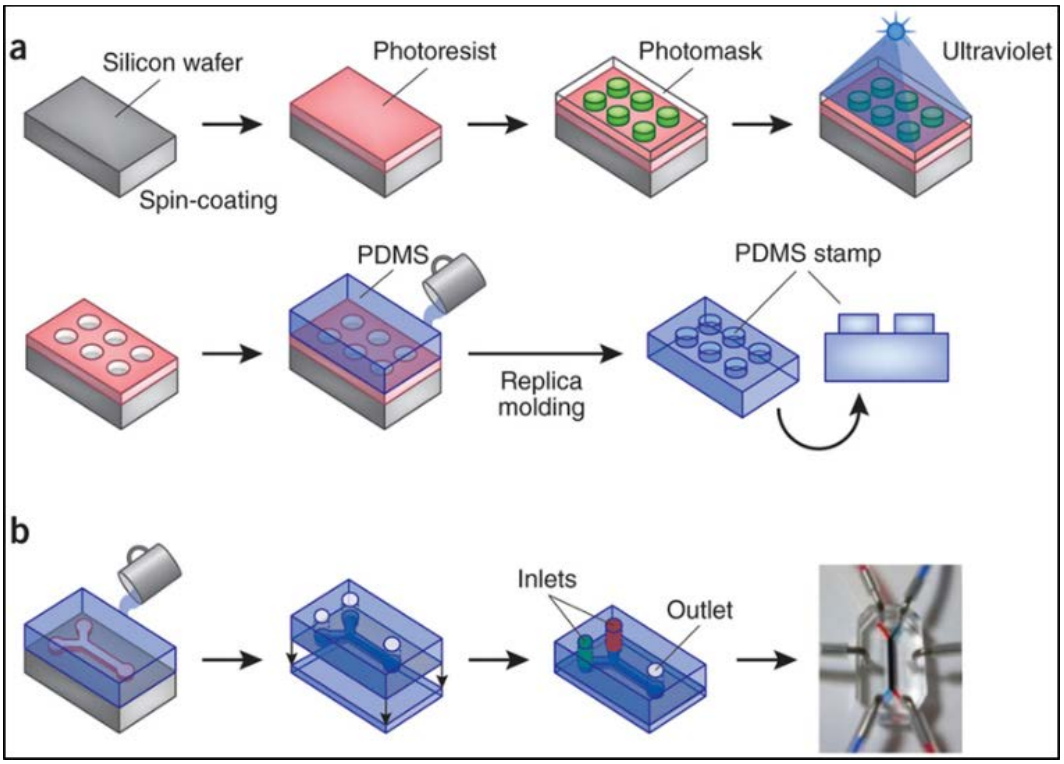

Figure 8 Fabrication of Microfluidics Chips. Reprinted by permission [121] from Springer Nature, Copyright (2014).

Microfluidic reactors can be operated in either continuous- flow [122] or droplet flow mode [123]. Continuous-flow microfluidics includes manipulating liquid flow continuously through

microchannels while droplet-based microfluidics includes generating the droplets. It is generally accepted as continuous-flow microfluidics is more suitable for generating nanoparticles (**Figure 9**) such as quantum dots [124], titanium dioxide nanorods [125]or polymeric nanoparticles [126]. Intended size distributions can be obtained in continuous-flow microfluidics by varying flow rates or concentrations of liquids.

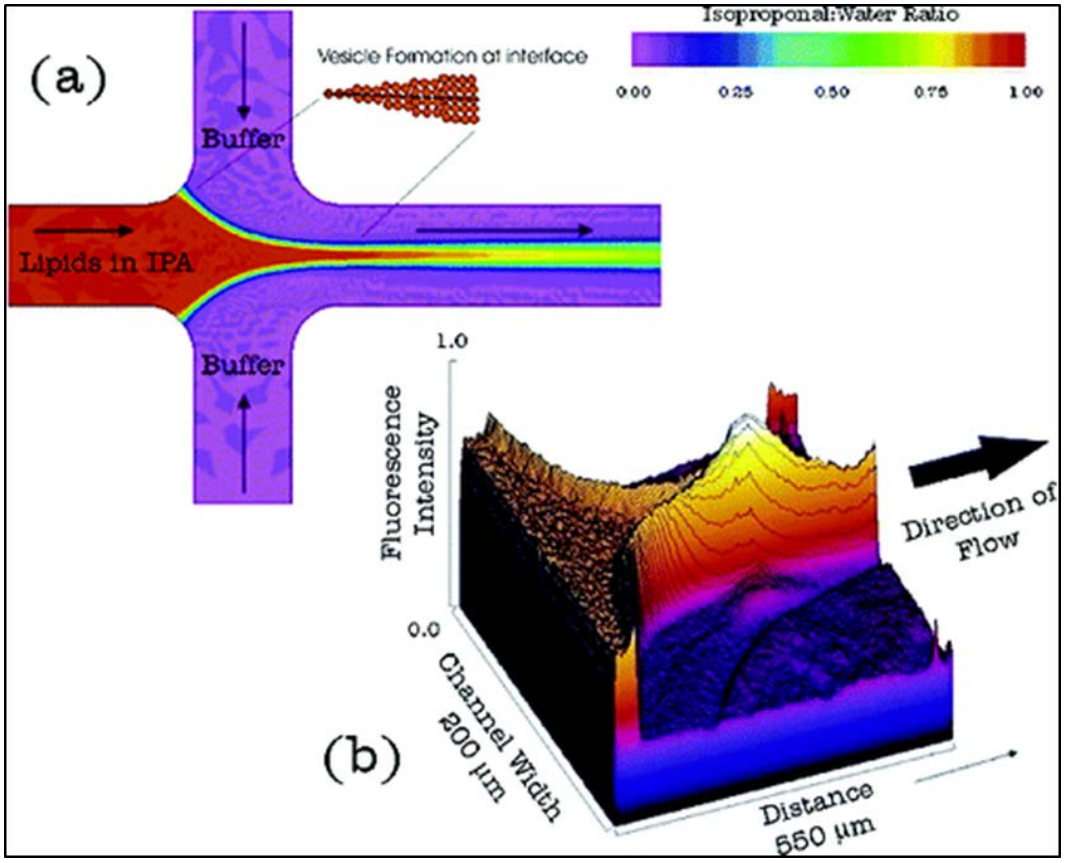

Figure 9 a) Liposome formation process in microfluidic channels. The colours represent the concentration ratios of IPA to aqueous buffer. b) 3D image of fluorescence intensity in the focused region in liposome formation. This figure reproduced from [127] (Andreas Jahn, Wyatt N. Vreeland, Michael Gaitan, and Laurie E. Locascio, Journal of the American Chemical Society 2004 126 (9)), 2674-2675, DOI: 10.1021/ja0318030, a public domain work funded by NIST.

The Reynolds number (Re) can characterize the flow of fluid through microfluidic channels. Laminar flow occurs when fluids flow in parallel layers without a disruption between the layers, which is in contrast to the turbulent flow which means a chaotic flow [128]. When the Re value is lower than 2000 the flow is laminar; flow is turbulent if the Re value is greater than 4000; between these values, transitional flow prevails [129, 130]. Re can be calculated with the formula below [131] as $Re=\rho uL/\mu$, where: ρ is the density of the fluid (kg/m3), u is the velocity of the fluid with respect to

the object (m/s), L is a characteristic linear dimension (m) and μ is the dynamic viscosity of the fluid (Pa·s or N·s/m2 or kg/m·s).

Jahn et al have demonstrated the controlled synthesis of nano-sized liposomes using microfluidic production method [127]. The microfluidic chip employed in this project was fabricated as having five inlets and three outlets. In experimental phase, solution of isopropyl alcohol (IPA) containing dissolved lipids was injected into the central inlet channel while free water was conveyed through two side inlet channels. The stream of IPA and dissolved lipids were focused by two aqueous streams at the cross junction of the chip. The flow rates of solutions mainly depend on the width of the channel since the width of the channel can limit the flow rate because of pressure. When IPA diffuses into aqueous solutions at the interface, lipids were self-assembled into vesicles i.e., liposomes. Flow rate represents the volume of fluid passes per unit time; flow rate ratio represents the ratio of the flow rates between fluids, and total flow rate represents the total value of the flow rates of fluids passes per unit time. The size of the produced liposome was controlled by changing the flow rate ratio (FRR) or total flow rate (TFR). The experiment demonstrated that by altering the flow rate of IPA containing dissolved lipids from 2.4 mm/s to 59.8 mm/s, the size of the liposomes was controlled in a range of 100 to 300 nm [127]. The article demonstrates the production of liposome populations is achievable by microfluidics method with various sizes in a controllable way by manipulating the flow rates or the shape along with the dimensions of the channels in a microfluidic chip without further purification or post-processing steps [33]. This approach also gives rise for adapting other applications into microfluidics such as drug encapsulation or drug delivery [132, 133].

However, there are still significant limitations that hinder industrial translation of microfluidic production; these can be mostly attributed to the small dimensional scale of the microfluidic architectures, and include high manufacturing costs, the complexity of device's operation, low particle production rates (up to a few mg/min [134]), and low device's lifetime (i.e. due to potential channel blockages caused by impurities or precipitation) [24-26]. On the other hand, millimetre-scale flow reactors (referred to as 'millifluidic reactors' or 'millireactors') have been recently developed and employed to produce both inorganic and organic nanomaterials, at volumetric flow rates up to 18 mL/min [25, 27-33]. Notably, scaling-up in these earlier studies enabled increased particle production capacity, while still retaining the fluidic controllability over particle's properties. Moreover, given their larger dimensions, devices could be manufactured using cost-effective and user-friendly techniques compared to conventional microfabrication methods [27, 28, 34].

Millifluidics can be defined as the flow and manipulation of higher amount of fluids in channels with dimensions of 1 mm across [135]. Millifluidic channels offer similar benefits comparing to

microfluidics technology, but also the fabrication of millifluidic reactors are much easier as the size is increased. The fabrication of a millifluidic reactor (or millireactor) in a relatively shorter time compared to a microfluidic reactor was demonstrated, using a 3D printer [28]. Also, the synthesis of organic and inorganic materials was demonstrated by using millimetre scale reactors [25, 27-33, 135].

1.3.6.3 Stability of liposomes

The stability of liposomes refers to the physical or chemical properties of liposomal formulations in terms of maintenance. As liposome structure can undergo degradation over time, the size or the encapsulation properties of the vesicle may change. Oxidative or hydrolytic degradation is believed to be the main mechanism that can lead to a change in size or leakage of the materials due to the change in permeability of the bilayer. Oxidative degradation may cause by performing experiments in high temperatures, working in an environment, which let expose of oxygen, or working with unpurified lipids. Performing experiments in the absence of oxygen or deoxygenating samples by passing nitrogen may help in protection from oxidative degradation. Performing experiments using saturated lipids such as distearoylphosphatidylcholine or dipalmitoylphosphatidylcholine (DPPC) instead of unsaturated lipids can be another solution to prevent degradation [8].

When pH levels close to neutral, the rate of degradation is at the lowest level, whilst it increases at either higher or lower pH levels. Formulations obtained by active loading for instance may suffer from hydrolysis. Aqueous solutions are more vulnerable to hydrolysis due to the presence of water and temperature may trigger the degradation, which can be prevented by refrigeration. Lyophilisation, which means freeze-drying of the sample to obtain a dried state of the formulations, can be performed to reduce the degradation and also increases the shelf-life [136].

Sterilization also is an important process to have the product free from viable organisms in the pharmaceutical industry. Filtration, γ-irradiation, UV-sterilization and ethylene oxide are some of the methods to obtain a sterilized sample. Filtration is a commonly practised method as it does not involve any process which can lead the liposome to disrupt, such as the use of heat, chemicals or radiation. However, filtration is only applicable to liposomes with a size under 200 nm and also it has to be performed in aseptic conditions.

1.3.6.4 Characterization of liposomes

Production of liposomal formulations is followed by various characterization methods to understand whether the samples are suitable for intended application considering properties such

as concentration, lamellarity, diameter, EE% and dispersity in terms of size distribution. The concentration of the phospholipids in the liposomal solution can be measured by spectrophotometric methods either by Bartlett Assay or by Stewart Assay. Following the destruction of the phospholipids in the solution, UV absorbance by a spectrophotometer employed in this method to check the inorganic phosphate [137]. Size determination of the liposomes can be characterized by Dynamic Light Scattering (DLS) method, which is easy and rapid but this method provides a mean diameter of the liposome bulk. In addition, zeta potential value, which is the surface charge of the liposomes, can be obtained [28]. Transmission electron microscopy (TEM) provides a characterization directly about the size and the morphology of the liposomes individually but the sample should be stained since the liposomes do not have a contrast to be visible by TEM [138]. Cryogenic electron microscopy (cryo-TEM) or atomic force microscopy can also be used to have detailed information about the structure and the size but these facilities are expensive and not easy to access. Gel exclusion chromatography can also be employed for size determination [139].

The fluidity of the liposome membrane can be characterized by differential scanning calorimetry in terms of temperature dependency. This feature is related to the phase transition temperature of the liposomes where the hydrocarbon chains may undergo phase transition from gel to crystalline or vice versa depending on the temperature. The phase transition temperature is important for determining storage condition, the possibility of drug leakage, in other words, the stability properties of the liposomes and provides information on whether the vesicle has reversible phase transition ability. Freeze-fracture electron microscopy or differential scanning calorimetry can be performed to investigate these properties on the liposomes [140].

The internal volume of the liposome is another important property that one should bear in mind. It can be defined as aqueous entrapped volume per unit quantity of lipids. By replacing the medium with an inert fluid such as deuterium oxide and then employing nuclear magnetic resonance spectroscopy the internal volume of water can be measured [8, 140].

Especially for drug delivery applications, measuring the encapsulation or the entrapment efficiency is one of the crucial steps. Before performing any application to observe the performance of the liposome solution, unencapsulated material in the solution must be removed. Once the free material is separated, the material that remained in the solution can be assumed as 100% encapsulated. The percentage of the loaded material into the liposomes in the solution means the efficiency in terms of encapsulation. EE% can be calculated by subtracting the amount of unencapsulated material from the amount of initial total drug and dividing by the total drug added. Commonly used separation technics for this purpose are centrifugation, dialysis and gel filtration

chromatography [8, 11]. The quantification of the materials in the solution can be carried out by spectrophotometry, fluorescence spectrophotometry or electrochemical methods. Following that, drug release trials can be performed via in vitro diffusion cells which can provide outcomes about pharmacokinetics and the bioavailability of the drug [141].

1.4 Summary

Considering cancer disease, which is one of the leading death causes is mainly treated by radiotherapy or chemotherapy or surgery (complete removal of cancerous tissue) [35, 142], the treatment can affect cancerous tissues as well as healthy tissues [143]. Liposomes, which are being used as nanocarriers of the pharmaceutical actives, have been proposed to minimize the side effects by entrapping drugs on the lipid bilayer or inside their aqueous area [14]. Even though the first liposomal drug, Doxil® (Liposomal Doxorubicin), minimizes the toxicity, novel drug delivery systems built by different approaches may contribute critical data to the area of drug delivery [64]. Novel drug delivery systems such as photothermal drug release via thermosensitive liposomes [97] were built up combining different disciplines like nanotechnology, medicine and chemistry. Metallic nanoparticles such as gold nanoclusters or SNPs with surface plasmon resonance properties give the chance of manufacturing drug delivery applications that can provide targeted delivery of the drug using irradiation as a triggering mechanism. AgNPs can provide a temperature increase inside liposomes by converting light energy to heat energy [109] and trigger liposome's lipid bilayer to phase transition from gel to liquid [97] so that liposomes can release drugs at the targeted site. In addition to various batch production methods, microfluidic or millifluidic tools provide easy and rapid production for liposomal drug delivery applications. Continuous-flow millireactors, which provides time-saving, lower cost and controllable nanoparticle production compared to conventional batch methods, will also be preferred as the production method in addition to batch methods in the study.

Chapter 2 Synthesis of Liposomes[1]

2.1 Introduction

Liposomes are polymolecular aggregates (i.e., polymolecular assemblies) of certain amphipathic molecules, formed in aqueous solution. They typically consist of an aqueous core enclosed within one or more bilayers of natural or synthetic amphipathic molecules (typically glycerophospholipids, i.e. lipids that contain a glycerol-3-phosphate unit) [144, 145]. Their unique architecture provides a useful platform for incorporating hydrophilic and/or hydrophobic molecules within the core and/or the bilayer, which has opened the way for the usage of liposomes as nanocarrier systems in pharmaceutical, cosmetic, and nutraceutical applications [146]. For instance, liposomes have demonstrated potential for delivering pharmaceutical actives to pathological sites within the body, with high efficacy and minimal toxicity. This is largely attributed to their nanostructure-dependent physico-chemical properties (size, surface charge and/or hydrophilicity) together with their high biocompatibility and biodegradability, thereby reducing undesired side effects [10, 90]. As a result, a number of liposome-based drug delivery systems have been developed, including conventional liposomes (mainly composed of phospholipids, with or without cholesterol), PEGylated liposomes and ligand-targeted liposomes [14], among which Doxil® and AmBisome® are exemplar formulations currently in clinical use [64, 147].

In the context of particulate-based drug delivery, the particle geometry (particularly its size and size distribution) plays a critical role on its performance *in vivo*, as it affects bio-distribution, endocytosis, clearance, targeting efficiency, drug release rate, encapsulation efficiency and stability [148-152]. In this regard, some of the quality control measures for food-grade or pharmaceutical-grade liposomal products involve determining the geometry and surface charge of the lipid vesicles [153]. In drug delivery applications, liposomes typically have a diameter in a range of 50 to 100 nm, which is deemed suitable for achieving vesicle's penetration through the blood vessel wall and escaping elimination by the reticuloendothelial system [67, 68, 150]. The dispersity of a liposome preparation is another important parameter affecting its performance *in vivo*; it is often quantified from dynamic light scattering (DLS) measurements through the dispersity index, a dimensionless numerical value ranging from 0 (i.e., for a sample with a uniform particle hydrodynamic radius) to 1 (i.e., for a sample that presents a very high particle size dispersity, often characterized by multiple

[1] The whole content in this chapter (Chapter 2) was published in *Pharmaceutics* journal published monthly online by MDPI 135. Yanar, F., et al., *Continuous-Flow Production of Liposomes with a Millireactor under Varying Fluidic Conditions.* Pharmaceutics, 2020. **12**(11): p. 1001.

size populations) [150, 154]. For polymer-based nanoparticles, dispersity index values smaller than 0.3 are generally considered to correspond to a sample of sufficiently low size dispersity for drug delivery applications [110, 150].

In principle, the formation of liposomes occurs when the phospholipid molecules encounter an aqueous environment and spontaneously arrange into a planar bilayer structure in order to minimize interactions between the hydrophobic acyl chain of the molecules and the aqueous phase. The formed planar bilayers subsequently enclose to generate a vesicular structure. For a given chemical formulation, the geometry of the resulting vesicle is primarily dependent upon the preparation process [151, 155, 156]. Currently, the batch methods most commonly employed for liposome production involve a series of steps, which often include (i) lipid dissolution in organic solvents, (ii) solvent evaporation, and (iii) hydration of the formed dry lipid film. However, such production methods suffer from significant drawbacks including limited control over process parameters to produce nanoscale vesicles with desired features, requiring additional post-production steps to achieve desired particle dimensional properties [110, 157]. These challenges become particularly critical when translating from laboratory-based synthesis to industry-scale production [110, 158].

More recently, microfluidic-based devices have been employed as an alternative technique to produce liposomes with controllable size and in a continuous-flow format. In microfluidic devices, a lipid alcohol solution typically mixes with a water phase under highly controlled fluidic conditions, within microscale architectures with cross-sectional dimensions in the order of tens to hundreds of micrometers [33, 118]. Microfluidic reactors with a range of channel designs, such as T- or Y-shaped mixers [120, 159] have been employed to produce different types of vesicular systems (including liposomes) under various flow conditions, such as hydrodynamic focusing [160] and droplet-based [28, 161] regimes. Compared to traditional batch methods, microfluidic approaches have shown advantages in many aspects, including precise control over the transport of fluids, chemical species and heat, and the potential for tuning vesicle properties on-demand [23]. However, there are still significant limitations that hinder industrial translation of this technology; these can be mostly attributed to the small dimensional scale of the microfluidic architectures, and include high manufacturing costs, complexity of device's operation, low particle production rates (up to 4 mg/min [134]), and low device's lifetime (i.e. due to potential channel blockages caused by impurities or precipitation) [24-26].

To address these challenges, millimetre-scale flow reactors (referred to as 'millifluidic reactors' or 'millireactors') have been recently developed and employed to produce both inorganic and organic

nanomaterials, at volumetric flow rates up to 18 mL/min [25, 27-33]. Notably, scaling-up in these earlier studies enabled increased particle production capacity, while still retaining the fluidic controllability over particle's properties. Moreover, given their larger dimensions, devices could be manufactured using cost-effective and user-friendly techniques compared to conventional microfabrication methods [27, 28, 34].

Although there is considerable interest in the scaling-up of liposome production [162-166], in the literature review, a systematic investigation of continuous-flow liposome production in a millifluidic reactor has not been carried out yet. In particular, only limited research has been performed to investigate the relationship between liposome dimensions and production-/formulation-related parameters, such as inlet volumetric flow rates, lipid concentration, chemical composition, and fluid temperature. Moreover, a systematic comparison between millifluidic and batch liposome production techniques has not been fully carried out yet.

The aim of the present study was therefore to demonstrate controllable production of liposomes using an easy-to-manufacture millifluidic reactor, at a range of varying operating conditions and lipid formulations. Moreover, the stability of the produced liposomes was evaluated and production performance was compared with a commonly used batch 'ethanol-injection' method.

2.2 Materials and Methods

2.2.1 Materials

Ethanol (99.9%), cholesterol (Chol, Sigma Grade 99%) from sheep's wool, dipalmitoylphosphatidylcholine (DPPC, >99%), octadecylamine (ODA, 99.0%, stearylamine), and polyoxyethylene (40) stearate (PEG-40) were obtained from Sigma Aldrich, Gillingham, UK. PHOSPHOLIPON®90G (purified phosphatidylcholine, or PC, from soybean lecithin) was kindly provided as a gift by Phospholipid GmbH (Lipoid, Ludwigshafen, Germany). Syringe pumps (AL-1010) were purchased from World Precision Instruments (Hertfordshire, UK), and 20 mL BD-Plastipak syringes with luer lock connectors were obtained from Fisher Scientific (Loughborough, UK). Male luer lock rings, polytetrafluoroethylene tubing, and magnetic stirrers (UC152D) were supplied by Cole-Parmer (St. Neots, UK). The tubing that was employed to connect the outlet port of the millireactor to the collection vial was 21.5 cm long (inner diameter: 0.5 mm; outer diameter: 1.6 mm) and was purchased from Cole-Parmer (St. Neots, UK).

2.2.2 Design and fabrication of millireactors

The millireactor geometry comprised two inlets with rectangular cross-sections (width: 0.4 mm, height: 1 mm) and one outlet, and a 60 mm long serpentine-like mixing channel (radius of curvature: 1.15 mm) having a square cross-sectional area of 1.0 x 1.0 mm. The curve shaped inlet channels were separated by a 0.2 mm wide septum. The geometrical layout of the millireactor and a photograph of the manufactured device (containing a coloured dye) are illustrated in **Figure 10A**&**B**, respectively.

The fabrication of the reactor was performed following a previously reported protocol, combining micromilling with replica moulding (referred to as µMi-REM) [34]. Briefly, the mould was designed in Autodesk Inventor Pro 2016 (Autodesk®, San Rafael, CA, USA). A negative mould was then micromilled into a block of acrylic, and epoxy resin was cast over it to obtain a positive master mould. Liquid polydimethylsiloxane (PDMS, from Sylgard® 184, Dow Corning Corporation, Michigan, MI, USA) was produced by mixing a PDMS monomer with curing agent (10:1 by weight). PDMS was subsequently degassed and poured over the master mould, and cured overnight at ambient temperature to obtain a replica of the millifluidic channel architecture. Inlets/outlet ports were created through the PDMS layer using a biopsy punch (1.5 mm in diameter) with a plunger (Miltex®, Fischer Scientific, Loughborough, UK). Bonding of the PDMS layer with a 50 x 70 mm glass slide (Corning® microscope slides, Sigma Aldrich, Gillingham, UK) was achieved via surface activation with oxygen plasma (using the TePla 300 plasma asher, PVA TePla AG, Wettenberg, Germany). The fabrication of the millireactor was performed by Dr Ali Mosayyebi.

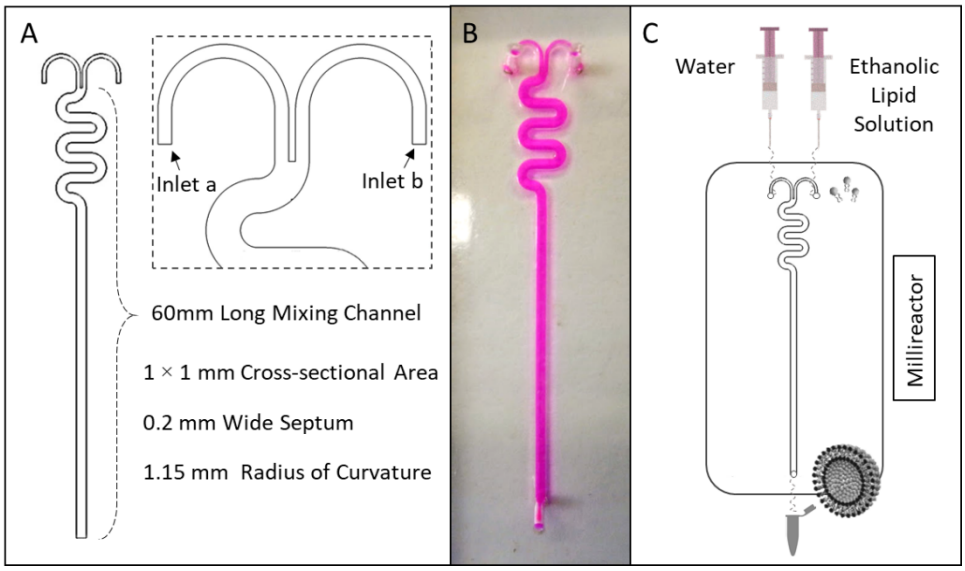

Figure 10 (A) Millireactor geometrical characteristics, (B) top view photograph of the millireactor, and (C) schematic illustration of the experimental approach for liposome production using the millireactor.

2.2.3 Liposome production

All lipids (PC, DPPC, Chol, ODA, and PEG-40) were dissolved in ethanol. In continuous-flow liposome production by solvent exchange mechanism, the ethanolic lipid solution and water were injected separately into the two inlets of the millireactor. A schematic of the experimental set-up for the production of liposomes using the millireactor is illustrated in **Figure 10C**.

Different flow conditions were investigated, corresponding to variations in both the flow rate ratio (FRR) and the total flow rate (TFR). Herein, the FRR is defined as the ratio between the inlet volumetric flow rates of water and the ethanolic lipid solution, and TFR as the total volumetric flow rate (i.e., the sum of ethanol and water flow rates). Liposomes were produced either at room temperature (RT) or 65 °C by placing the millireactor on a hot plate. In the latter case, the ethanolic lipid solution and distilled water (in separate syringes) were kept in a beaker containing water at 65 °C, prior to injection in the millifluidic device. The operational parameters (TFR, FRR, and temperature) and chemical formulations for each liposome batch are reported in **Table 3**. All data reported represent the mean values taken from three independent measurements of samples, with the corresponding standard deviations. Batch production of liposomes was also carried out using an ethanol injection technique [159], by manually injecting the ethanolic lipid solution in water, within a vial (4 mL) under magnetic stirring (at RT). Different volume ratios (VRs) of the aqueous phase to the ethanolic lipid solution were investigated, corresponding to FRR values of 5, 10, 25 and 50.

Table 3 The operational parameters (TFR, FRR, and temperature) and chemical formulations used in each experiment.

Batch code[1]	Fluidic parameters			Lipid composition (mM)[3]					Temperature	Size (Z-average)	Dispersity	Z-potential
	TFR (mL/min)	FRR	Reynolds number[2]	PC	DPPC	Chol	ODA	PEG-40	(°C)	(nm)		(mV)
#1 PC	1	5	9.79	100	-	-	-	-	RT	171.9 ± 2.7	0.285 ± 0.042	ND
#2 PC	1	10	13.17	100	-	-	-	-	RT	170.5 ± 4.6	0.241 ± 0.030	ND
#3 PC	1	25	16.18	100	-	-	-	-	RT	169.0 ± 0.8	0.133 ± 0.025	ND
#4 PC	1	50	17.30	100	-	-	-	-	RT	179.8 ± 2.4	0.188 ± 0.009	ND
#5 PC	5	5	48.95	100	-	-	-	-	RT	177.9 ± 1.8	0.279 ± 0.029	ND
#6 PC	5	10	65.83	100	-	-	-	-	RT	173.4 ± 2.0	0.252 ± 0.016	ND
#7 PC	5	25	80.88	100	-	-	-	-	RT	184.2 ± 1.5	0.320 ± 0.008	ND
#8 PC	5	50	86.52	100	-	-	-	-	RT	214.0 ± 3.3	0.375 ± 0.010	ND
#9 PC	10	5	97.90	100	-	-	-	-	RT	228.4 ± 9.5	0.437 ± 0.036	ND
#10 PC	10	10	131.66	100	-	-	-	-	RT	240.3 ± 9.2	0.481 ± 0.018	ND
#11 PC	10	25	161.75	100	-	-	-	-	RT	253.9 ± 3.0	0.494 ± 0.020	ND
#12 PC	10	50	173.04	100	-	-	-	-	RT	272.5 ± 7.4	0.522 ± 0.011	ND
#13 PC	1	10	13.17	16	-	-	-	-	RT	122.1 ± 0.5	0.145 ± 0.013	−3.4 ± 0.3
#14 PC	1	10	13.17	50	-	-	-	-	RT	217.3 ± 4.3	0.094 ± 0.021	−13.2 ± 0.5
#15 PC	1	5	9.79	200	-	-	-	-	RT	245.6 ± 4.0	0.469 ± 0.086	ND

#16 PC	1	5	9.79	40	-	-	-	-	RT	150.5 ± 5.4	0.240 ± 0.043	ND
#17 PC	1	5	9.79	5	-	-	-	-	RT	125.4 ± 1.1	0.220 ± 0.006	ND
#18 PC	1	10	13.17	14.4	-	1.6	-	-	RT	110.9 ± 2.6	0.184 ± 0.033	ND
#19 PC	1	10	13.17	12.8	-	3.2	-	-	RT	143.0 ± 0.4	0.175 ± 0.006	ND
#20 PC	1	10	13.17	11.2	-	4.8	-	-	RT	134.5 ± 1.4	0.146 ± 0.022	−0.3 ± 0.2
#21 PC	1	10	13.17	9.6	-	6.4	-	-	RT	142.3 ± 1.5	0.082 ± 0.023	ND
#22 PC	1	5	9.79	11.2	-	4.8	-	-	RT	80.0 ± 0.2	0.117 ± 0.017	ND
#23 PC	1	15	14.75	11.2	-	4.8	-	-	RT	135.8 ± 1.0	0.087 ± 0.018	ND
#24 PC	1	20	15.63	11.2	-	4.8	-	-	RT	141.5 ± 0.9	0.075 ± 0.006	ND
#25 PC	1	10	13.17	12.8	-	1.6	1.6	-	RT	92.9 ± 0.2	0.167 ± 0.006	15.6 ± 0.3
#26 DPPC	1	10	13.17	-	16	-	-	-	RT	66.7 ± 0.6	0.244 ± 0.002	7.8 ± 0.7
#27 DPPC	1	5	9.79	-	11.2	4.8	-	-	RT	162.8 ± 1.6	0.167 ± 0.046	ND
#28 DPPC	1	10	13.17	-	11.2	4.8	-	-	RT	185.2 ± 1.7	0.212 ± 0.004	3.7 ± 0.4
#29 DPPC	1	15	14.75	-	11.2	4.8	-	-	RT	198.8 ± 1.2	0.208 ± 0.012	ND
#30 DPPC	1	20	15.63	-	11.2	4.8	-	-	RT	201.1 ± 0.6	0.219 ± 0.007	ND
#31 DPPC	5	5	48.95	-	11.2	4.8	-	-	RT	131.9 ± 1.0	0.085 ± 0.028	ND
#32 DPPC	5	10	65.83	-	11.2	4.8	-	-	RT	139.7 ± 1.3	0.073 ± 0.002	ND
#33 DPPC	5	15	73.75	-	11.2	4.8	-	-	RT	136.9 ± 0.4	0.089 ± 0.016	ND
#34 DPPC	5	20	78.13	-	11.2	4.8	-	-	RT	138.6 ± 1.9	0.088 ± 0.011	ND
#35 DPPC	10	5	97.90	-	11.2	4.8	-	-	RT	105.9 ± 1.1	0.093 ± 0.017	ND
#36 DPPC	10	10	131.66	-	11.2	4.8	-	-	RT	97.3 ± 0.6	0.103 ± 0.012	ND
#37 DPPC	10	15	147.50	-	11.2	4.8	-	-	RT	94.9 ± 0.9	0.085 ± 0.011	ND
#38 DPPC	10	20	156.26	-	11.2	4.8	-	-	RT	88.4 ± 1.1	0.069 ± 0.015	ND
#39 DPPC	1	10	13.17	-	12.8	1.6	1.6	-	RT	232.4 ± 1.1	0.701 ± 0.120	25.9 ± 1.6
#40 DPPC	1	10	13.17	-	13.6	-	1.6	0.8	RT	54.4 ± 0.5	0.144 ± 0.020	29.8 ± 3.0
#41 DPPC	1	15	14.75	-	13.6	-	1.6	0.8	RT	54.8 ± 0.9	0.130 ± 0.007	45.6 ± 3.4
#42 DPPC	1	20	15.63	-	13.6	-	1.6	0.8	RT	56.6 ± 0.7	0.158 ± 0.013	36.3 ± 2.7
#43 DPPC	1	10	13.17	-	12.8	-	1.6	1.6	RT	75.3 ± 0.3	0.190 ± 0.016	17.4 ± 0.7
#44 DPPC	1	15	14.75	-	12.8	-	1.6	1.6	RT	81.3 ± 1.0	0.209 ± 0.010	20.8 ± 0.5
#45 DPPC	1	20	15.63	-	12.8	-	1.6	1.6	RT	77.2 ± 1.0	0.195 ± 0.007	29.8 ± 2.9
#46 DPPC	1	5	9.79	-	11.2	4.8	-	-	65	177.6 ± 2.1	0.222 ± 0.017	ND
#47 DPPC	1	10	13.17	-	11.2	4.8	-	-	65	196.1 ± 1.5	0.238 ± 0.023	ND
#48 DPPC	1	15	14.75	-	11.2	4.8	-	-	65	186.7 ± 1.9	0.154 ± 0.005	ND
#49 DPPC	1	20	15.63	-	11.2	4.8	-	-	65	195.8 ± 2.7	0.224 ± 0.017	ND
#50 DPPC	5	5	48.95	-	11.2	4.8	-	-	65	138.7 ± 2.3	0.076 ± 0.019	ND
#51 DPPC	5	10	65.83	-	11.2	4.8	-	-	65	143.5 ± 1.0	0.101 ± 0.006	ND
#52 DPPC	5	15	73.75	-	11.2	4.8	-	-	65	124.9 ± 1.3	0.094 ± 0.026	ND
#53 DPPC	5	20	78.13	-	11.2	4.8	-	-	65	125.6 ± 1.9	0.085 ± 0.015	ND
#54 DPPC	10	5	97.90	-	11.2	4.8	-	-	65	101.1 ± 0.7	0.044 ± 0.009	ND
#55 DPPC	10	10	131.66	-	11.2	4.8	-	-	65	93.9 ± 1.2	0.055 ± 0.008	ND
#56 DPPC	10	15	147.50	-	11.2	4.8	-	-	65	90.6 ± 0.4	0.057 ± 0.008	ND
#57 DPPC	10	20	156.26	-	11.2	4.8	-	-	65	86.6 ± 1.7	0.066 ± 0.008	ND
#58 PC*	-	5*	-	100	-	-	-	-	RT	193.6 ± 2.9	0.260 ± 0.012	ND
#59 PC*	-	10*	-	100	-	-	-	-	RT	192.1 ± 2.7	0.242 ± 0.007	ND
#60 PC*	-	25*	-	100	-	-	-	-	RT	193.2 ± 1.7	0.302 ± 0.030	ND
#61 PC*	-	50*	-	100	-	-	-	-	RT	208.2 ± 24.5	0.325 ± 0.056	ND

Each liposome batch is reported together with its corresponding fluidic parameters, chemical formulation, and the physico-chemical properties of the end product. Values of liposome size, dispersity and zeta potential

represent the mean of three measurements with the corresponding standard deviation. Flow rate ratio (FRR) is defined as the ratio between the inlet volumetric flow rates of water and the ethanolic lipid solution, and TFR as the total volumetric flow rate (i.e. the sum of ethanol and water flow rates). [1]The batch code given represents the number of the produced liposome batch along with its fluidic parameters, chemical formulation, and the resultant size and dispersity values. [2]Reynolds number was calculated based on the volumetric ratios of water and ethanol, considering the values of TFR and FRR. [3]Given parameters represent the amount of the phospholipid (phosphatidylcholine soybean (P90G) or dipalmitoylphosphatidylcholine (DPPC)), stabilizer (cholesterol (Chol) and/or octadecylamine (ODA)), or polyoxyethylene (40) stearate (PEG-40) in the liposome batch, reported in millimolar (mM) concentration. * The liposome batch was produced using the ethanol injection technique as a batch method; FRR values in millifluidic production correspond to the volume ratio (VR) of water to ethanolic lipid solution in batch production. ND: Not determined.

2.2.4 Liposome characterisation

The mean diameters, size dispersities, and zeta potentials of the produced liposome dispersions were determined by DLS technique, using a Zetasizer Nano ZS (Malvern Instruments Ltd., Malvern, UK). Dimensional and zeta potential measurements were performed at 25 °C, using polystyrene semi-micro (Fisherbrand™ (FB55147), Fisher Scientific, Loughborough, UK) cuvettes and folded capillary cell (DTS1070, Malvern Instruments Ltd., Malvern, UK) type cuvettes, respectively. Samples used for DLS analysis had a volume of 1 mL (without dilution). The viscosity values used for DLS measurements were calculated using the Zetasizer Software 7.12, by considering the effects of different FRRs and VRs on the fluid's viscosity (see part **2.2.4.1**) [167]. The dimensions of the resultant liposomes were given as the Z-average, which represents the intensity-weighted mean hydrodynamic size of the particulate dispersion. The Z-average value is a widely used dimensional parameter determined using DLS according to ISO 13321 and ISO 22412, and is recommended as a robust way of quantifying and reporting the liposome's mean size [168].

All measurements were performed three times per sample. The values for liposome size (Z-average), dispersity and zeta potential were calculated by taking the average of three measurements. The standard deviation was also calculated from these three measurements (using Microsoft Excel).

The produced liposomes were imaged by transmission electron microscopy (TEM). 5 μl of the sample was placed on a carbon-coated grid and allowed to adsorb for 30 seconds; any excess amount was removed with a filter paper (Whatman). Liposomes were negatively stained by adding 5 μL of 5% ammonium molybdate containing 1% trehalose on the grid (for 30 seconds), and the excess amount was again removed using a filter paper. TEM images were taken using the FEI Tecnai T12 machine.

2.2.4.1 Viscosity of the ethanol/water solution

Figure 11 shows the dynamic viscosity of the ethanol/water mixture, at varying amounts of water, determined using the Zetasizer software.

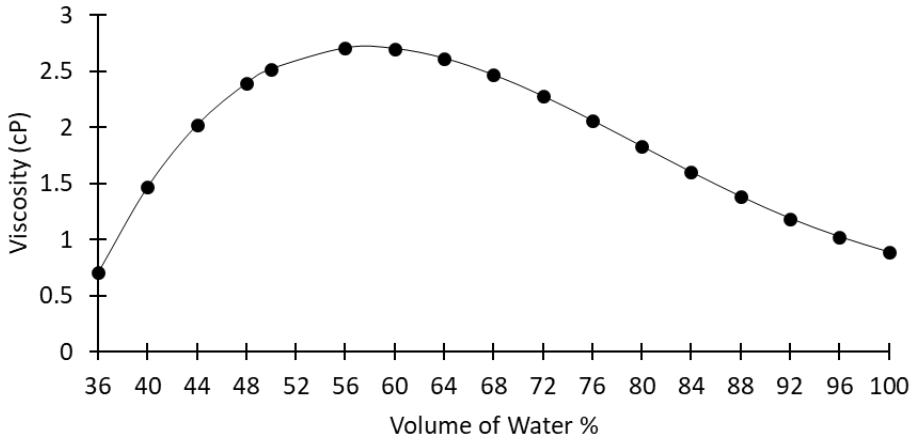

Figure 11 Data represent the viscosity values used in the DLS measurements (in cP). Depending on the flow rate ratio (FRR) used, the volume ratio of ethanol and water was calculated theoretically and the viscosity values were extrapolated using the software (Zetasizer) provided by Malvern.

The concentration of the water-ethanol mixture was calculated theoretically by considering the varied amount of water at different FRRs, and was input in the Zetasizer software to obtain the viscosity values reported in **Figure 11**. The reported values were in turn input in the DLS software for determination of liposome size and dispersity.

The calculation of the viscosity of the water-ethanolic lipid solution mixture was performed using the Zetasizer software at a temperature of 25 °C by considering the flow rate values. The obtained resultant suspension was kept at room temperature for at least one hour after production, and the sample was characterized using DLS technique on the same day using the relevant calculated viscosity values (**Figure 11**). Since the synthesis of liposomal solutions was performed in a controllable environment and the sample was kept at a constant temperature after production, it was believed that the viscosity of the dispersion was equal to the theoretically calculated value.

2.3 Results and Discussion

2.3.1 Millifluidic reactor's design rationale

The design of the millifluidic reactor includes two curved inlet channels, which are separated by a septum before merging into the mixing channel. This design feature was introduced to ensure that the inlet flow streams could meet parallel to each other, and differs from conventional microfluidic hydrodynamic focusing architectures where the inlet channels typically meet at an angle in the range of 30°-90°. It was hypothesised that the proposed design configuration would prevent flow instabilities at the intersection between inlet channels, which may occur particularly at the higher flow rates investigated.

The mixing channel design had a serpentine-like architecture to enhance mixing efficiency between water and ethanol by increasing the residence time of chemical species within the device (compared to a straight channel) and by inducing advection-dominated transport, e.g. due to the formation of secondary flows within the channel's cross-section (also known as Dean flows) [169]. The fluidic and mixing performance of the device was modelled using Computational Fluid Dynamics (CFD) simulations (see **Figure 12** and **Figure 13**). Values of Reynolds and Dean number in the mixing channel of the device, at the different TFRs investigated, are reported in **Table 4.** Numerical results show that increasing the TFR resulted in greater mixing efficiency, which is likely due to stronger secondary flows. At any given TFR, increasing the FRR also resulted in greater mixing efficiency [170].

2.3.1.1 Calculation of Reynolds number (Re) and Dean number (De)

Table 4 summarises the values of Reynolds number (Re) and Dean number (De) in the mixing channel of the millifluidic reactor, calculated at different total flow rates (TFR).

Table 4 Values of Reynolds number and Dean number in the mixing channel of the millifluidic device, at the different total flow rates (TFR) investigated.

TFR (mL/min)	Reynolds number	Dean Number
1	13.1	8.6
5	65.8	43.4
10	131.6	86.8

The Reynolds number (Re) and Dean number (De) were calculated from $Re= \rho VD/\mu$ and $De= ((D/2r)^{0.5})Re$, respectively, where ρ is the fluid density, V is the mean velocity of the fluid, D is the channel hydraulic diameter, μ is the fluid dynamic viscosity, and r is the radius of curvature of the mixing channel centreline. The density of the ethanol-water mixture was calculated based on the FRR,

and the dynamic viscosity was obtained from the viscosity values reported in **Figure 11**. Values were calculated considering a flow rate ratio (FRR) of 10.

2.3.1.2 Numerical simulation of the transport of fluids and chemical species within the millifluidic device

The transport of fluid and chemical species (ethanol and water) within the millifluidic device was characterised using computational fluid dynamics (CFD) simulations. The geometry of the millireactor was designed using Inventor Pro 2016 (Autodesk®, USA), and geometrical meshing was performed using ICEM CFD 17.0 (Ansys Inc., USA). A total number of 1'661'007 mesh volumes (selected mesh size of 0.05 mm) of tetrahedral shape was employed. Ansys® Fluent 17.0 was employed to solve for mass and momentum conservation equations (i.e., Navier-Stokes), and for advection-diffusion equations. Selected TFR and FRR values, corresponding to experimental conditions tested, were simulated numerically. Boundary conditions were set as: constant mass flow at the inlet cross-sections, atmospheric pressure at the outlet, and no-slip boundary condition at the channel inner walls. The diffusion coefficient of ethanol in water was set to 1×10^{-9} m^2/s [167], and fluids were assumed incompressible and Newtonian.

In order to quantify the mixing performance of the device, the relative mixing index (RMI) was calculated for each simulated flow condition. RMI was defined as the ratio of the standard deviation of ethanol mass fraction over the outlet cross-section to the standard deviation of ethanol mass fraction in the unmixed state (just after the junction between inlets), following an approach previously reported in the literature [170].

Figure 12 shows the calculated values of relative mixing index at different values of flow rate ratio and total flow rate, demonstrating an increase in mixing efficiency with increasing both TFR and FRR.

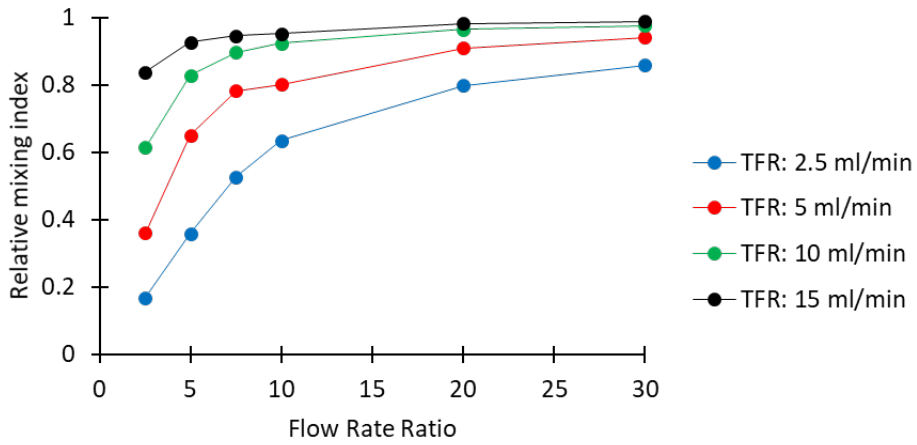

Figure 12 The numerically calculated relative mixing index of water and ethanol, based on the selected total flow rates (TFR) and flow rate ratios (FRR).

Figure 13 instead shows contours of ethanol mass fraction plotted over selected cross-sectional surfaces along the mixing channel of the millifluidic device, at varying operational TFRs and FRRs.

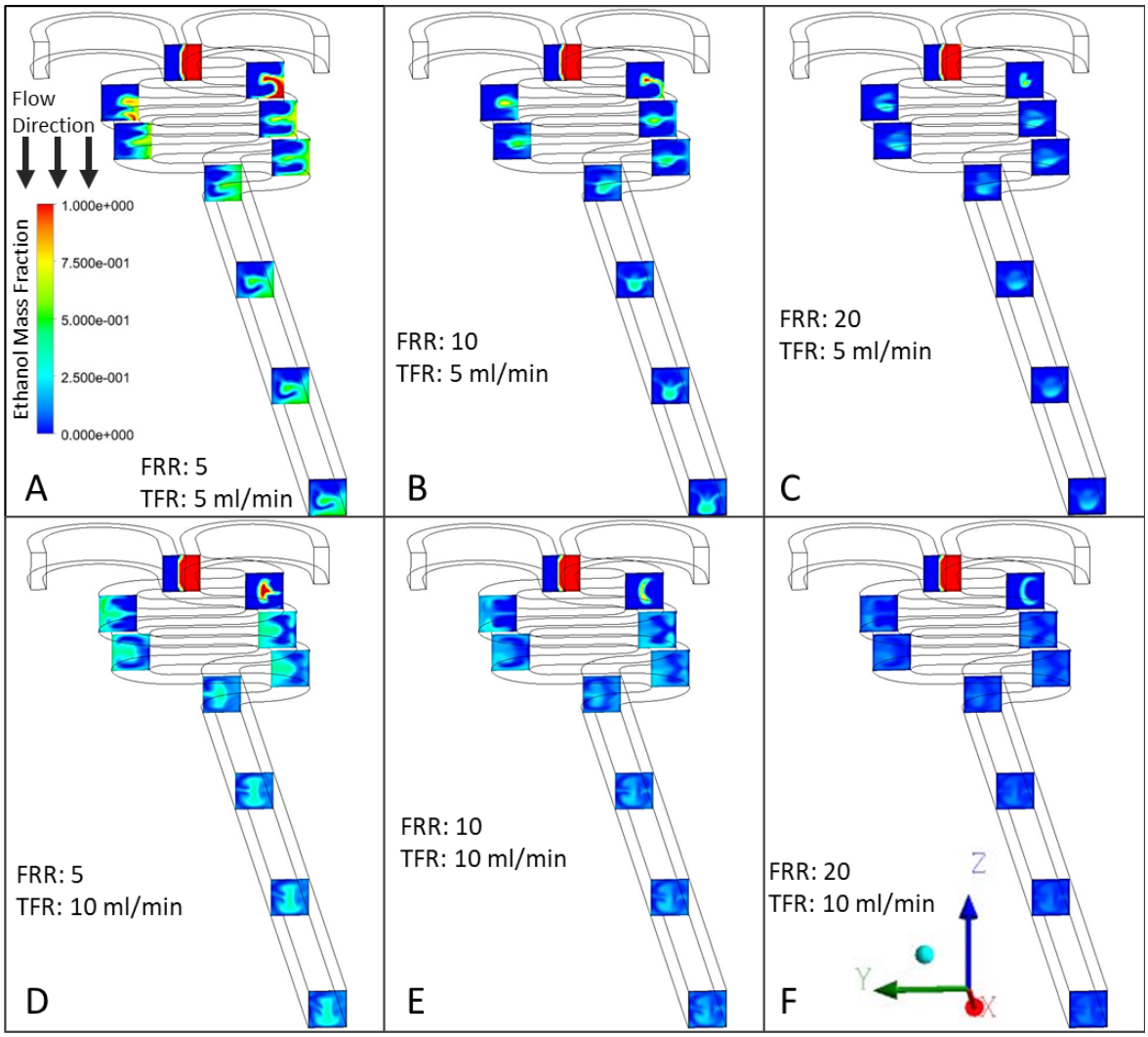

Figure 13 Contour plots of the ethanol mass fraction, plotted over different cross-sectional surfaces from the entrance of the mixing channel until the channel's outlet. The red and blue colours represent the ethanol and water phases, respectively. Mixing

between the two phases along the millifluidic reactor can be appreciated. (A) TFR = 5 mL/min, FRR = 5. (B) TFR = 5 mL/min, FRR = 10. (C) TFR = 5 mL/min, FRR = 20. (D) TFR = 10 mL/min, FRR = 5. (E) TFR = 10 mL/min, FRR = 10. (F) TFR = 10 mL/min, FRR = 20. TFR: Total flow rate, and FRR: flow rate ratio (aqueous/ethanolic lipid solution).

Figure 13 shows the mixing profile of water and ethanol in the serpentine shaped millireactor on different flow conditions. It can be seen that the ethanol portion in the mixture was decreased when the higher FRR applied, as expected. Also, the mixing profile was changed when applying higher TFR, indicating an increase in mixing efficiency, as supported with the data in **Figure 12**. Also, the contour plots of ethanol mass fraction demonstrated that the mixing in the serpentine channel was dominated by advection rather than diffusion.

2.3.2 Methodological rationale

The first set of experiments was designed to examine the effect of TFR and FRR on the size, dispersity and stability of liposomes. The selected values of operational parameters are comparable to those typically used in continuous-flow liposome production by solvent exchange mechanism [23]. Experiments were conducted employing two different lipid compositions, namely a cost-effective model lipid (PC, at 100 mM) and a formulation that is often used in commercial medicines (DPPC/Chol, at 11.2:4.8 mM) [10]. The storage stability of PC (100 mM) liposomes was also evaluated; in these experiments, liposomes were produced at a constant TFR (1 mL/min) and different FRRs (5, 10, 25 and 50). Further experiments were carried out to investigate the effects of varying the amount and/or type of the liposome constituents. These included (a) different concentrations of PC (5, 40, 100, and 200 mM) at constant TFR (1 mL/min) and FRR (5); (b) different molar ratios of PC/Chol (9:1, 8:2, 7:3, and 6:4) at constant TFR (1 mL/min) and FRR (10), corresponding to different amounts of cholesterol; and (c) different formulations of phospholipid (PC vs. DPPC) and stabilizer (Chol vs. ODA), in the presence or absence of a PEG-40 moiety (at a fixed TFR of 1 mL/min and varying FRRs). Zeta potential measurements were also performed on selected formulations, in order to evaluate the effect of lipid type on liposome surface charge. Formulations investigated had the same total concentration (16 mM) and included pure, cholesterol-containing, and octadecylamine- and cholesterol-containing PC and DPPC liposomes. Additionally, PC liposomes with a greater lipid concentration (50 mM) and DPPC liposomes containing PEG-40 (at varying concentrations) were characterised to investigate the effect of lipid and stabilizer concentration on zeta potential, respectively.

In the third set of experiments, the effect of temperature on the production of DPPC/Chol liposomes was investigated at either room temperature or 65 °C. In these experiments, the reactor was operated at varying TFRs (1, 5, and 10 mL/min) and FRRs (5, 10, 15, and 20).

Finally, a comparison between liposomes produced by millifluidics and ethanol injection (i.e. as a model for a conventional batch technique) was carried out, whereby the volume ratios (VRs) of the aqueous phase to the ethanolic lipid solution in the batch method were consistent with the FRR values in the millireactor.

2.3.3 Effects of TFR and FRR on liposome size

The effect of fluidic parameters on liposome size and dispersity were assessed. Please refer to **Table 3** (batch code #1 PC to #12 PC) for the corresponding experimental conditions and lipid composition. The experimental results are illustrated in **Figure 14**.

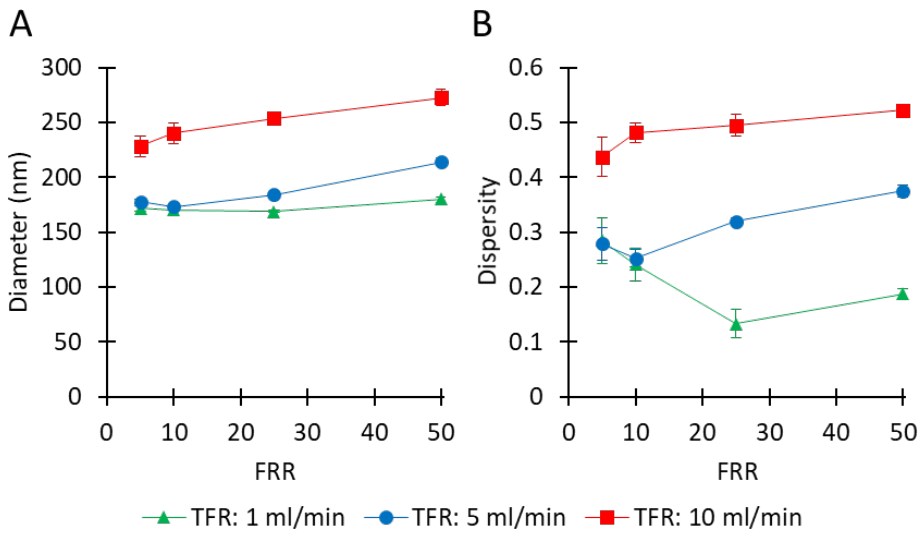

Figure 14 Effects of total flow rate (TFR) and flow rate ratio (FRR) on liposome Z-average size (A) and dispersity (B). Liposomal formulations (PC, 100 mM) were produced at TFR = 1 ml/min, 5 ml/min, 10 ml/min and FRR (aqueous phase/ethanolic lipid solution) = 5, 10, 25, 50. Data represent the mean of three measurements with corresponding standard deviation. Refer to **Table 3** (batch code #1 PC to #12 PC) for the corresponding experimental conditions, lipid composition, and numerical data of mean values and standard deviation.

Figure 14A shows that, at a given TFR, the mean liposome diameter overall increased by increasing the FRR, ranging from 169 nm (at TFR = 1 mL/min and FRR = 25) to 272 nm (at TFR = 10 mL/min and FRR = 50). At TFR = 1 mL/min, it varied in a relatively small range (from 170 nm to 179 nm), whilst increased from 177 nm to 214 nm at TFR = 5 mL/min, and ranged from 228 nm to 272 nm at TFR = 10 mL/min. Concerning the effect of TFR, at any given FRR, a greater TFR generally resulted in larger

liposomes. Values of dispersity are reported in **Figure 14B**, and ranged from 0.13 to 0.52. At TFR = 10 mL/min, increasing the FRR from 5 to 50 resulted in an increase in dispersity from 0.43 to 0.52. At TFR = 1 mL/min, increasing FRR from 5 to 25 resulted in a decrease in dispersity (from 0.28 to 0.13), while an increase in FRR from 25 to 50 resulted in a marginal increase in dispersity (from 0.13 to 0.18). A similar trend was observed at TFR = 5 mL/min; when FRR was increased from 5 to 10 the dispersity remained almost unchanged (from 0.27 to 0.25), followed by an increase (from 0.25 to 0.37) when FRR was further increased from 10 to 50.

In summary, these results indicate that liposome size strongly depends on the imposed flow settings. The TFR was found to be directly correlated with both liposome size and size dispersity. However, diverging effects of FRR were observed at different values of TFR. At TFR = 10 mL/min, changing FRR from 5 to 50 caused an increase in both liposome size and dispersity. Conversely, at TFR = 5 mL/min or 1 mL/min, increasing the FRR didn't show a significant effect at first and a subsequent tendency for an increase in liposome size. Overall, the liposome batch presenting the most suitable characteristics (for pharmaceutical applications) was obtained when operating the millireactor at TFR = 1 mL/min and FRR = 25; notably, samples produced at these operating conditions had Z-average size of 169 nm and dispersity of 0.13, and the final lipid concentration in the end-product was 3.8 mM (corresponding to 2.91 mg/mL).

To examine a formulation that is relevant to pharmaceutical applications [10], DPPC/Chol was used for experiments under similar flow conditions. Please refer to **Table 3** (batch code #27 DPPC to #38 DPPC) for the corresponding experimental conditions and lipid composition. The results are shown in **Figure 15**.

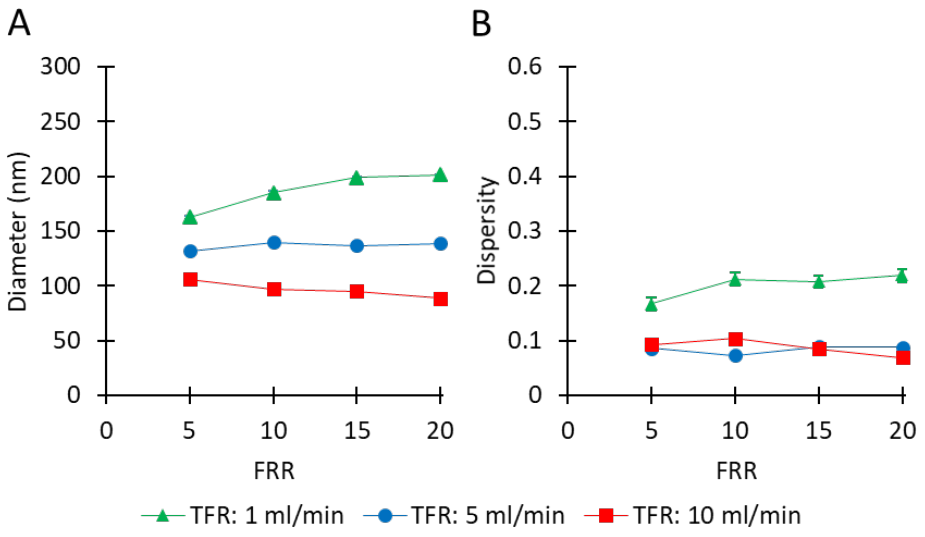

Figure 15 Effects of total flow rate (TFR) and flow rate ratio (FRR) on liposome Z-average size (A) and dispersity (B). Liposomal formulations (DPPC, 16 mM) were produced at TFR = 1 ml/min, 5 ml/min, 10 ml/min and FRR (aqueous phase/ethanolic lipid solution) = 5, 10, 15, 20. Data represent the mean of three measurements with corresponding standard deviation. Refer to **Table 3** (batch code #27 DPPC to #38 DPPC) for the corresponding experimental conditions, lipid composition, and numerical data of mean values and standard deviation.

Figure 15A shows that the largest liposomes were obtained at TFR = 1 mL/min, in a range from 162 nm to 201 nm (by increasing FRR from 5 to 20). At TFR = 5 mL/min, there was no significant change observed in liposome size (from 131 nm to 138 nm) with increasing FRR from 5 to 20. When TFR was set to 10 mL/min, increasing FRR resulted in a marginal decrease in liposome size from 105 nm to 88 nm. Concerning the effect of TFR, at any given FRR, a greater TFR resulted in smaller liposomes. The dependence of liposome size on FRR varied depending on the TFR; an increase of FRR caused either a decrease (at TFR = 10 mL/min) or an increase (at TFR = 1 mL/min) in liposome size. The values of dispersity are reported in **Figure 15B** and varied in a range of 0.06 to 0.22. No specific trend was observed when increasing FRR from 5 to 20, at TFR = 10 mL/min (dispersity = 0.06 - 0.09), TFR = 5 mL/min (dispersity = 0.09 - 0.07) and at TFR = 1 (dispersity = 0.17 - 0.22). The optimal operating conditions for this formulation corresponded to TFR = 10 mL/min and FRR = 20, where the obtained liposome sample had an average size of 88 nm and dispersity of 0.07. The final total lipid concentration of the liposome samples ranged between 0.48 mg/mL (FRR = 20) and 1.67 mg/mL (FRR = 5).

The results described above (**Figure 14** & **Figure 15**) indicate that liposome dimensional properties likely depended on an interplay between fluidic and chemical conditions, including TFR, FRR, lipid concentration and type. When using the PC (100 mM) formulation, increasing TFR (at any given FRR) resulted in the production of liposomes with relatively higher diameter and size dispersity (**Figure 14**); conversely, when using DPPC/Chol (11.2:4.8 mM), both liposome size and size dispersity generally reduced with increasing TFR (**Figure 15**).

In previous studies, the liposome size was found to be almost insensitive to changes in TFR whilst it was inversely related to FRR [33, 171, 172]. In these studies, liposomes were produced using the microfluidic hydrodynamic focusing (MHF) approach using microscale reactors (with a cross-section ranging between 36 to 320 μm and 10 to 320 μm in depth and width, respectively) having a cross-flow geometry, whereby vesicle formation is primarily governed by diffusion-dominated mixing between water and an organic solvent. In a previous investigation using a scaled-up MHF device with channel cross-section of 1 mm × 1 mm (i.e., a size that is comparable to the one used in this study), the liposome size was directly related to FRR whilst it was inversely related to TFR [33].

Additionally, liposome size was found to be inversely related to both TFR and FRR in studies where the mixing process was dominated by advection rather than diffusion, such as in zigzag-shaped microchannels [173] or semi-circular contraction-expansion array microchannels [174].

It is generally accepted that, in the liposome formation process by solvent exchange mechanism, bi-layered fragments (BFs) first form at the water-organic solvent interface, which then self-assemble into liposomes (in milliseconds) upon increased polarity of the surrounding medium [110, 158]. This process is affected by the volumetric ratio between aqueous and ethanolic phases and the local lipid concentration (both depending on FRR), and by the mixing efficiency (which depends on TFR, for a given FRR). In the present study, increasing the TFR resulted in faster and more effective mixing between ethanol and water, likely due to stronger secondary flows associated with the channel's curvature. This is confirmed by the results of numerical simulations shown in **Figure 12** & **Figure 13**, which show increased mixing efficiency at greater TFRs. It can be hypothesized that the rapid increase in polarity associated with a faster mixing process would in turn cause BFs to rapidly self-assemble into liposomes of a smaller diameter. Increasing the FRR also resulted in greater mixing efficiency (see numerical results reported in **Figure 12** & **Figure 13**), overall resulting in a decrease in liposome diameter. These predictions are consistent with the results obtained when using a lower lipid concentration (e.g., 16 mM total concentration for DPPC/Chol liposomes, **Figure 15**).

On the other hand, when a greater lipid concentration was employed (e.g. 100 mM for PC liposomes, see **Figure 14**), the significantly larger number density of lipid molecules may have increased the possibility of BFs to collide and assemble into larger liposomal structures or other supramolecular lipid aggregates. This occurrence may become more prominent with increasing the TFR, due to the stronger secondary flows, and may also explain the observed additional peak in the DLS spectra (at approximately 1000 nm) at TFR = 10 mL/min, in both intensity-based and volume-based size distribution (see **Figure 16** for representative size distribution plots). The reasons, however, remain unclear for why increasing FRR resulted in larger particles, at a TFR of 10 mL/min (**Figure 14**).

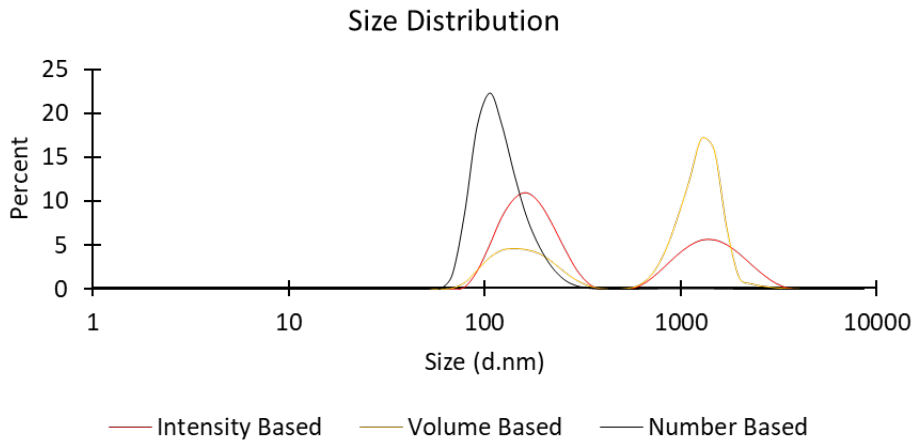

Figure 16 Representative size distributions (intensity-, volume-, and number-based) of liposome batches prepared by millifluidics using a serpentine-shaped millireactor. Liposomal formulations (PC, 100 mM) were produced at total flow rate (TFR) = 10 ml/min and flow rate ratio (FRR, aqueous phase/ethanolic lipid solution) = 10. Refer to **Table 3** (batch code #10 PC) for the corresponding experimental conditions and lipid composition.

The liposome size distributions shown in **Figure 16** were determined by taking into account the scattering intensity of each particle fraction. The peak observed at a particle size of ~1000 nm in the intensity-based distribution potentially originated from aggregates or larger vesicles, since the particle's scattering intensity is proportional to the square of the particle's molecular weight. The number- and volume-based distributions are instead derived from the intensity-based distributions using Mie theory. Whilst a peak at ~1000 nm appeared in the volume-based distribution, it could not be detected in the number-based distribution; this is likely due to the fact that these larger particulate structures represent only a relatively small proportion of the overall number of particles in the dispersion [168].

Overall, it appears that whilst liposome size at the lower lipid concentrations is dominated by the rapidity and efficiency of mixing between ethanol and water, at the greater lipid concentrations the increased number density of lipid molecules plays a dominant role. This observation has not been reported previously for millifluidic-based liposome production; however, further investigations are required to fully understand the mechanisms behind vesicle formation at the fluidic conditions employed in this study.

2.3.4 Evaluation of liposome stability upon storage

The storage stability of liposomes was assessed by analysing four different batches. Please refer to **Table 3** (batch code #1 PC to #4 PC) for the corresponding experimental conditions and lipid composition. Samples were kept in glass vials at 4 °C for up to 42 days, and size measurements were

taken on Day 0 (just after production), Day 7, Day 14 and Day 42. Changes in liposome size over time are reported in **Figure 17**.

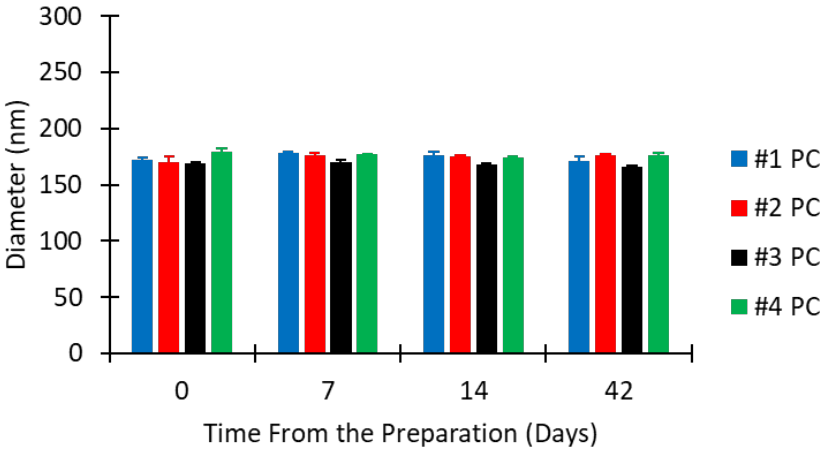

Figure 17 Dimensional stability of liposomes as a function of flow rate ratio (FRR). Liposomal formulations (PC, 100 mM) were produced at total flow rate (TFR) = 1 ml/min, and FRR (aqueous phase/ethanolic lipid solution) = 5, 10, 25, 50. Data represent the mean of three measurements with corresponding standard deviation. Refer to **Table 3** (batch code #1 PC to #4 PC) for the corresponding experimental conditions, lipid composition, and numerical data of mean values and standard deviation.

Figure 17 shows that there was no significant change in the size of liposome batches over time. The maximum variation in liposome size was within ±4% of the initial diameter, for all liposome batches analysed. All liposome batches prepared were thus reasonably stable over the test period of six weeks, which is consistent with previous studies reporting on the stability of liposomes produced by microfluidics [169, 175]. Considering the general requirements for shelf-life of pharmaceutical products, stability measurements over longer periods may be required for certain applications.

2.3.5 Effect of lipid concentration on liposome size

Considering the above reported results, further investigations were carried out to assess the effect of varying the concentration of PC. Please refer to **Table 3** (batch codes #17 PC, #16 PC, #1 PC, #15 PC) for the corresponding experimental conditions and lipid composition. The millifluidic device in these experiments was operated at constant fluidic conditions, which resulted in a final lipid concentration ranging between 0.63 and 25.3 mg/mL.

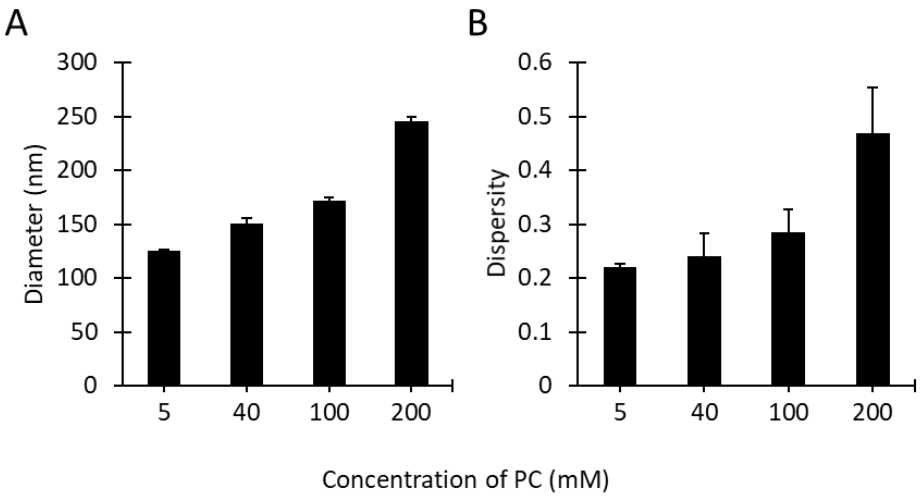

Figure 18 Effect of lipid concentration on liposome size (A) and dispersity (B). Liposomal formulations (PC) were produced at concentrations of 5 mM, 40 mM, 100 mM and 200 mM with total flow rate (TFR) = 1 ml/min and flow rate ratio (FRR, aqueous phase/ethanolic lipid solution) = 5. Data represent the mean of three measurements with corresponding standard deviation. Refer to **Table 3** (batch codes #17 PC, #16 PC, #1 PC, #15 PC) for the corresponding experimental conditions, lipid composition, and numerical data of mean values and standard deviation.

As shown in **Figure 18**, increasing PC concentration resulted in an increase of liposome diameter and size dispersity. Specifically, with increasing the initial PC concentration from 5 mM to 200 mM the liposome diameter increased from 125 nm to 245 nm (**Figure 18A**), and the dispersity from 0.21 to 0.46 (**Figure 18**B). Both these increments were more pronounced at concentrations > 100 mM. These findings confirm the observations reported above (see **Figure 14**), and are also consistent with other studies describing the production of liposomes by microfluidic approaches [33, 176]. Increasing the initial concentration of lipids likely resulted in a greater number density of lipid molecules available to form supramolecular aggregates of larger size and broader size distribution.

2.3.6 Effect of cholesterol on liposome size

Cholesterol is an important constituent of cell membranes and is widely used in liposomal formulations, as it changes the permeability and modifies the stability of liposomes [146]. It is also known to modulate the rigidity of a lipid bilayer, depending on the lipid constituents used [177]. In the literature review, a systematic investigation of the characteristics of cholesterol-containing liposomes produced by millifluidics has not been carried out yet. Therefore, in order to study the effect of cholesterol on the size of liposomes produced *via* millifluidics, different batches were produced by varying the amount of cholesterol relative to PC. Please refer to **Table 3** (batch code #18 PC to #21 PC) for the corresponding experimental conditions and lipid composition.

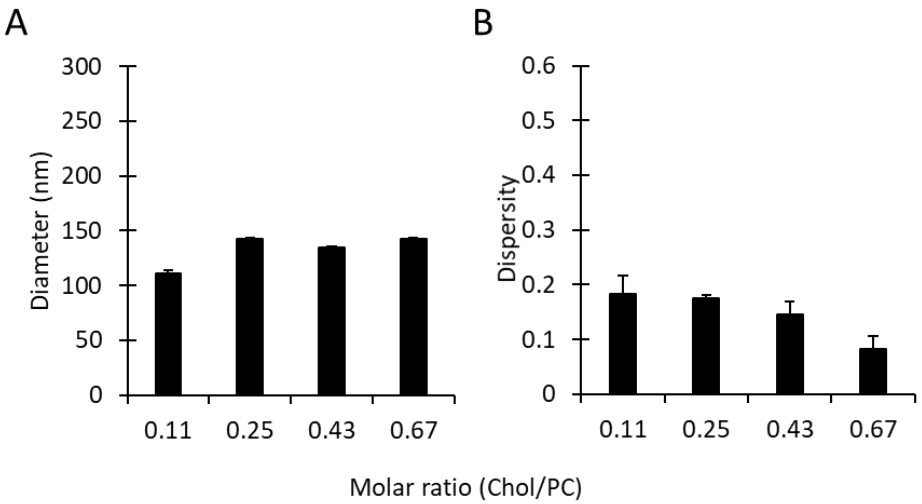

Figure 19 Effect of cholesterol concentration (in the molar range 1:9 to 1:1.5, with a total concentration of 16 mM) on liposome size (A) and dispersity (B). Liposomal formulations (PC/Chol) were produced at total flow rate (TFR) = 1 ml/min and flow rate ratio (FRR, aqueous phase/ethanolic lipid solution) = 10 with changing Chol/PC molar ratios (0.11, 0.25, 0.43, 0.67). Data represent the mean of three measurements with corresponding standard deviation. Refer to **Table 3** (batch code #18 PC to #21 PC) for the corresponding experimental conditions, lipid composition, and numerical data of mean values and standard deviation.

As it can be observed in **Figure 19**, no significant differences were observed in liposome batches prepared with different amounts of cholesterol. Increasing the cholesterol concentration from 1:9 to 1:1.5 in a molar range resulted in an increase in the liposome diameter from 110 nm to 142 nm and a slight decrease in dispersity from 0.18 to 0.08. The marginal change in liposome size due to the addition of cholesterol could be attributed to the formation of gaps between lipid molecules resulting from the intercalation of cholesterol within the membrane bilayer, causing an expansion of the membrane as reported in earlier investigations [178]. Moreover, the corresponding decrease in the amount of PC favoured the production of liposomes with a narrower size distribution, which is consistent with the results shown in **Figure 18**. Nevertheless, it is interesting to note that – in some previous studies – an increase in liposome size has been observed upon increasing cholesterol concentration [178, 179], with size changes depending on the lipid type and the amount of cholesterol added [180]. In summary, results demonstrated that liposomes made of different molar ratios of PC/Chol and having a therapeutically relevant size can be produced using the developed millifluidic device.

2.3.7 Effect of liposome composition on their dimensional properties

Earlier investigations of liposome production by millifluidics have predominately focused on a limited number of model lipid formulations. Since liposome properties are very often dependent upon their lipid composition [181], a further verification of the reactor's performance was carried out by producing liposomes of different formulations comprising PC, DPPC, Chol, ODA and PEG-40. PC (soybean) is one of the most common lipids used in liposomal formulations due to its abundance in animals and plants, and DPPC is often used in thermosensitive formulations and is often a key constituent in membrane models [182]. Cholesterol is known to increase the rigidity of a lipid bilayer [146], and PEG-40 is used to achieve steric stabilization of the liposome for applications including drug loading and release [183]. In addition, ODA (a cationic molecule) is often employed to produce positively charged liposomes in drug delivery applications [184]. Please refer to **Table 3** (batch codes #22 PC, #20 PC, #23 PC, #24 PC, #27 DPPC, #28 DPPC, #29 DPPC, #30 DPPC #40 DPPC, #41 DPPC, #42 DPPC, #43 DPPC, #44 DPPC, #45 DPPC) for the corresponding experimental conditions and lipid composition. The overall results are shown in **Figure 20**.

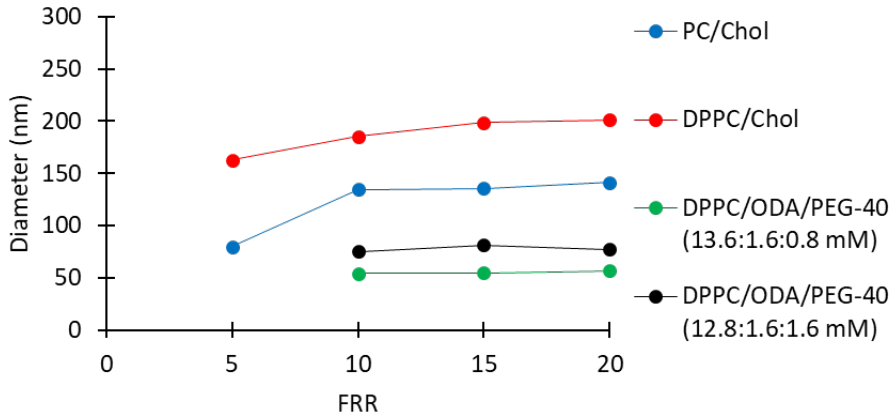

Figure 20 Z-average size of liposomes consisting of different lipid formulations. Liposomal formulations (PC/Chol, DPPC/Chol, DPPC/ODA/PEG-40, DPPC/ODA/PEG-40) were produced at a concentration of 16 mM, with total flow rate (TFR) = 1 ml/min and flow rate ratio (FRR, aqueous phase/ethanolic lipid solution) = 5, 10, 15, 20. Data represent the mean of three measurements with corresponding standard deviation. Refer to **Table 3** (batch codes #22 PC, #20 PC, #23 PC, #24 PC, #27 DPPC, #28 DPPC, #29 DPPC, #30 DPPC #40 DPPC, #41 DPPC, #42 DPPC, #43 DPPC, #44 DPPC, #45 DPPC) for the corresponding experimental conditions, lipid composition, and numerical data of mean values and standard deviation.

Figure 20 shows that the liposome size of PC/Chol and DPPC/Chol liposomes increased from 79 nm to 141 nm and from 162 nm to 201 nm, respectively, when increasing FRR from 5 to 20. The difference in size between the two formulations may be due to the superior fluidity of the

unsaturated fatty acids in the PC double layer. It has been previously reported that an increase in fluidity results in a decrease in liposome size [185]. Moreover, it has been shown that lipids with shorter chains lead to the formation of larger liposomes [186, 187], which may be due to the reduced thickness of the bilayer when a shorter chain length lipid is employed, e.g. the alkyl chain lengths of DPPC (16:0) vs. PC (18:2/16:0), leading to reduced membrane bending modulus [188] and lower line tension [189]. The resulting difference in size between PC/Chol and DPPC/Chol liposomes could be a combination of both aforementioned effects.

For the positively charged liposomes (DPPC/ODA/PEG-40), **Figure 20** shows that increasing the FRR didn't have a significant effect on liposome size, while simultaneously decreasing the amount of DPPC and increasing the amount of PEG-40 increased the liposome size. The observed increase in liposome size with increasing the content of PEG-40 is consistent with a previously reported investigation [190]. Please refer to **Table 3** for the zeta potential values of DPPC/ODA/PEG-40 liposomes (batch code #40 DPPC to #45 DPPC).

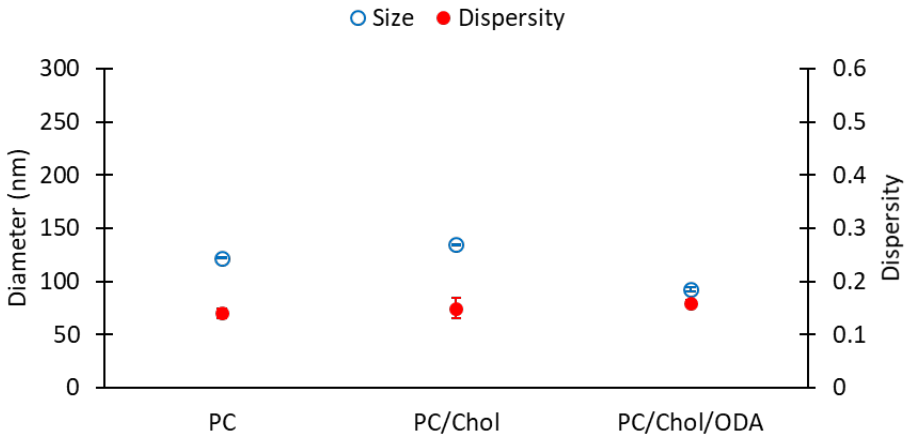

Figure 21 Z-average size (left Y-axis, empty blue circles), and dispersity (right Y-axis, filled red circles) of liposomes consisting of different lipid formulations. Liposomal formulations (PC, PC/Chol, PC/Chol/ODA) were produced at a concentration of 16 mM with total flow rate (TFR) = 1 ml/min and flow rate ratio (FRR, aqueous phase/ethanolic lipid solution) = 5. Data represent the mean of three measurements with corresponding standard deviation. Refer to **Table 3** (batch codes #13 PC, #20 PC, #25 PC) for the corresponding experimental conditions, lipid composition, and numerical data of mean values and standard deviation.

For comparison, PC, PC/Chol and PC/ODA/Chol liposomes were evaluated, and results are shown in **Figure 21**. Please refer to **Table 3** (batch codes #13 PC, #20 PC, #25 PC) for the corresponding experimental conditions and lipid composition. **Figure 21** shows that the size of liposomes slightly

changed upon addition of cholesterol to PC (diameter of 122.1 nm and 134.5 nm for PC and PC/Chol liposomes, respectively) likely due to an increase in the rigidity of the membrane bilayer [177], while a slight decrease in size was observed upon the incorporation of ODA (diameter of 92.8 nm). No significant difference was observed in the dispersity of liposomes across formulations (**Figure 21**).

In addition, zeta potential values and TEM images of selected formulations are shown in **Figure 22** & **Figure 23**, respectively. Please refer to **Table 3** (batch codes #14 PC, #13 PC, #20 PC, #25 PC, #26 DPPC, #28 DPPC, #39 DPPC) for the corresponding experimental conditions and lipid composition.

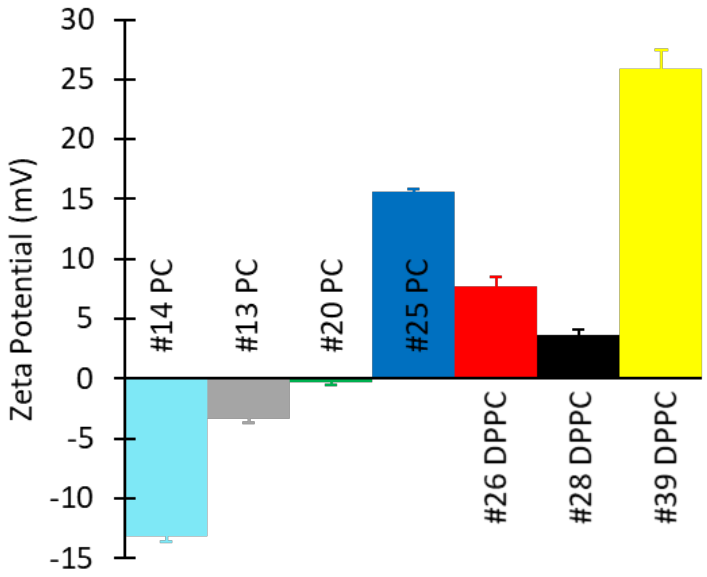

Figure 22 Zeta potential values of liposomes consisting of different lipid formulations (PC, PC, PC/Chol, PC/Chol/ODA, DPPC, DPPC/Chol, DPPC/Chol/ODA respectively) and different concentrations (50 mM, 16 mM, 11.2:4.8 mM, 12.8:1.6:1.6 mM, 16 mM, 11.2:4.8 mM, 12.8:1.6:1.6 mM respectively). Liposomal formulations were produced at total flow rate (TFR) = 1 ml/min and flow rate ratio (FRR, aqueous phase/ethanolic lipid solution) = 10. Data represent the mean of three measurements with corresponding standard deviation. Refer to **Table 3** (batch codes #14 PC, #13 PC, #20 PC, #25 PC, #26 DPPC, #28 DPPC, #39 DPPC) for the corresponding experimental conditions, lipid composition, and numerical data of mean values and standard deviation.

Zeta potential values of the produced liposomes (**Figure 22**) show that PC formulations in the absence of ODA were negatively charged, whilst DPPC liposomes were positively charged (even in the absence of ODA). Other authors have similarly reported a slightly positive value of zeta potential for DPPC liposomes, and they have attributed this to the software used to carry out the calculations [191]. As expected, the addition of ODA caused a further increase in zeta potential. Coherently with our findings (**Figure 20**, **Figure 21** and **Figure 22**), it was previously reported that incorporation of ODA in liposomes resulted in slight decrease in liposome size and an increase in surface charge [33,

192]. In this study, the highest zeta potential value was observed for DPPC/ODA/PEG-40 (batch code #41 DPPC) liposomes (+45.56) and the lowest for PC (batch code #14 PC) liposomes (−13.16).

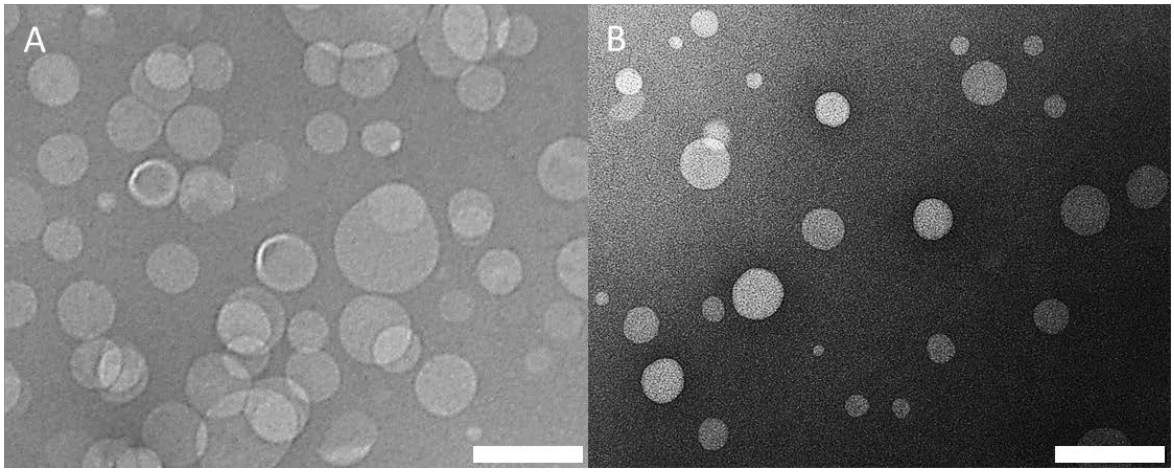

Figure 23 TEM images of liposome formulations of (A) PC/Chol and (B) PC/ODA/Chol at concentrations of 11.2:4.8 mM and 12.8:1.6:1.6 mM. Liposomal formulations were produced at total flow rate (TFR) = 1 ml/min and flow rate ratio (FRR, aqueous phase/ethanolic lipid solution) = 10. Please refer to **Table 3** (batch codes #20 PC and #25 PC) for the corresponding experimental conditions and lipid composition. Scale bars: 200 nm.

Representative TEM images are also illustrated in **Figure 23**, showing the morphology of liposomes produced from different formulations. The size of PC/Chol liposomes (**Figure 23A**) was also calculated by analysing the TEM images (**Figure 24A** & **B**) using a custom-built particle detection software (MATLAB R2020, based on the *imfindcircle* function). It was found that the value obtained from DLS (Z-average: 134.5 nm and dispersity: 0.15) was slightly larger than the one calculated from the images (number average diameter: 97.7 ± 29.8 nm and dispersity: 0.09); this small difference in diameter may be due to differences in the size quantification method, which is already reported and discussed in the literature [193, 194].

Figure 24A illustrates a representative TEM image of liposomes (PC/Chol 11.2:3.8 mM) produced by millifluidics. **Figure 24B** shows the outcome of the particle detection script (written in MATLAB) employed to detect circular objects (i.e. liposomes) in the TEM images and quantify their diameter.

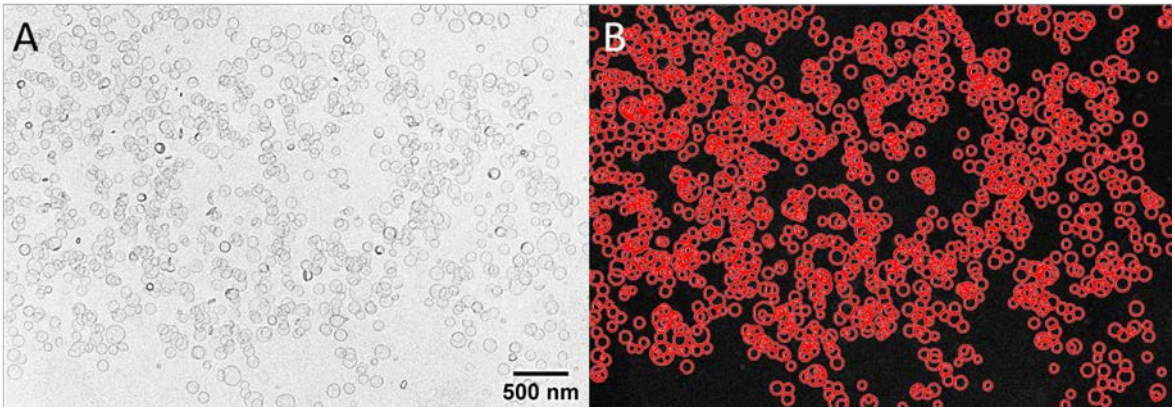

Figure 24 (A) Shows a representative TEM image used to calculate the liposome diameter. Liposomes comprised of PC/Chol (11.2:3.8 mM) and were produced using the millifluidic reactor, at total flow rate (TFR) = 1 mL/min and flow rate ratio (FRR, aqueous phase/ethanolic lipid solution) = 10. (B) The TEM image was processed using a custom-built software (MATLAB, R2020) that detected the circular objects (i.e. liposomes) in the image and calculated their diameter.

The image-based method of calculation of the mean diameter was based on a determination of the number average diameter of detected circles in the TEM images. The method implemented by MATLAB uses the function "imfindcircles", which detects circles in an image *via* the Hough transform. The method can also discriminate between overlapping circles, and provides the diameter of each individual circle. The average liposome diameter (97.7 ± 29.8 nm) was calculated by dividing the sum of the diameter values of each circle to the number of circles detected. The dispersity (0.09) was calculated by taking the square of the standard deviation divided by the mean diameter [195].

Overall, these experiments further confirmed that liposomes of varying therapeutically-relevant formulations can be produced using the developed millifluidic reactor, resulting in end-products with relatively uniform morphology, and of concentrations and dimensions that are relevant to pharmacological products. Here, therapeutically-relevant formulations are considered to be the ones having lipid composition and concentration comparable to those in commercial medicinal products using liposomes. The liposomal samples produced using millifluidic reactor have also been found to have similar size and dispersity to liposomes used in the pharmaceutical field [33].

2.3.8 Effect of production temperature on liposome size

An evaluation of the effect of production temperature on the size of DPPC/Chol liposomes was performed by comparing liposomes produced at room temperature (RT) and 65 °C. The higher temperature was selected to be at least 10°C above the phase transition temperature of DPPC (the reported value for the T_m of pure DPPC is indeed 41.5 °C). Thus, experiments were carried out to

examine whether any size change occurred when liposomes were formed above T_m by millifluidic approach. Please refer to **Table 3** (batch codes #27 DPPC to #38 DPPC, and #46 DPPC to #57 DPPC) for the corresponding experimental conditions and lipid composition. Results are shown in **Figure 25**.

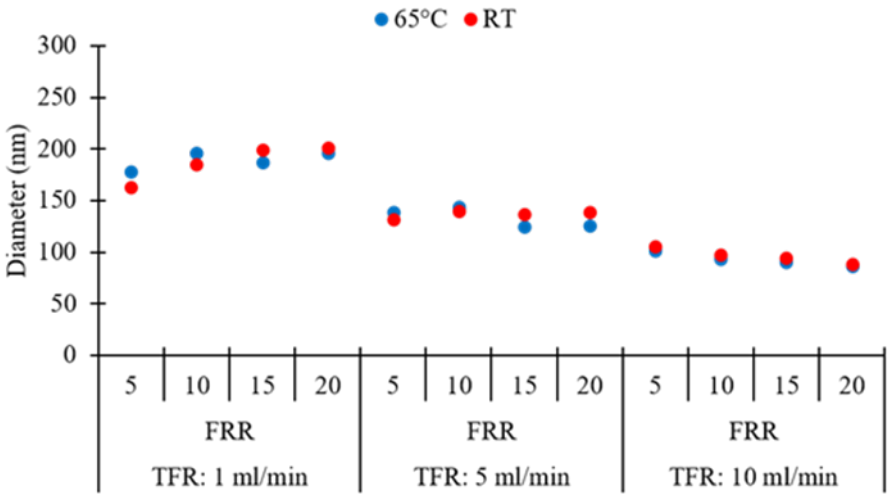

Figure 25 Effect of temperature on Z-average of different liposome batches, obtained at different values of total flow rate (TFR) and flow rate ratio (FRR). RT: Room temperature. Liposomal formulations (DPPC/Chol, 11.2:4.8 mM) were produced at TFR = 1 ml/min, 5 ml/min, 10 ml/min and FRR (aqueous phase/ethanolic lipid solution) = 5, 10, 15, 20. Data represent the mean of three measurements with corresponding standard deviation. Refer to **Table 3** (batch codes #27 DPPC to #38 DPPC, and #46 DPPC to #57 DPPC) for the corresponding experimental conditions, lipid composition, and numerical data of mean values and standard deviation.

It was found that increasing the temperature had an insignificant effect on both liposome size and dispersity ($p > 0.05$, between or within groups corresponding to 65 °C and RT). All liposome populations exhibited similar values of Z-average size (**Figure 25**) and dispersity (refer to **Table 3**), at the given TFR and FRR. A previous study found that the size of DPPC-based liposomes was larger when liposomes are prepared below the T_m of the lipid but became smaller when they formed at temperatures near the phase-transition temperature; however, the liposome size was found to be less dependent on temperature ($p > 0.05$) when liposome formation occurred above T_m [196]. These findings also demonstrate that the millifluidic reactor can sustain temperatures up to 65 °C, without evidence of performance deterioration.

2.3.9 Comparison between batch and millifluidic-based liposome production

Only a limited body of work has been previously conducted to systematically compare millifluidic reactors with batch production methods. In this study, we compared the performance of the millifluidic reactor with a conventional batch ethanol-injection method, under comparable physico-chemical conditions. Batch production was carried out by first dissolving lipids in ethanol and then rapidly injecting the ethanolic lipid solution in the aqueous phase [33]. Please refer to **Table 3** (batch codes #1 PC to #4 PC, and #58 PC to #61 PC) for the corresponding experimental conditions and lipid composition.

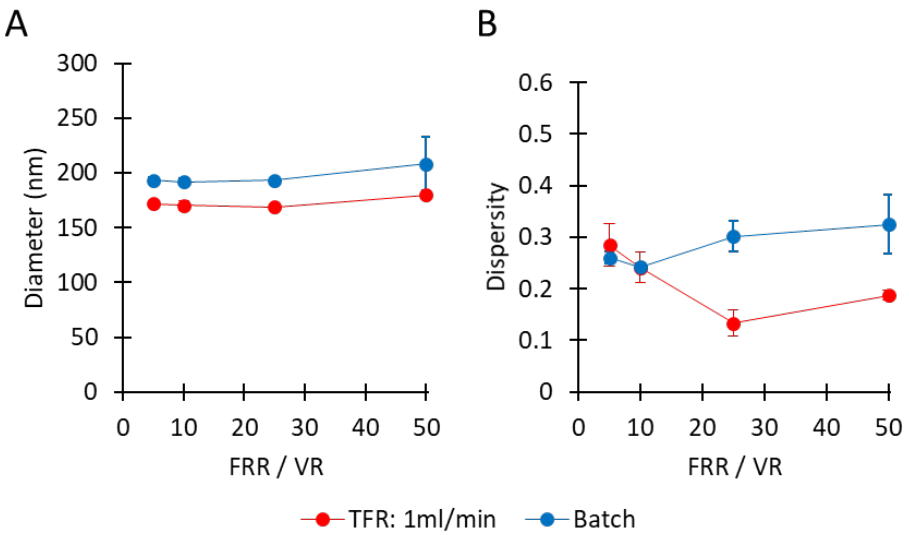

Figure 26 Comparison of production techniques in terms of liposome size (A) and dispersity (B). Methods of production included millifluidic-based (red) and batch ethanol injection (blue) methods. Liposomal formulations labelled in red comprised of PC (100 mM) and were produced using the millifluidic reactor, at total flow rate (TFR) = 1 mL/min and flow rate ratio (FRR, aqueous phase/ethanolic lipid solution) = 5, 10, 25, 50. Liposomal formulations labelled in blue comprised of PC (100 mM) and were produced using batch ethanol injection method at volume ratio (VR, aqueous phase/ethanolic lipid solution) = 5, 10, 25, 50. Data represent the mean of three measurements with corresponding standard deviation. Refer to **Table 3** (batch codes #1 PC to #4 PC, and #58 PC to #61 PC) for the corresponding experimental conditions, lipid composition, and numerical data of mean values and standard deviation. FRR: flow rate ratio, VR: volume ratio, TFR: total flow rate.

Figure 26A compares the size of liposomes produced by millifluidic and batch methods. In both cases, the increase of FRR/VR caused only a very marginal change in liposome size (from 171 nm to 179 nm in millifluidics, and from 193 nm to 208 nm in batch production). Notably, liposomes produced by millifluidics were smaller than those produced by batch method, while a similar

dependence of liposome diameter on FRR/VR was observed for both methods. An analogous finding was previously reported in a study comparing ethanol injection with a microfluidic hydrodynamic focusing (MHF) microscale reactor [33]. Overall, the millireactor produced slightly smaller liposomes with a narrower size distribution (**Figure 26B**) when compared to the batch production method, which could be attributed to the greater controllability of the mixing process in the millifluidic environment.

2.4 Conclusions

The use of microfluidic technology for the production of nanoscale vesicular systems, such as liposomes, has not been fully translated to an industrial scale yet. This may be due to limitations of microfluidic-based reactors, such as low production rates, limited lifetime, and high manufacturing costs. However, millimetre-scale flow reactors (also known as millifluidic reactors or millireactors) have the potential to achieve higher production rates and are highly suitable for scalable and low-cost manufacturing. In this study, continuous-flow production of liposomes was demonstrated using a serpentine-shaped millifluidic reactor which could achieve production rates of up to 16.7 mg/min. The ability of the millireactor to achieve tunable production of liposomes by varying key operational parameters was demonstrated. It was found that the lipid type, along with its concentration, had a significant effect on the resultant liposome populations. Notably, the millireactor was able to produce DPPC/Chol liposomes with a diameter (Z-average) of approximately 100 nm and dispersity ~0.1, when operated at a TFR of 10 mL/min with a lipid concentration of 16 mM. Also, the dimension of liposomes upon storage remained largely unchanged over time. Production of liposomes at different PC concentrations, ranging from 5 mM to 200 mM, was also demonstrated. Moreover, the reactor has proven to be suitable for the production of liposomes with a size (~100 nm; dispersity < 0.2) that is compatible with medicinal liposomal formulations, and this was demonstrated for a spectrum of different formulations that included cholesterol, charged moieties, and PEG-40. Finally, when compared to a more conventional batch method, millifluidics-based production generated liposomes with a more therapeutically relevant size and size dispersity, demonstrating its potential for mass production of liposomes in pharmaceutical applications. Future studies may investigate millifluidic-based drug loading efficiency upon different flow conditions, as well as further scaling-up of liposome production. The latter could be potentially achieved through parallelisation of multiple millireactors, development of hydraulic supply units of greater capacity, or the evaluation of millifluidic devices comprising even larger architectures.

Chapter 3 Encapsulation of Silver Nanoparticles in Liposomes

3.1 Introduction

Silver nanoparticles (AgNPs) are of significant interest in various fields of science because of their antimicrobial, optical and thermal behaviour [197]. These characteristics of AgNPs have paved the way for their usage in various fields, including electrochemistry, catalysis, food and pharmaceutical industries, and nanomedicine [15]. Moreover, AgNPs have been utilized as coatings in consumer products such as textiles, keyboards, food packaging [198], clothing [199], and medical products due to their antibacterial properties. In the field of medicine, AgNPs are used as imaging probes, plasmonic antennas and nanoprobes due to their ability to kill or damage cancer cells [16-18]. Additionally, AgNPs can be used in light-controlled drug delivery systems, and also be employed for real-time tracking and detection of cancerous tissues [99].

AgNPs can be synthesized in different shapes, including spherical, rod-like, triangular, or hexagonal [200], which can be tuned according to the method of synthesis. The differences in size and shape of the nanoparticles (NPs) dramatically influence the antimicrobial and optical effects of the nanoparticles [201]. It was demonstrated that AgNPs could cause greater toxicity in retinal endothelial cells when the particle size is reduced [202]. In another study, it was demonstrated that silver wires had a strong effect on alveolar epithelial cells in terms of cell viability and cytotoxicity although silver nanospheres (SNSs) had no effect [203].

Notably, the surface plasmon resonance wavelength of AgNPs is tuneable across visible and near infra-red (NIR) light, depending on the particle's size and shape. In addition to their ability to induce antibacterial effects, silver nanoprisms (SNPs) in particular have attracted significant attention due to their remarkable optical features, due to their SPR behaviour depending on sharp tip morphology that leads to higher absorption and scattering intensity (i.e. comparing to silver nanospheres (SNS)) [19, 20, 106]. Because of these properties, SNPs have been employed in a broad range of fields, including solar cells, catalysis and biomedical applications [204-207]. Given their unique optical behaviour, SNPs are also a potential tool for non-invasive tracking and imaging in cancer therapy.

Overall, the aforementioned properties of SNPs make them a potential tool for theranostic applications. However, as for conventional anticancer compounds, bio-distribution of AgNPs at high concentration may result in systemic toxicity arising from non-targeted delivery [208]. Therefore, encapsulation of AgNPs within a carrier could potentially reduce their systemic toxicity upon

administration. In efforts to achieve localised delivery of AgNPs while minimizing systemic toxicity, previous studies have reported that the delivery of AgNPs to target cells using liposomes showed greater toxicity compared to delivery of unencapsulated AgNPs [209, 210]. However, no previous study has investigated the synthesis and physico-chemical characterisation of SNPs encapsulated into liposomes, which could be employed as an anticancer agent or as a tracking system in bio-detection.

Liposomes are vesicular systems composed of natural or synthetic lipids (mainly phosphatidylcholines). They consist of a lipid bilayer shell encapsulating an aqueous compartment, and have shown characteristics of biocompatibility, biodegradability, increased biologic half-life, as well as the ability to be loaded with both hydrophilic and hydrophobic molecules [62-64]. Liposomal formulations can deliver a given bioactive agent to a specific site within the body while minimizing its negative side effects since the agent is confined within the liposome and healthy tissues are thus not directly exposed to it [67, 211, 212]. All of these features make liposomes an attractive vehicle for the transport and delivery of anticancer compounds.

Considering the potential pharmaceutical applications in localised delivery of SNPs, this study aimed to demonstrate and evaluate the encapsulation of SNPs into liposomes, which was performed using the continuous-flow millireactor (described in section **2.2.2** and **2.3.1**). Following the synthesis of liposomal dispersions, the efficiency of different methods including centrifugation, gel filtration and agglomeration on the removal of unencapsulated SNPs were evaluated by using size distribution plots obtained using DLS. Also, the SNS encapsulation in liposomes, which was previously demonstrated in the literature [209], was similarly evaluated using size distribution plots in a similar approach, to investigate the effectiveness of the characterization method, as a comparison.

3.2 Materials and Methods

3.2.1 Materials

Ethanol (99.9%), cholesterol (Chol, Sigma Grade 99%) from sheep's wool, dipalmitoylphosphatidylcholine (DPPC, >99%), octadecylamine (ODA, 99%, stearylamine), polyoxyethylene (40) stearate (PEG-40), HEPES (≥99.5%) and sodium hydroxide pellets were obtained from Sigma Aldrich (Gillingham, UK). PHOSPHOLIPON®90G (purified phosphatidylcholine, or PC, from soybean lecithin) was kindly provided as a gift by Phospholipid GmbH (Lipoid, Ludwigshafen, Germany). Silver nitrate (AgNO3 99%), tri-sodium citrate dihydrate (TSCD), polyvinylpirrolidone (PVP, average molecular weight $AM_w \approx 29{,}000\ gmol^{-1}$), hydrogen peroxide

(H_2O_2, 30% by weight (wt-%)), and sodium borohydride (NaBH4, 99%), were obtained from Sigma Aldrich (Gillingham, UK) and used as purchased. All water employed was Milli-Q.

For millifluidic-based production of liposomes encapsulating SNPs, syringe pumps (AL-1010) were purchased from World Precision Instruments (Hertfordshire, UK), and 20 mL BD-Plastipak syringes with luer lock connectors were obtained from Fisher Scientific (Loughborough, UK). Male luer lock rings, polytetrafluoroethylene (PTFE) tubing, and a hot plate stirrer (UC152D) were supplied by Cole-Parmer (St. Neots, UK). The tubing that was employed to connect the outlet port of the millireactor to the collection vial was 21.5 cm long (inner diameter: 0.5 mm; outer diameter: 1.6 mm) and was purchased from Cole-Parmer (St. Neots, UK).

3.2.2 Synthesis of liposomes

All lipids (PC, DPPC, Chol, ODA, and PEG-40) were first dissolved in ethanol. In continuous-flow liposome production by solvent exchange mechanism, the ethanolic lipid solution and aqueous phase (water or HEPES (20 mM, pH 7.4)) were injected separately into the two inlets of the millireactor, which was fabricated using a previously reported protocol combining micromilling with replica moulding (referred to as µMi-REM) [28, 34, 135]. A schematic of the experimental set-up for the production of liposomes using the millireactor is illustrated in **Figure 27A.**

For millifluidic-based production, experiments were conducted at different flow dynamic conditions, corresponding to variations in both flow rate ratio (FRR) and total flow rate (TFR). Herein, the FRR is defined as the ratio between the inlet volumetric flow rates of water and the ethanolic lipid solution, and TFR as the total volumetric flow rate (i.e., the sum of ethanol and water flow rates). Synthesis of liposomes was also carried out using an ethanol injection technique (**Figure 27C**) [159]. Detailed information of the millireactor fabrication process and liposome synthesis (using either millifluidic or batch methods) is also reported in sections **2.2.2** and **2.2.3,** respectively**.**

3.2.3 Synthesis of AgNPs

For the synthesis of SNPs, 24 mL of solution containing TSCD (0.1 M, 0.375 mL), silver nitrate ($AgNO_3$, 0.05 M, 0.05 mL), PVP (0.7 mM, 0.375 mL) and hydrogen peroxide (H_2O_2, 30 wt.%, 0.125 mL) was stirred vigorously at room temperature. After 7 minutes, a freshly prepared solution of sodium borohydride (NaBH4, 25.00 mM, 1.00 mL) was rapidly injected. After about 30 minutes, the solution colour changed from yellow to orange-brown, then to green-blue through to blue after a further 5 - 10 minutes. The stirring was subsequently stopped and the resultant SNP dispersion was stored at +4 °C. For the synthesis of SNSs, 24.75 mL of solution containing TSCD (0.1 M, 1.5 mL), silver nitrate (AgNO3, 0.05 M, 0.2 mL) and PVP (0.7 mM, 1.5 mL), was stirred vigorously at room

temperature. After 7 minutes of stirring, a freshly prepared solution of sodium borohydride ($NaBH_4$, 25 mM, 0.25 mL) was rapidly injected. After about 10 - 15 minutes the solution's colour changed from light yellow to yellow-orange. The stirring was then stopped, and the resultant SNS dispersion was stored at +4 °C. The synthesis of AgNPs was performed by Dr Domenico Andrea Cristaldi and Dr Harriet Kimpton.

3.2.4 Synthesis of liposome-AgNP dispersions

Synthesis of liposomal dispersions encapsulating SNPs was performed following a similar protocol to the one used for liposome production. Briefly, the ethanolic lipid dispersion and the SNP dispersion were injected separately into the two inlets of the millireactor, and the resultant dispersion was collected from the outlet of the millireactor.

The synthesis of liposomal dispersions encapsulating SNSs using an ethanol injection technique [159] was performed by manually injecting the ethanolic lipid solution into the SNS dispersion, within a vial (4 mL) under magnetic stirring (see **Figure 27C**). The dispersion was stirred for 4 minutes.

The operational parameters (flow conditions, lipid composition and separation method) for each liposomal dispersion are reported in **Table 5**. Dispersions including liposomes containing SNSs or SNPs were labelled as Lipo/SNSs and Lipo/SNPs, respectively. A schematic of the experimental set-up for the production of liposomes encapsulating AgNPs (referred to as Lipo/AgNPs) using the millireactor is illustrated in **Figure 27A**.

Liposomal dispersions were produced either at room temperature (RT) or 65 °C by placing the millireactor on a hot plate stirrer. In the latter case, the ethanolic lipid solution and the aqueous or AgNP phase (in separate syringes) were kept in a beaker containing water at 65 °C, prior to injection in the millifluidic device. For the synthesis of Lipo/SNPs (**Table 5**, batch code #13 and #14), where the HEPES was used in aqueous phase instead of water), the SNP dispersions were diluted (1:1 v/v) using HEPES (40 mM, pH 7.4) before production. For the production of Lipo/SNP sample (**Table 5**, batch code #14)**,** where the positively charged lipids used for the synthesis, the SNPs was 1:1 v/v added to the dispersion after liposomes (20 mM, pH 7.4) had formed.

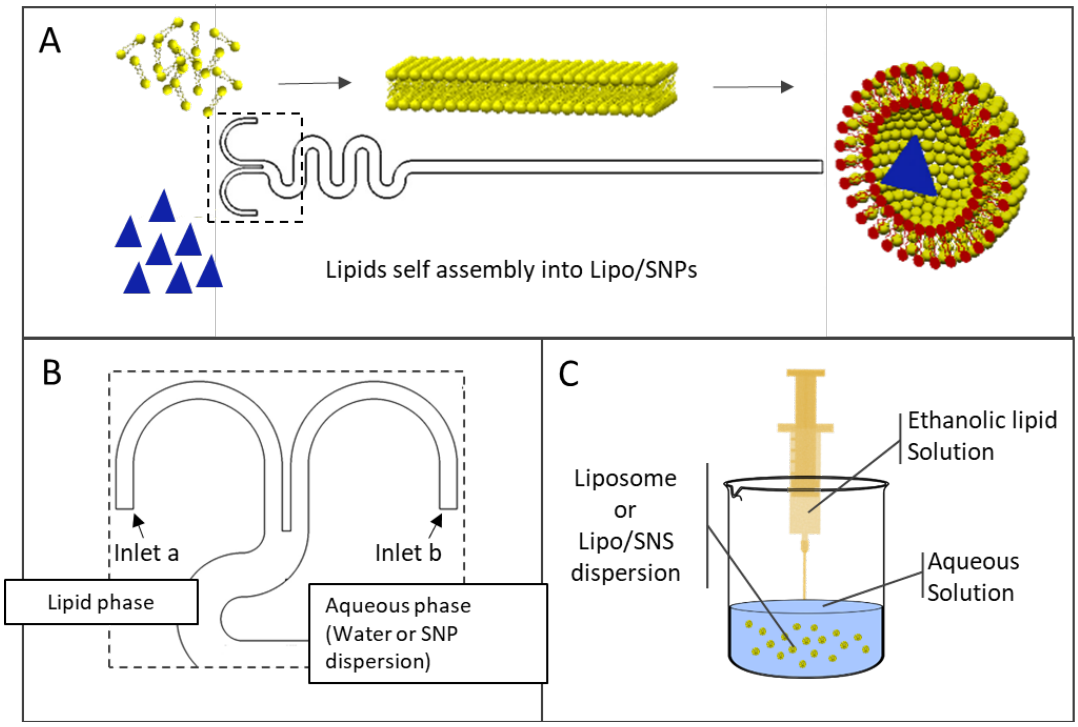

Figure 27 (A) Schematic illustration of the experimental approach for liposome or Lipo/SNP production using the millireactor, and (B) schematic of the device's inlet section with indication of the injected media. (C) Liposome or Lipo/SNS production using the ethanol injection method.

Table 5 **The operational parameters and chemical formulations of liposomal dispersions.**

Batch code[1]	Sample	Flow conditions	Lipid composition (mM)[2]					Separation Method
		TFR:FRR	PC	DPPC	Chol	ODA	PEG-40	
#1	Liposome	1:10	11.2	-	4.8	-	-	-
#2		1:10	-	12.8	-	1.6	1.6	
#3	Liposome or Lipo/SNS	1:10[3]	16	-	4	-	-	Centrifugation (30000G)
#4	Liposome or Lipo/SNP	1:10	20	-	-	-	-	Centrifugation (10000G - 50000G)
#5		1:10	40	-	-	-	-	
#6		1:10	60	-	-	-	-	
#7[5]		1:10	-	7	3	-	-	Gel Filtration
#8		1:10	50	-	-	-	-	Agglomeration
#9		5:10	28	-	12	-	-	-
#10		1:25	100	-	-	-	-	
#11[4]		1:10	16	-	-	-	-	
#12[4,6]		1:3	-	14.4	-	1.6	0.01	

The experimental conditions for liposomal dispersions are reported together with the corresponding fluidic parameters, chemical formulation, and the separation method performed. Flow rate ratio (FRR) is defined as the ratio between the inlet volumetric flow rates of the aqueous phase and the ethanolic lipid solution, and TFR as the total volumetric flow rate (i.e. the sum of the flow rates of ethanol and aqueous phases).[1] The batch code given represents the number of the produced liposome sample or Lipo/AgNP (SNS or SNP) sample along with its fluidic parameters, chemical formulation, and the separation method. [2] Given parameters represent the amount of the phospholipid (phosphatidylcholine soybean (P90G) or dipalmitoylphosphatidylcholine (DPPC)), stabilizer (cholesterol (Chol) and/or octadecylamine (ODA)), or polyoxyethylene (40) stearate (PEG-40) in the liposome or Lipo/AgNP sample, reported in millimolar (mM) concentration. [3]The liposome or Lipo/SNS sample was produced using the ethanol injection technique, and given parameters (1:10) corresponds to the volume ratio (VR) of ethanolic lipid solution to water (or SNS dispersion), respectively. [4] Synthesis of the samples was performed using HEPES (20 mM, pH 7.4) as the aqueous phase instead of water. [5]The parameters for this batch code were also employed for the production of Lipo/SNSs or Lipo/SNPs for the calculation of EE%, using the

centrifugation technique as a separation method. The centrifugation forces used were 30000G and 50000G for Lipo/SNS and Lipo/SNP samples, respectively. [6] The sample was synthesized at 65 °C.

3.2.5 Separation of unencapsulated AgNPs and quantification of EE%

3.2.5.1 Centrifugation and gel filtration

Separation of unencapsulated AgNPs (SNPs or SNSs) using centrifugation was performed at 10000G and 50000G for Lipo/SNPs, and 30000G for Lipo/SNSs. Liposome-AgNP dispersions (Lipo/SNP or Lipo/SNS) were centrifuged at 4°C using an ultracentrifuge (OptimaTM MAX-XP Tabletop ultracentrifuge, TLA-55), within 1.5 mL micro centrifuge polypropylene tubes (from Beckman Coulter, Luton, UK), and the supernatant was subsequently harvested.

The encapsulation efficiency (EE%) was calculated using the equation (Eq. 1) given below [209]. The concentration of AgNPs (SNSs or SNPs) in the dispersions was calculated using the absorbance-concentration curves (see paragraph **3.3.2**). Absorbance of the supernatant and the pellet were quantified using a UV-Vis spectrometer (UV-Vis) in a FLUOstar Omega plate reader from BMG LABTECH (Aylesbury, UK).

$$EE\% = \frac{\text{Total amount of AgNP} - \text{Amount of AgNP in the supernatant}}{\text{Total amount of AgNP}}\ x\ 100 \qquad \textbf{(Eq. 1)}$$

Separation of unencapsulated SNPs using gel filtration was performed as follows. 1 gram of Sephadex G-50 (Sigma Aldrich, Gillingham, UK) was mixed with 10 mL of water. After swelling, the gel was carefully put in a 20 mL syringe, which was used as the column. 1 mL of the sample (liposome or Lipo/SNP) was diluted up to 5 mL, and added to the column. The samples eluted out from the column were collected as fractions of 1 mL.

3.2.5.2 Agglomeration of SNPs

The separation of unencapsulated SNPs by the agglomeration approach was performed using SNPs that were not coated by PVP. Briefly, 24 mL of solution containing tri-sodium citrate dihydrate (TSCD) (100 mM, 0.025 mL), silver nitrate ($AgNO_3$, 50 mM, 0.05 mL), and hydrogen peroxide (H_2O_2, 30 wt.%, 0.125 mL) was stirred vigorously at room temperature. After 7 minutes, a freshly prepared solution of sodium borohydride ($NaBH_4$, 25 mM, 1.00 mL) was rapidly injected. The solution went pale yellow in colour. After a further 5-10 minutes, the solution changed rapidly through orange to light blue. The stirring was then stopped and the resultant SNP dispersion was used to synthesize Lipo/SNPs in continuous-flow production as described in paragraph **3.2.4.** The synthesis of AgNPs was performed by Dr Harriet Kimpton.

Here, it was hypothesized that SNPs synthesized without PVP would agglomerate over time and sediment at the bottom of the vial as the mass of the aggregate increased. The empty liposomes and liposomes encapsulating SNPs would instead remain suspended, which would enable separation and removal of unencapsulated SNPs.

3.2.6 Characterization of liposomal dispersions

3.2.6.1 Size distribution and zeta potential measurements

The size distribution and zeta potential of the liposomal dispersions were characterised by dynamic Light Scattering (DLS) technique, using a Zetasizer Nano ZS (Malvern Instruments Ltd., Malvern, UK). The measurements were performed at 25 °C, using polystyrene semi-micro (Fisherbrand™ FB55147, Fisher Scientific, Loughborough, UK) cuvettes and folded capillary cell (DTS1070, Malvern Instruments Ltd., Malvern, UK) type cuvettes, respectively. Samples used for size measurements had a volume of 1 mL (without dilution). Viscosity values used for DLS measurements were calculated using the Zetasizer Software 7.12, by considering the effects of different FRRs or VRs on the fluid's viscosity (see paragraph **2.2.4.1**) [167].

Evaluations of the liposomal size distribution were carried out by considering the intensity-based distributions, as recommended in the ISO 13321 and ISO 22412 [168, 195]. However, number or volume-based distributions were given as additional plots when needed, to provide further details of the dimensional properties of the dispersions.

The rationale for mainly using intensity-based distributions for evaluating the dimensional properties of liposomal dispersions are summarised below. Firstly, the refractive index (RI) of the material is not taken into consideration in the calculation of intensity-based distributions, while it is used to determine volume and number-based distributions. This is important for dispersions including more than one type of nanomaterial (i.e., for Lipo/AgNP samples), as the conversion of intensity-based distributions to number or volume-based distributions may lead to inaccurate results. In this study, the lipid RI value was chosen as the overall RI of Lipo/AgNP dispersions due to difficulties in the estimation of the actual RI for the mixture. Secondly, the conversion from intensity to volume or number-based distribution assumes that the dispersion is homogenous and all of the nanoparticles are spherical. In this study, it was assumed that the Lipo/SNPs do not have a fully spherical structure due to anisotropic shape of SNPs or SNP attached liposomes, and that the dispersion was not homogeneous due to possible aggregation. Based on the aforementioned reasons, the use of intensity-based distributions rather than number and volume-based distributions was found more reliable [213].

It is also important to note that the data used in the size distribution plots were obtained by selecting the "*the multiple narrow modes (high resolution)*" option in the Zetasizer software. This mode is recommended for samples that can contain discrete populations [168, 195]. Notably, selection of this option resulted in multiple peaks in the size distribution plots, indicating the presence of multiple populations in the sample, while the "*general purpose (normal resolution)*" mode showed only one peak in the size distribution plots for most samples.

3.2.6.2 TEM analyses

Liposomal dispersions were imaged using the transmission electron microscopy (TEM) technique; 5 µL of the sample was placed on a carbon-coated grid and allowed to adsorb for 30 s, and any excess amount was removed with a filter paper (Whatman). Liposomal dispersions with or without AgNPs were negatively stained by adding 5 µL of 5% ammonium molybdate containing 1% trehalose on the grid (for 30 s), and the excess amount was again removed using a filter paper. TEM images were captured using the Tecnai T12 (FEI, Hillsboro, OR, USA). The characterization of SNS and SNP samples using TEM was performed following the same protocol, but without the negative staining step. The EE% of SNPs in liposomes was also calculated from TEM images by manually based counting method using the equation reported below.

$$EE\% = \frac{\text{Total amount of SNPs in the image} - \text{free (unencapsulated) SNPs in the image}}{\text{Total amount of SNPs in the image}}\ x\ 100 \qquad \textbf{(Eq. 2)}$$

3.2.6.3 TEM analyses of resin embedded Lipo/SNP

The Lipo/SNP samples were also characterized with an additional TEM-based process, in order to gain additional evidence and information of SNPs encapsulation. This process involved the embedding of Lipo/SNP dispersions into a resin, which was subsequently cut into thin sections. TEM images of the same section were taken at different angles in order to obtain a 3D image, so that the location of nanoparticles could be characterized more effectively.

Briefly, 1 mL of Lipo/SNP dispersion was mixed with the fixative glutaraldehyde (2.5% concentration) and incubated for 1 hour. Subsequently, the sample was embedded in alginate for 20 minutes and rinsed twice with water for 10 minutes. Then, the sample was mixed with osmium tetroxide (1% concentration) as a post-fixative, and incubated for 1 hour. The sample was rinsed again, and uranyl acetate (2.5% concentration) was added. After 20 minutes, the sample was rinsed five times with ethanol for 10 minutes, at increasing ethanol concentration (30 - 50 - 70 - 95 - 100%) each time. Then, a 50:50 acetonitrile:resin mixture was added to the sample and incubated overnight. Finally, the sample was embedded in fresh resin and polymerized at 60°C for 24 hours.

The obtained embedded sample of liposomes was cut using an ultra-microtome to obtain very thin slices with a thickness of approximately 800-900 Å. Slices were then placed on a carbon-coated grid and imaged using a TEM machine.

TEM analyses and sample preparations were performed at the Biomedical Imaging Unit in Southampton General Hospital, with the assistance of technical staff.

3.3 Results and Discussion

3.3.1 Methodological rationale

A range of experiments was designed for the evaluation of AgNP encapsulation in liposomes. Experiments were carried out first by applying different separation techniques (e.g., centrifugation, gel filtration, and agglomeration) to perform and assess separation of unencapsulated SNPs because the SNP loaded liposomes are of interest as the unencapsulated SNPs might provide undesirable toxicity. Secondly, the liposomal dispersions were characterized by using TEM and DLS (without separation) to quantify EE%. The Lipo/SNP samples used throughout the study were synthesized using continuous-flow production. Different separation technics were performed, first to obtain a dispersion including only liposomes encapsulating SNPs as a platform that can be potentially employed in pharmaceutical applications, and secondly to calculate EE% if possible.

Also, SNS encapsulation in liposomes was performed using the ethanol injection method, and encapsulation was evaluated using TEM and DLS. The aim here was to determine the efficiency of the characterization method by examining the encapsulation performance of two different nanoparticles in the same way.

The Lipo/SNS samples (20 mM) that were synthesized using ethanol injection, were evaluated in terms of separation after centrifugation (30000g) using size distribution plots. A similar approach was followed for Lipo/SNP samples that were synthesized by continuous-flow production. The characterization of Lipo/SNP samples was performed at three different lipid concentrations (20, 40, 60 mM) and two different centrifugal forces (10000g and 50000g). Different centrifugal forces and lipid concentrations were tested to observe any effect on separation efficiency and EE%, respectively.

The separation of SNPs was evaluated using a gel filtration process. The resultant samples were characterized using DLS, UV-Vis or TEM. An agglomeration technique was also employed as a third method of separation. Synthesized SNPs and Lipo/SNPs were characterized just after production,

and 4 weeks after production for the evaluation of separation, which was made by comparing the initial and final results based on DLS or UV-Vis.

In the second set of experiments, the evaluation of encapsulation was performed for Lipo/SNP samples (without carrying out any separation process); the samples were characterised directly after production using TEM and DLS techniques. Here, two types of lipids were employed to examine the effect of negative and positive charge, on the interaction between liposomes and SNPs.

3.3.2 Absorption spectra of AgNP dispersions

The absorption spectra of stock SNSs (100 µL) and stock SNPs (100 µL) mixed with 100 µL distilled water separately are shown in **Figure 28**. In addition, the absorption spectra of AgNP (SNS or SNP) and distilled water mixtures with a total volume of 200 µL at varying AgNP ratios are shown in **Figure 29**.

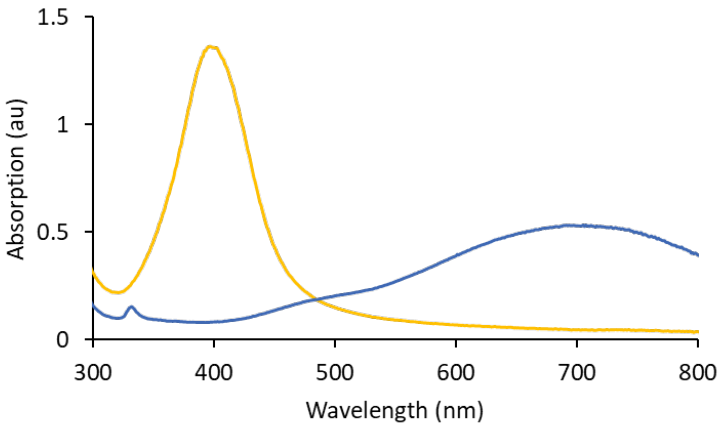

Figure 28 Absorbance spectra of stock SNS (yellow) and stock SNP (blue) dispersions.

The UV-Vis characterization of SNS and SNP stock dispersions showed peak values at around 400 nm and 700 nm, respectively, which confirms the shape-dependent optical behaviour of AgNPs and is consistent with the literature [214]. Dispersions were also measured at different concentrations, in order to generate the standard curves shown in **Figure 29**.

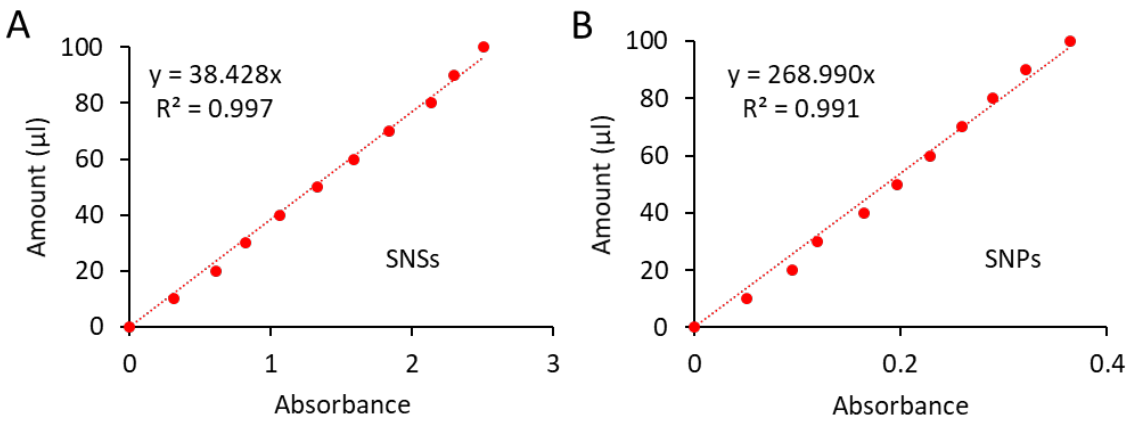

Figure 29 Standard curves for (A) SNSs and (B) SNPs. The concentration values of AgNPs was determined by mixing a certain amount of AgNP and water, up to a total volume of 200 µL.

Figure 29A and **Figure 29B** show the standard curves at different amounts of SNS and SNP samples respectively. The calculation was performed by measuring the absorbance of the SNP dispersions by dilution. The linear interpolating function was subsequently used to calculate unknown amounts of AgNP in experimental samples, which enabled the calculation of the EE%.

3.3.3 Dimensional properties of Liposomes and AgNPs

In this paragraph, the main properties of liposomes and AgNPs are discussed based on the size distribution plots and images obtained from DLS and TEM, respectively. The size distribution plots of selected liposome formulations and AgNPs are in shown in **Figure 30**. For the experimental conditions and production parameters of liposomes, refer to **Table 5** (batch codes #1 and #2).

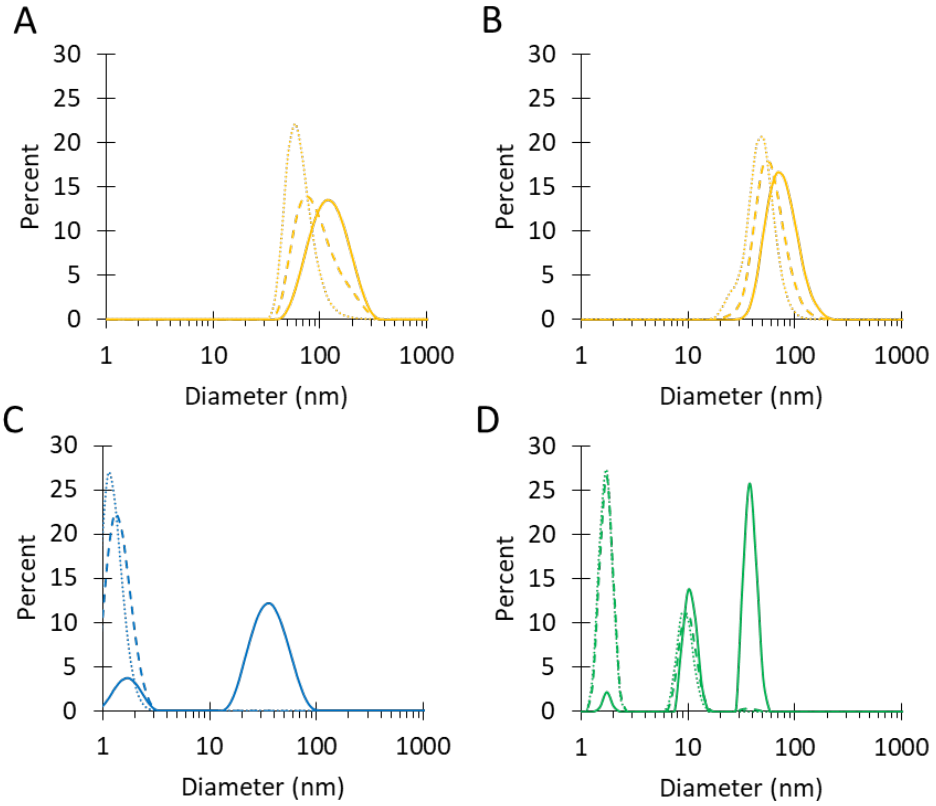

Figure 30 Representative size distribution plots of selected samples of (A) negatively and (B) positively charged liposomes (batch code #1 and #2 respectively, in **Table 5**), (C) SNPs and (D) SNSs. Liposomes comprised of PC/Chol (11.2:4.8 mM) and DPPC/ODA/PEG-40 (12.8:1.6:1.6 mM) and were produced using the millifluidic reactor, at total flow rate (TFR) = 1 ml/min and flow rate ratio (FRR, aqueous phase/ethanolic lipid solution) = 10. The solid, dashed, and dotted lines represent the size distributions for intensity, volume and number-based DLS analyses.

Figure 30A, **B**, **C** & **D** show the size distributions plots of negatively and positively charged liposomes along with SNSs and SNPs, respectively. The plots were obtained via DLS and are given as intensity, volume or number-based distributions. The interpretation of the size distributions was primarily made by considering the intensity-based distributions (see paragraph **3.2.6)**. For all populations, the number and intensity-based distributions showed the lowest and highest peak values, respectively, which is consistent with the literature [168, 213]. Based on the intensity-based distributions, the peak of anionic liposomes was at approximately 120 nm (**Figure 30A**), while it was lower than 100 nm for cationic liposomes (**Figure 30B**). The difference in size between positively and negatively charged liposomes was consistent with the data provided in the previous Chapter (please see paragraph **2.3.7**). However, the intensity, volume, and number-based plots showed similar distributions, and there were only small differences in size distribution plots for liposome sample. This showed that the dispersions were almost homogeneous and there were no

aggregates, which also indicated that the overall size dispersity of liposomes was acceptable (0.146 ± 0.022 and 0.190 ± 0.016 for negatively and positively charged liposomes, respectively).

However, the size distribution plots of AgNPs changed significantly when converting intensity-based to volume or number-based distributions. The peak values of intensity-based distributions of SNPs were around 2 and 35 nm (**Figure 30C**), while they were 2, 10 and 40 nm for SNSs (**Figure 30D)**. The number and volume-based distributions showed peaks at approximately 1 nm for SNPs and 2 - 10 nm for SNSs. This can be explained by possible aggregation of AgNPs and to the NP shape not being completely spherical. Here, it was expected for SNPs and SNSs to have average sizes between 15 - 50 nm and 1 - 15 nm, respectively. However, the size distributions showed different values than those expected, especially the volume and number-based distributions. The reason for the presence of a peak at ~1 nm in the volume and number-based distributions (for SNPs) was possibly related to the amount of small AgNPs, which could be greater than the amount of SNPs. As a result, the peak at ~35 nm (corresponding to SNPs) for intensity-based distribution could not be detected in both the number and volume-based distributions.

Similar behaviour was observed for SNSs. The peak at ~40 nm in the intensity-based distribution was not present in the volume and number-based distributions. This peak could be associated with the presence of SNS clusters. A second peak observed at ~10 nm potentially corresponded to the presence of SNSs in the dispersion.

It is important to note that the reported size values of nanoparticles obtained from DLS were slightly different than the actual size of nanoparticles since the DLS calculation method was based on the hydrodynamic radius of the nanoparticles [168]. Also, it was observed during measurements that AgNPs presented slightly different peaks over multiple runs (measurements included 11 runs for a single measurement); this could be related to possible NP aggregation, which could cause an overestimate of the NP size.

Another reason for the NP size to decreased when converting from intensity to volume or number-based distribution was related to the calculation method. The intensity, volume and number-based distributions were calculated by taking the 6^{th}, 3^{rd} and 1^{st} power of the particle radius respectively, and this results in the increase of the contribution of agglomerates to the size distribution [168, 213].

The liposomes, SNPs and SNSs were also characterized using TEM, and representative images are reported in **Figure 31**.

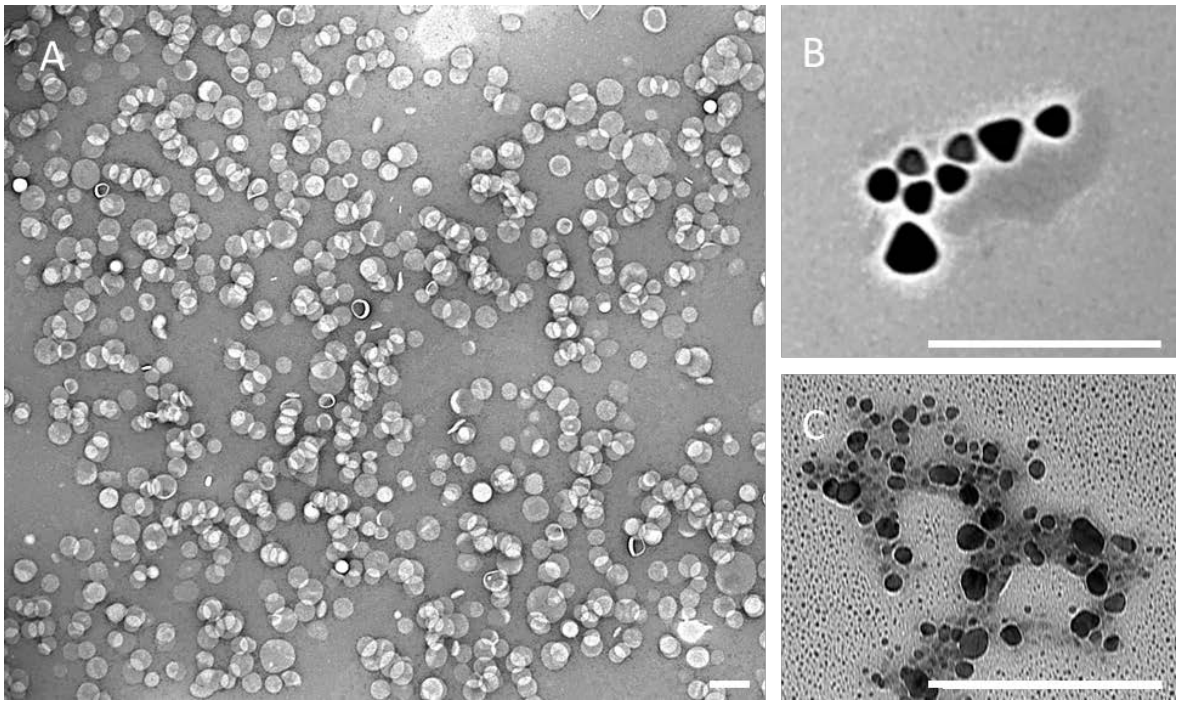

Figure 31 TEM images of selected representative samples of (A) liposomes (for experimental conditions refer to batch code #1 in **Table 5**), (B) SNPs and (C) SNSs. Liposomes comprised of PC/Chol (11.2:4.8 mM) and were produced using the millifluidic reactor, at total flow rate (TFR) = 1 ml/min and flow rate ratio (FRR, aqueous phase/ethanolic lipid solution) = 10. Scale bars: 200 nm.

Figure 31A, B & C show the TEM images of negatively charged liposomes, SNPs and SNSs, respectively. Liposomes were observed as separately dispersed, with some limited level overlapping in some regions. Relatively more intense areas in the image are likely to contain more stain compared to other areas. The corresponding size of liposomes measured from TEM images is reported in **Figure 24**.

SNPs were observed to have a triangular shape, particularly at the greater NP sizes, while they presented rounded corners when the size decreased. The SNSs were relatively heterogeneous in size and presented a more spherical shape when the size decreased. Additionally, SNSs were observed to form clusters, supporting the findings from the size distribution measurements (see **Figure 30D** solid line).

3.3.4 Evaluation of encapsulation in Lipo/SNSs

The evaluation of SNS encapsulation in liposomes was performed by characterizing the pellet and supernatant along with SNS, liposome and Lipo/SNS samples. The centrifugation method was employed for the separation of unencapsulated SNSs from the Lipo/SNSs dispersion. Results were

given as size distributions based on intensity, volume or number in **Figure 32**. For the experimental conditions, refer to **Table 5** (batch code #3). Each sample was also analysed diluted to assess differences due to potential aggregations and to observe values more precisely.

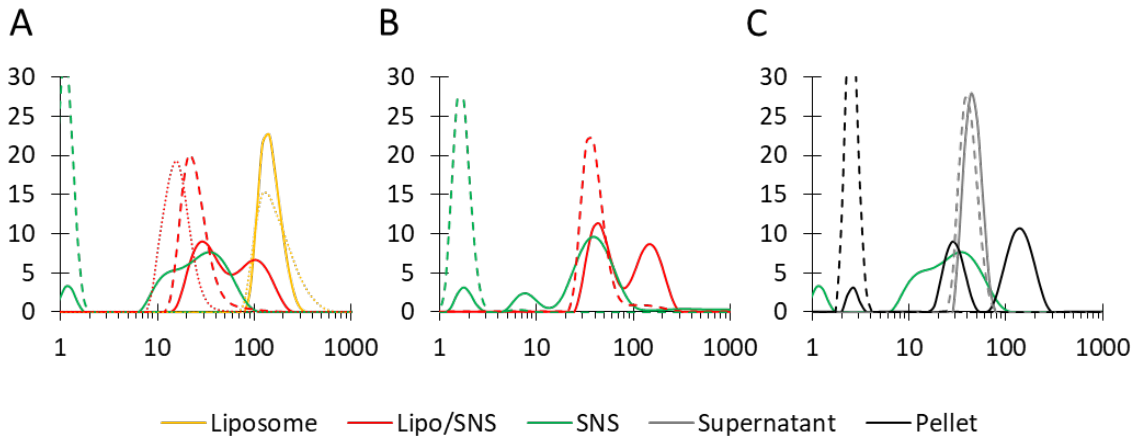

Figure 32 Size distribution plots of (A) liposome, SNS and Lipo/SNS, (B) 1:10 diluted SNS and Lipo/SNS, (C) pellet and supernatant after centrifugation. Y and X axes represent percentage of distributions and diameter (nm) respectively. The solid, dashed and dotted lines represent the size distributions for intensity, volume and number. Liposomal samples comprised of PC/Chol (16:4 mM) and were produced using ethanol injection technique, at volume ratio (VR, aqueous phase/ethanolic lipid solution) = 10. For the experimental conditions please refer to **Table 5** (batch code #3).

Evaluation of SNS encapsulation from the size distribution plots was made based on the differences in peak values. Considering the results in **Figure 32A**, liposomes showed a peak at ~120 nm, and SNSs showed a broad peak at ~40 nm, respectively. However, the Lipo/SNS showed two peaks at ~30 and ~100 nm. It was hypothesised that the higher peak corresponded to liposomes interacting with SNSs, and the lower peak to free SNSs. Based on the volume or number-based distribution of Lipo/SNS, it can be assumed that the amount of free SNSs is much greater than the SNSs interacting with liposomes. Considering that the liposome number-based distribution had a peak at a similar diameter as the intensity distribution (indicating absence of agglomerates), and that the amount of SNSs was relatively greater compared to liposomes (see volume or number-based distribution of Lipo/SNSs), it was hypothesised that the presence of two peaks in the intensity-based distribution of Lipo/SNS confirmed the interaction between liposomes and SNSs. **Figure 32B** shows the results of measurements on the diluted samples. Lipo/SNS dispersions presented two peaks at around 40 and 150 nm, which potentially corresponded to SNSs (or clusters of SNSs) and liposomes interacting with SNSs, respectively. The dilution of the samples caused the distribution peaks to be prominent for both samples. The amount of SNSs (corresponding to peaks at around 2 nm and 8 nm) could not be detected when the SNSs were mixed with liposomes, which also supported the hypothesis that SNSs were encapsulated into liposomes. **Figure 32C** shows the distribution plots for the pellet and

supernatant. The peak for the supernatant at ~55 nm possibly corresponded to the empty liposomes, suggesting that the centrifugation force was not high enough to pellet all the liposomes down (i.e., only larger liposomes may pellet down during centrifugation). However, the pellet showed peaks at around 20 nm and 150 nm, which possibly indicated free SNSs and Lipo/SNSs. Also, the smaller peak of the pellet (at ~3 nm) was thought to be the result of a leak of small AgNPs from liposomes that occurred during the dilution of the pellet.

Additionally, it must be noted that the size distribution plots obtained by selecting the "*general purpose (normal resolution)"* in the Zetasizer software (see part **3.2.6.1**), showed one main peak for Lipo/SNS samples at ~100 nm, supporting that the encapsulation of SNSs in liposomes was achieved. Similar approaches investigating encapsulation of SNSs into liposomes based on size distribution plots are also reported in the literature [209, 210]. It is important to note that, a peak value indicating SNPs in the size distribution plots can be observed, however, there was no indication of AgNPs observed in the reported plots in literature, which can be explained by the effect of the selected option when obtaining distribution plots from the software (see part **3.2.6.1**).

As mentioned earlier, it is important to note that the centrifugation force used was not sufficient to pellet all the liposomes down. It is considered that this centrifugation value was chosen relatively lower to prevent all SNS from pelleting and forming a solid cluster at the bottom of the bottle. Additionally, it can be concluded that sample dilution could help to obtain better results as the possibility of potential clusters would be lower, but also using lower concentrations of lipids and AgNPs may provide more reliable results since the sample would be more homogeneous. Overall, the separation using centrifugation was found to be useful in understanding any possible interactions between SNS and liposomes, but it would require additional tests to determine the most suitable centrifugation parameters along with the concentration of the lipids and SNSs.

The Lipo/SNS sample was also characterized using TEM before the centrifugation process. The images are shown in **Figure 33**.

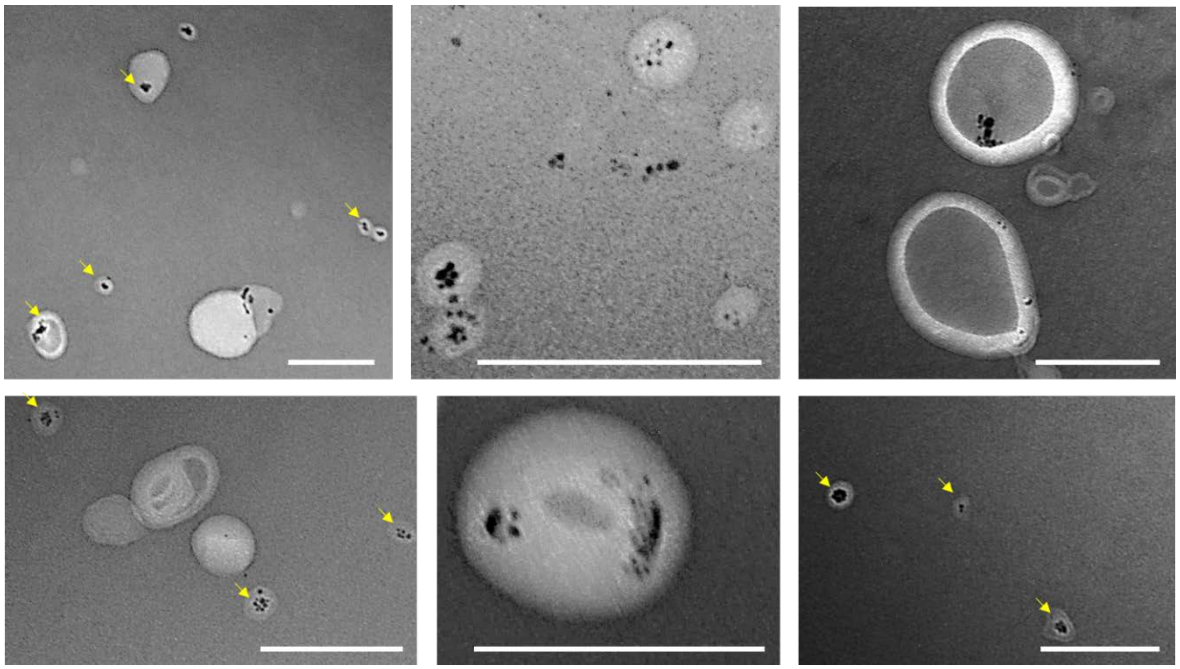

Figure 33 TEM images of Lipo/SNS samples. Scale bars: 200 nm. Liposomal samples comprised of PC/Chol (16:4 mM) and were produced using ethanol injection technique, at volume ratio (VR, aqueous phase/ethanolic lipid solution) = 10. For the experimental conditions, please refer to **Table 5** (batch code #3). The arrows point towards some of the encapsulated SNSs in liposomes.

Figure 33 shows different images of the same sample of Lipo/SNS. The SNSs (relatively darker and smaller structures) were observed as mostly associated with the surface or located inside the lipid bilayers of liposomes. Based on the location of SNSs in liposomes, it can be concluded that the lipophilic properties of the SNSs were more dominant. Overall, the images showed that the encapsulation of SNSs in liposomes was achieved to some extent. Based on the images, it was assumed that SNS encapsulation occurred in a relatively small proportion of liposomes.

Finally, the EE% of SNSs in liposomes was calculated using a liposomal dispersion synthesized with continuous-flow millireactor. For the experimental conditions please refer to **Table 5** (batch code #7). The EE% was found as 76.88 ± 28.69 %, by measuring the amount of SNSs in the supernatant. In accordance with the results obtained from size distribution plots and TEM, the encapsulation of SNSs was confirmed qualitatively and quantitatively in liposomal dispersions synthesized using ethanol injection method and continuous-flow millireactor, respectively.

3.3.5 Synthesis of Lipo/SNPs

3.3.5.1 Evaluation of separation using centrifugation

The evaluation of SNP encapsulation in liposomes was performed as reported in previous paragraphs (see paragraph **3.3.4**). Centrifugation was employed for the separation of

unencapsulated SNPs from the Lipo/SNP sample. Liposome, SNP and Lipo/SNP samples (i.e. both pellet and supernatant) were characterized using size distribution plots. For the experimental conditions refer to **Table 5** (batch code #4, #5 and #6). The size distributions of samples are shown in **Figure 34**.

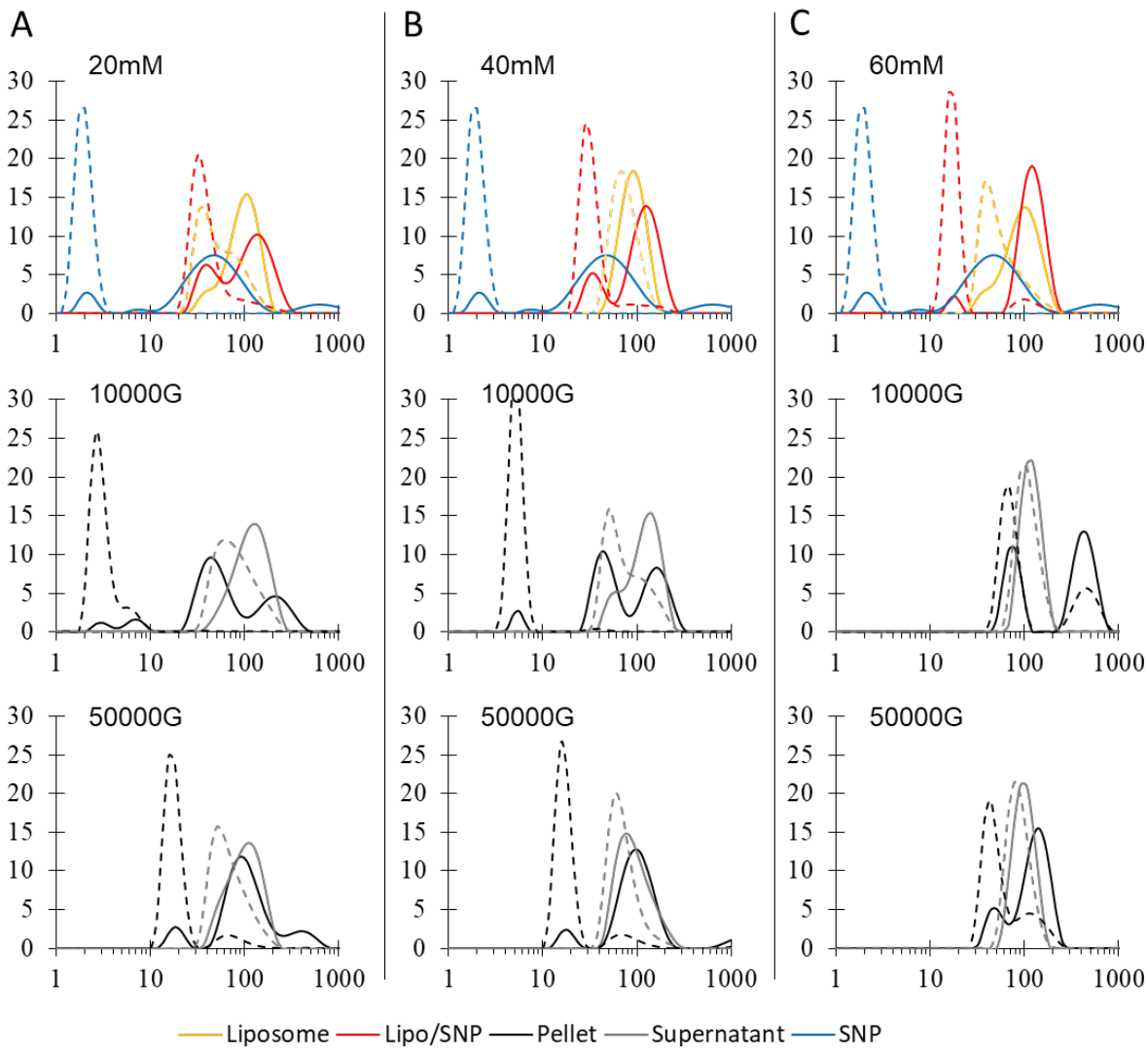

Figure 34 Size distribution plots of liposome, SNP, Lipo/SNP, with pellet and supernatant obtained after centrifugation at 10000g and 50000g centrifugal force. Plots correspond to lipid concentrations of (A) 20 mM (B) 40 mM and (C) 60 mM. Y and X axes represent percentage of distributions and diameter (nm) respectively. The solid and dashed lines represent the size distributions for intensity and volume respectively. Liposomal samples comprised of PC (20 mM, 40mM, 60mM) and were produced using the millifluidic reactor, at total flow rate (TFR) = 1 ml/min and flow rate ratio (FRR, aqueous phase/ethanolic lipid solution) = 10. For the experimental conditions please refer to **Table 5** (batch codes #4, #5 and #6).

Figure 34 shows the size distribution plots of liposomes, SNPs and Lipo/SNPs, including both supernatant and pellet, after centrifugation. The plots in the figure are vertically divided into three sections (A, B and C) depending on the lipid concentration used for the synthesis of liposomal dispersions (namely 20, 40 and 60 mM, respectively). Each panel shows the liposome, SNP and Lipo/SNP in the first raw, and the supernatant and pellet obtained after centrifugation using 10000G and 50000G in the second and third raws, respectively.

Figure 34A shows that the peak values were at around 50 and 100 nm for SNPs and liposomes, respectively. For Lipo/SNPs, two peaks were present at about 40 nm and 150 nm, which was possibly indicating free SNPs and SNPs encapsulated in liposomes. The peak of liposomes increased from around 100 nm to around 150 nm, which might indicate that SNPs were entrapped in the lipid bilayers leading to an increase in the final liposome size.

The middle plot of **Figure 34A** (after 10000g centrifugation), showed that the pellet had two peaks at around 40 and 200 nm while the supernatant had a peak at ~120 nm (corresponding to the liposomes). This observation might indicate that a centrifugal force of 10000g was enough to pellet the SNPs but not the liposomes. On the other hand, the peaks observed for the pellet possibly belonged to free SNPs and SNPs encapsulated in liposomes due to an increase in size. The bottom plot of **Figure 34A** (after 50000g centrifugation), showed similar values, but an additional peak was observed at ~400 nm, which was possibly associated with an agglomeration of SNPs and liposomes, due to the higher centrifugal force. Considering the volume-based distributions for SNPs, a peak at ~2 nm was observed. This peak was observed also in the pellet after centrifugation at 10000g, but it was not observed after centrifugation at 50000g. It could be assumed that the higher centrifugal force resulted in more NPs to pellet down including small-sized AgNPs, so that the NPs with a higher diameter (at ~10 nm) dominated the plot, and the peak at ~2 nm disappeared. Another explanation might be that, the resuspension of the pellet (after 10000g centrifugation) caused the release of smaller AgNPs from liposomes, but the AgNPs could not be released because the vesicles were packed more tightly in the pellet that formed with a higher centrifugal force (50000g).

In **Figure 34B & C,** similar results to those mentioned above were obtained. However, the Lipo/SNPs with higher lipid concentration (60 mM) showed two discrete peaks (after 10000g). Also, it was observed that, for the Lipo/SNPs, the percentage of the higher peak – which may indicate liposomes encapsulating SNPs – was increased when the lipid concentration increased. Based on these findings, it could be assumed that the greater amount of lipids resulted in higher EE%. The reason why this peak might be attributed to Lipo/SNPs rather than empty liposomes is the presence of a peak higher than 100 nm (indicating empty liposomes) despite the high number of SNPs.

Based on the analysis of supernatant and pellet, it was observed that the percentage of liposomes (or liposomes encapsulating SNPs) in the pellet increased for each sample when the lipid concentration increased. Additionally, the amount of relatively smaller SNPs decreased. These findings also likely indicated encapsulation of SNPs in liposomes.

It is important to note that, when the distributions were plotted by selecting the 'normal distribution' option (see paragraph **3.2.6**), only one peak was observed for Lipo/SNSs corresponding to the size of liposomes (or liposomes encapsulating SNSs). However, in the case of Lipo/SNPs, this was observed only in some measurements. The underlying reason could be attributed to size differences between AgNPs. Notably, SNSs could have been encapsulated more efficiently within liposomes due to their smaller size and spherical shape, as opposed to SNPs that had a larger size and sharp edges. It should also be noted that the presence of the second peak in Lipo/SNPs size distribution could be potentially attributed to the presence of SNP clusters, which would scatter light for effectively than SNSs.

To the best of the author's knowledge, no previous study has evaluated the encapsulation of SNPs in liposomes. However, as mentioned in previous paragraphs, the encapsulation of SNSs in liposomes has been evaluated elsewhere following a similar experimental approach (i.e., based on particle's size distribution plots). Here, the evaluation of SNP's encapsulation in liposomes was discussed based on the size distribution plots after sample centrifugation. Overall, the centrifugation process was found to be partly effective for the separation of unencapsulated SNPs due to possible aggregates; however, by combining it with DLS measurements, it allowed qualitative assessment of successful encapsulation of SNPs into liposomes.

Finally, the EE% of SNPs in liposomes was calculated using a liposomal dispersion synthesized with the continuous-flow millireactor. For the experimental conditions please refer to **Table 5** (batch code #9). The EE% was equal to 81.62 ± 28.99 %, and was determined by measuring the amount of SNPs in the supernatant. Considering the findings for this section, it can be concluded that the encapsulation of SNPs here was confirmed qualitatively and quantitatively in liposomal dispersions synthesized using continuous-flow based production method.

3.3.5.2 Evaluation of separation using a gel filtration technique

The evaluation of encapsulation of SNPs in liposomes was performed by employing a gel filtration technique for the separation of unencapsulated SNPs from the Lipo/SNP dispersion. It should be noted that the process of gel filtration for separation is a well-studied and commonly employed technique [215]. Samples of liposomes, SNPs and Lipo/SNPs were run through the gel and the

collected samples were characterized using DLS, UV-Vis or TEM. For the experimental conditions refer to **Table 5** (batch code #7). Initial tests were performed on the liposomes alone. The collected samples (i.e. after travelling through the gel) were characterized using DLS, and results are shown in **Figure 35**.

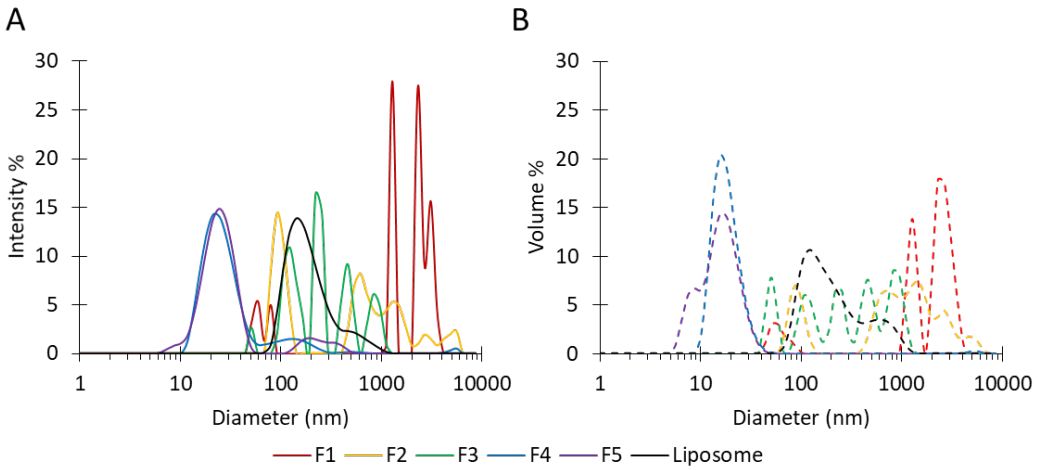

Figure 35 (A) Intensity and (B) volume-based size distributions of samples collected after gel filtration. Plots F1 to F5 represent the first and last collected samples respectively. Liposomes comprised of DPPC/Chol (7:3 mM) and were produced using the millifluidic reactor, at total flow rate (TFR) = 1 ml/min and flow rate ratio (FRR, aqueous phase/ethanolic lipid solution) = 10. For the experimental conditions refer to **Table 5** (batch code #7).

Figure 35A shows the intensity-based size distributions of the collected samples. The peaks were found to be decreasing in size, starting from the first sample to the last sample collected, starting from ~4000 nm to the last occurring at ~20 nm. This demonstrated that the bigger liposomes were collected first and the smallest liposomes were collected last during the gel filtration process, as expected. Also, it is important to note that the red plots belonged to the first collected sample (F1), which was believed to include aggregates. **Figure 35B** shows the volume-based size distributions, which were similar to the intensity distributions, corroborating that the filtration process worked successfully for liposomes alone. However, the collected samples showed multiple narrow peaks at different diameters ranging from 20 nm to 4000 nm, indicating that the liposome sample was highly heterogeneous in size. Another reason could be the presence of aggregates in the sample. It must be noted that the data here were presented as intensity and volume distributions, also with multimodal peaks (see paragraph **3.2.6.1**), that all allowed additional peaks to be shown, even if a very small amount of a liposome of different size. This effect was observed more clearly when analysing the data using number-based distributions (**Figure 36**) where the size peaks were calculated based only on the number of liposomes in the dispersion, resulting in the observation of

the highest peak values at ~120 nm. Overall, the filtration process proved to be effective when applied to liposomes alone.

The number-based size distribution of liposome samples was shown below, along with the distributions of collected samples after the filtration process.

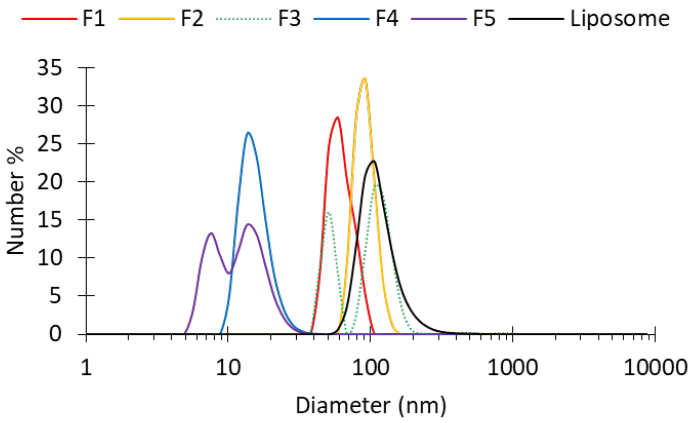

Figure 36 Number-based size distributions of samples collected after the produced liposome dispersion travelled through the gel. Plots F1 and F5 represent the first and last collected samples, respectively. Liposomes comprised of DPPC/Chol (7:3 mM) and were produced using the millifluidic reactor, at total flow rate (TFR) = 1 ml/min and flow rate ratio (FRR, aqueous phase/ethanolic lipid solution) = 10. For the experimental conditions refer to **Table 5** (batch code #7).

A similar analysis process for performed on the SNPs alone. The collected samples after filtration through the gel was characterized using UV-Vis, and results are shown in **Figure 37**.

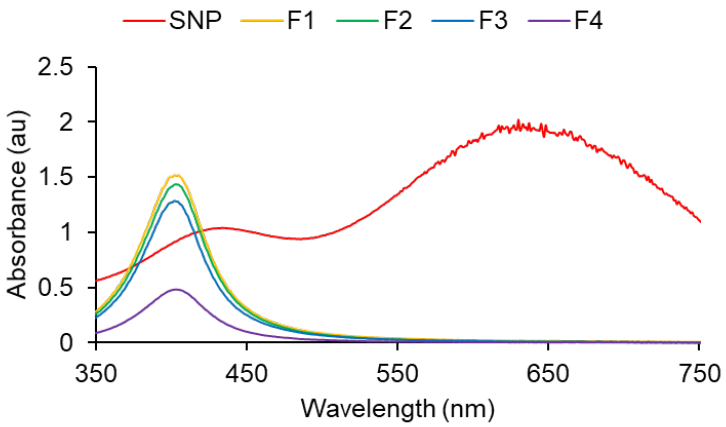

Figure 37 The absorbance of the samples collected after the SNPs travelled through the gel. Plots F1 to F4 represent the first and last collected samples, respectively.

Figure 37 shows the absorbance of collected samples after SNPs travelled through the sephadex gel. Here, the collected samples were characterized by UV-Vis. The absorbance of the SNP sample used for this experiment had a peak at ~630 nm (SNP), however the collected samples (from F1 to F4) showed a peak at ~400 nm. An explanation could be that the triangular shaped nanoparticles (SNPs) converted into spherical shaped nanoparticles (SNSs) during the gel filtration process. A colour change from blue to yellow was also observed in the column during the filtration process. Also, it must be noted that, some of the SNPs were blocked in the gel, probably due to the edge tips, and only the collectable samples (F1 to F4) were analysed. These findings suggest that SNPs converted into SNSs during the filtration process, or that only spherical shaped nanoparticles could pass through the gel.

Finally, the filtration process was performed for the separation of unencapsulated SNPs from Lipo/SNP samples. The collected samples (after Lipo/SNPs filtration) were characterized using UV-Vis and TEM. The results are shown in **Figure 38** and **Figure 39**, respectively.

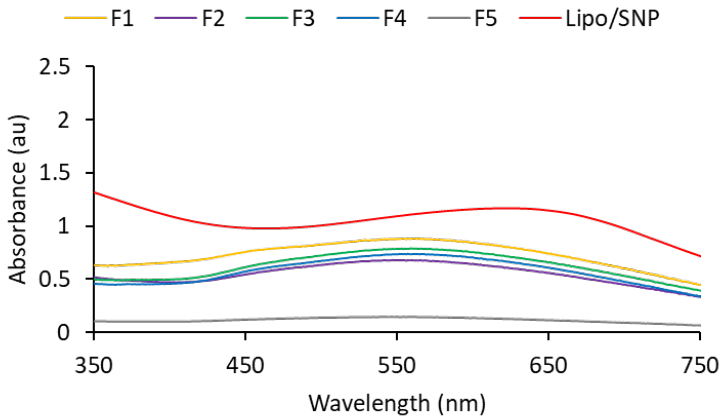

Figure 38 The absorbance of the samples collected after Lipo/SNP travelled through the gel. Plots F1 and F5 represent the first and last collected samples, respectively. Liposomal samples comprised of DPPC/Chol (7:3 mM) and were produced using the millifluidic reactor, at total flow rate (TFR) = 1 ml/min and flow rate ratio (FRR, aqueous phase/ethanolic lipid solution) = 10. For the experimental conditions, refer to **Table 5** (batch code #7).

Figure 38 shows the absorbance of Lipo/SNPs and of the collected samples after the gel filtration process. The collected samples did not show similar peaks when compared to the Lipo/SNP sample. The absorbance peak was at ~650 nm for the Lipo/SNP sample, while there was a broad peak at ~575 nm for the collected samples. It is interesting to note that, contrary to the findings in the previous section (see **Figure 37**), there was no yellowish colour observed during the process and none of the collected samples showed an absorbance at ~400 nm, which would have been an indication of SNSs in dispersion. The collected samples instead presented the same blue colour as

Lipo/SNP sample. Also, similar to the separation of SNPs alone, a certain amount of the sample was stuck in the gel.

Based on these findings, it might be concluded that unencapsulated SNPs could not separate efficiently from the Lipo/SNPs during the gel filtration process. Possible reasons might be that, following the stuck of triangular-shaped AgNPs to the gel, relatively rounder (and bigger) AgNPs or AgNPs that interacted with liposomes travelled through the gel. In addition, the smaller AgNPs (mainly SNSs but also a proportion of small-sized SNPs) were thought to be encapsulated in liposomes since there was no absorbance peak observed at ~400 nm. Also, the colour of the unfiltered Lipo/SNPs and collected samples were identical. Besides, there was no absorbance peak observed at ~640 nm for the collected samples, which could be an indication for SNPs or Lipo/SNPs. Overall, the separation of unencapsulated SNPs using gel filtration could not be fully achieved; thus, there is a need to further research on the physico-chemical interactions between the gel and Lipo/SNPs.

Some of the collected samples after gel filtration were characterised using TEM, and the images are shown in **Figure 39**.

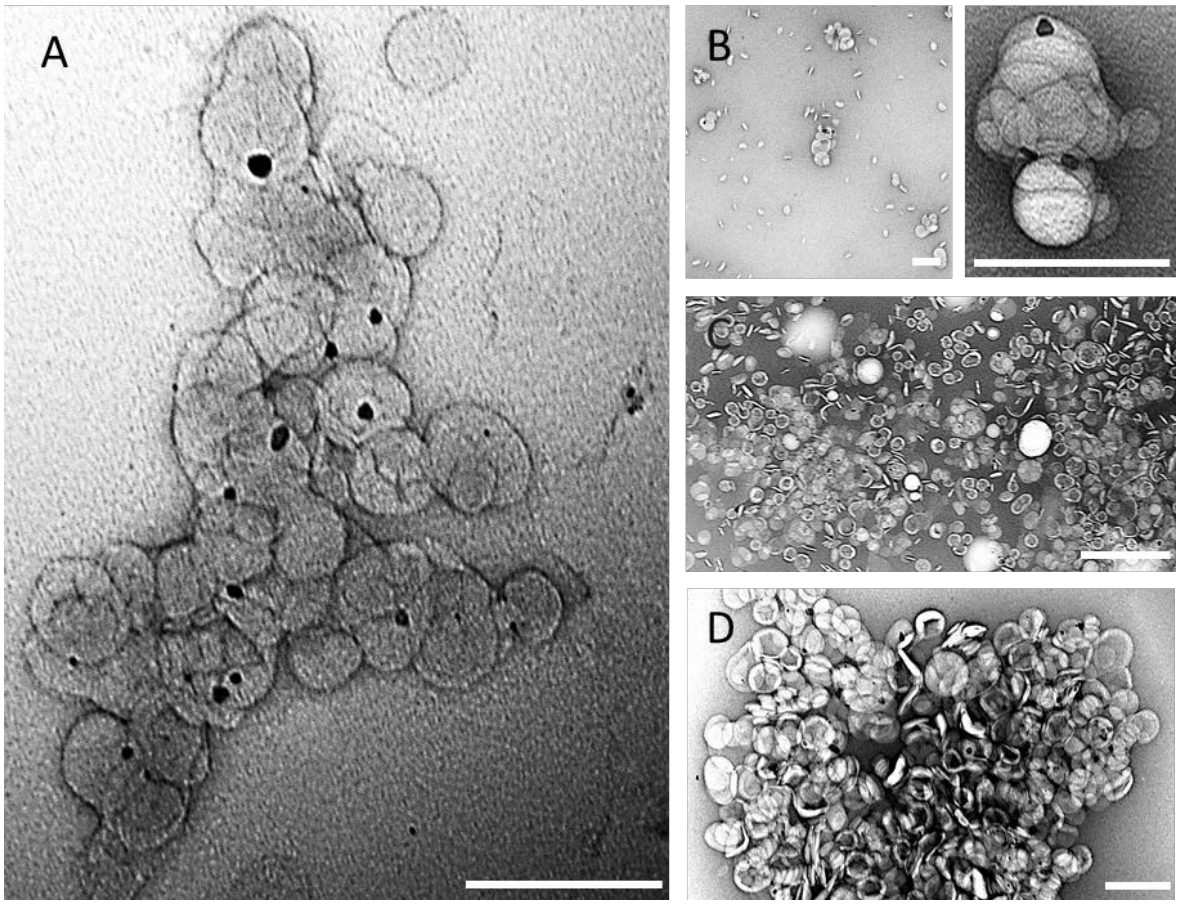

Figure 39 TEM images showing the (A) Lipo/SNP samples, and (B) first, (C) second, (D) third collected samples after filtration, respectively. The two images in panel (B) belong to same sample, and the image on the right corresponds to a higher magnification. Scale bars: 200 nm. The dark circular or triangular structures represent AgNPs and the relatively bigger circular structures represent liposomes. Liposomal samples comprised of DPPC/Chol (7:3 mM) and were produced using the millifluidic reactor, at total flow rate (TFR) = 1 ml/min and flow rate ratio (FRR, aqueous phase/ethanolic lipid solution) = 10. For the experimental conditions, refer to **Table 5** (batch code #7).

Figure 39A shows a TEM image of the Lipo/SNP sample, where a relatively high amount of SNPs encapsulated in the liposomes could be observed. During the TEM characterization, a high amount of empty liposomes was observed, while the amount of free SNPs was relatively low. This might be due to the negative staining process that could prevent SNPs from being detected, as they are dark in colour. Also, liposomes were observed as linked or superimposed to each other. Notably, a similar behaviour was observed for the collected samples (i.e. after filtration).

In **Figure 39B**, **C** & **D** show selected images illustrating successful encapsulation of SNPs in liposomes. Both liposomes and SNPs were observed as clusters, similar to the Lipo/SNP sample. It must be noted that, during the characterization process, the number of clusters appeared to be greater for the collected samples comparing to Lipo/SNP sample. The reason for this remains

unclear; however, it might be that the gel filtration process caused liposomes and SNPs to form a packed cluster. On the other hand, the amount of observed SNPs interacting with liposomes decreased in the final sample when compared to the Lipo/SNP sample. This suggests that the encapsulated SNPs were eluted first, and the empty liposomes were eluted only subsequently from the column. However, the findings reported for **Figure 38** showed no significant difference between the collected samples, which is inconsistent with TEM-based observations.

Overall, the gel filtration process was found to be only partly effective for the separation of unencapsulated SNPs. Considering all findings together, it was demonstrated that SNPs did not convert into SNSs upon filtration, and that the collected samples contained liposomes encapsulating SNPs (as shown in TEM images). These findings suggest that the filtration process should be investigated in greater detail in future experiments.

3.3.5.3 Evaluation of separation using the agglomeration approach

In this section, the separation of unencapsulated SNPs was performed using the agglomeration approach. SNPs were synthesized without PVP (i.e., as uncoated SNPs), and it was hypothesized that the unencapsulated SNPs in the dispersion would bind to each other, form aggregates, and eventually pellet down. However, the encapsulated SNPs in liposomes and empty liposomes would remain suspended in the fluid.

The SNP sample was firstly characterized by UV-Vis to determine whether the nanoparticles were aggregated or not within two hours after production, to observe any potential change in the absorption levels. However, the results shown in **Figure 40** did not provide sufficiently robust information, as the absorbance levels were not stable. This also showed that AgNPs in the dispersion were not as stable as expected.

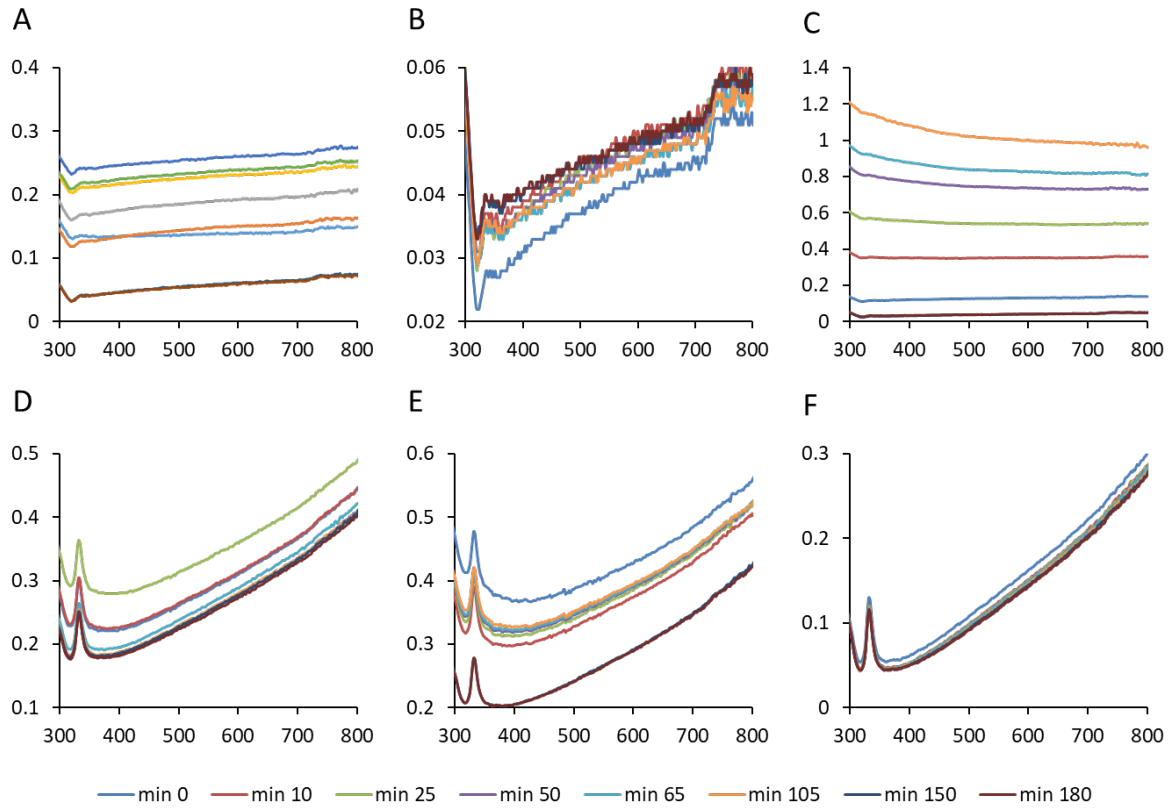

Figure 40 Absorbance values of SNPs synthesized without PVP, and plotted at different time points. A, B, C, D, E and F represent different samples taken from the same SNP sample. The absorbance of each sample was measured over time and plotted. Y and X axes represent absorbance and wavelength (nm) respectively.

The results belonged to different samples taken from the same vial, showing that the sample was highly heterogeneous and that the formation/deformation of SNPs was still occurring.

Further experiments were performed for longer time periods, to acquire more information for the formation of potential SNP agglomeration. Also, Lipo/SNP samples were synthesized using unstabilized SNPs by continuous-flow method using the millireactor, and the samples were kept at RT or +4°C for four weeks. For the experimental conditions, refer to **Table 5** (batch code #8). The Lipo/SNP samples were characterized just after production, and four weeks later, using DLS and UV-Vis. The results just after production are shown in **Figure 41**.

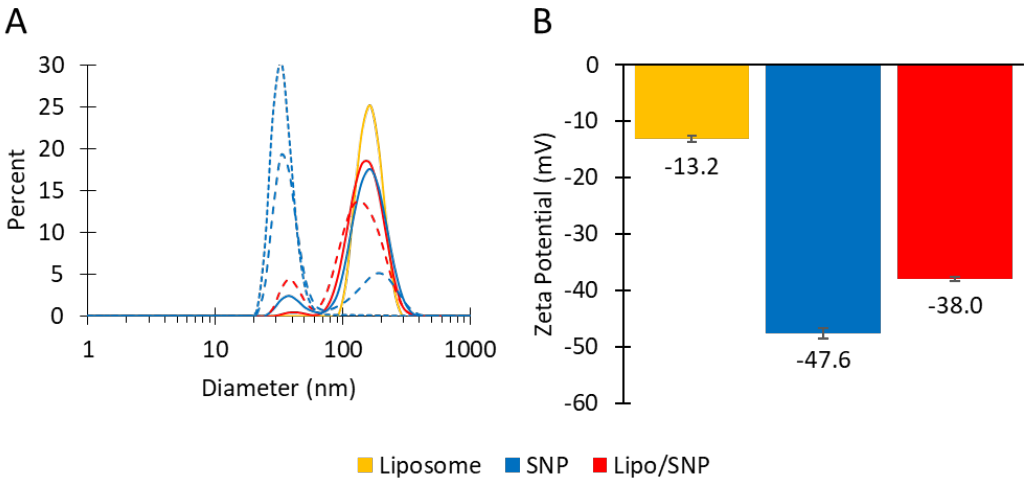

Figure 41 (A) Size distribution and (B) zeta potential values of liposome, Lipo/SNP and SNP samples. The solid line and dashed line represent the size distributions for intensity and volume respectively. Liposomal samples comprised of PC (50 mM) and were produced using the millifluidic reactor, at total flow rate (TFR) = 1 ml/min and flow rate ratio (FRR, aqueous phase/ethanolic lipid solution) = 10. For the experimental conditions, refer to Table 5 (batch code #8).

Figure 41A shows the size distribution plots of the liposome, SNP and Lipo/SNP samples just after production. The peak values for liposomes, SNPs and Lipo/SNPs were at ~160 nm, ~160 nm and ~150 nm respectively. Unlike previously shown, the peak value for the SNP sample was relatively higher than expected. However, the volume and number-based distribution plots showed similar values as previously shown, at ~25 nm. For the Lipo/SNP sample, there was one main peak observed at ~150 nm indicating liposomes or SNPs interacting with liposomes. The interaction was possibly confirmed with the volume-based distribution, showing that the peak at ~25 nm (indicating free SNPs) was relatively lower compared to the percentage of the SNP sample. In **Figure 41B,** the zeta potential values of liposome, SNPs and Lipo/SNP samples were shown to be -13.2 mV, -47.6 mV and -38 mV, respectively. Considering together the size distribution plots and the increased zeta potential value of the Lipo/SNP sample compared to SNPs, the interaction between liposomes and SNPs has occurred, and encapsulation was thought to be achieved to some extent. Here, the change in zeta potential value was thought of as an indication of an interaction between liposomes and SNPs [216]. Additionally, it must be noted that the zeta potential graph of Lipo/SNP sample had a single peak, suggesting that there were no discrete particles in the dispersion, and the liposomes had interacted with SNPs.

The samples were also characterized using DLS and UV-Vis, 4 weeks after production, as shown in **Figure 42** and **Figure 43**.

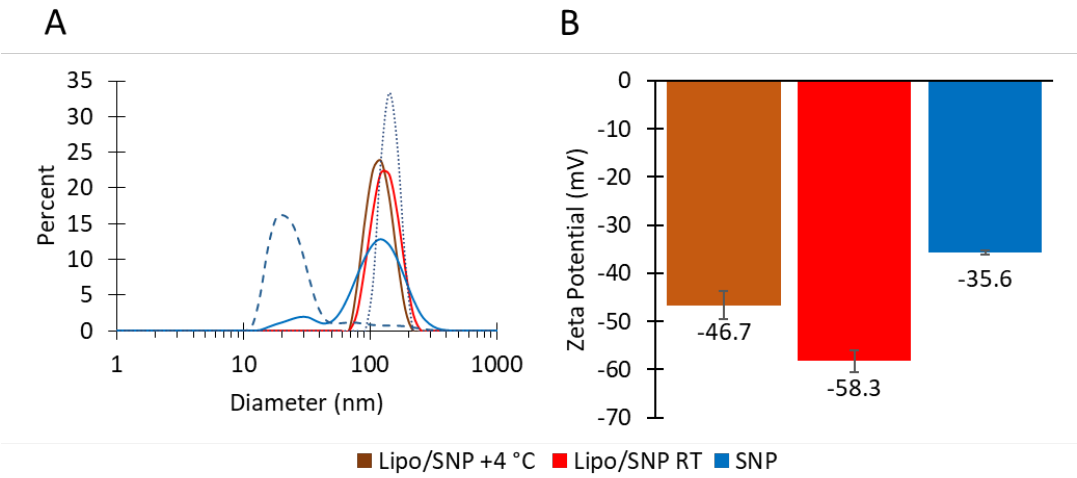

Figure 42 (A) Size distribution and (B) zeta potential values of liposome, Lipo/SNP and SNP samples four weeks after production. The solid, dashed and dotted lines represent the size distributions for intensity, volume and number respectively. Liposomal samples comprised of PC (50 mM) and were produced using the millifluidic reactor, at total flow rate (TFR) = 1 ml/min and flow rate ratio (FRR, aqueous phase/ethanolic lipid solution) = 10. For the experimental conditions refer to **Table 5** (batch code #8).

Figure 42 shows the size distribution plots of Lipo/SNP (+4 °C and RT) and SNP samples, at 4 weeks after production. It is important to note that the characterized aliquots were taken from the top of the vials. **Figure 42A** shows that there was no difference between the Lipo/SNP samples stored at +4 °C and RT, demonstrating that the storage conditions had no detectable effect on the final dimensional characteristics. The Lipo/SNP samples showed a peak at ~130 nm, indicating free liposomes, free SNPs or liposomes encapsulating SNPs. The size distribution plot of the SNPs showed a peak at ~20 nm and 130 nm. However, the number-based distributions showed a narrow peak at ~150 nm. These findings showed the existence of SNPs in the sample 4 weeks after production, even in the top layer of the vial. Additionally, the presence of SNPs was confirmed from the zeta potential measurements in **Figure 42B**.

Considering the results altogether (**Figure 41 and Figure 42),** it was observed that over four weeks the size distribution of the Lipo/SNP sample became more narrow, and changed from being 20-350 nm to 70-250 nm. The number-based distribution of SNPs, changed from level of 20 nm to 100 nm over four weeks, showing that an amount of the small nanoparticles or residuals disappeared, and the number of bigger SNPs dominated the plot. The disappearance of smaller nanoparticles over time was consistent with the size plot of the Lipo/SNPs (number-based distribution of SNPs in **Figure 41A** and **Figure 42A**). Based on these findings, it could be inferred that separation of

unencapsulated SNPs by agglomeration did not occur, as presence of SNPs was observed in the sample four weeks after production. However, the disappearance of smaller SNPs could be the result of flocculation [217], which caused AgNPs to become larger in size. However, the separation process was ineffective as the bigger AgNPs did not separate by gravity. It was thus observed that the agglomeration of SNPs occurred as expected due to the increased size; however, the SNPs remained suspended in the fluid.

Additionally, the samples were characterized by UV-Vis and results were shown below.

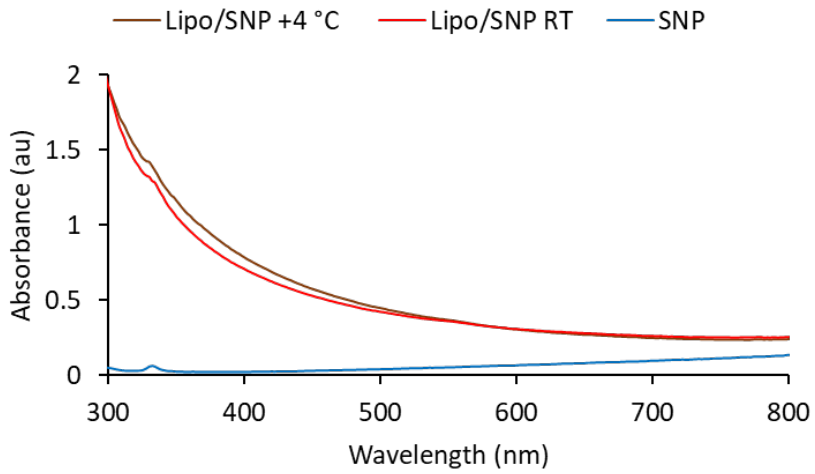

Figure 43 The absorbance of the samples four weeks after the production. Liposomal samples comprised of PC (50 mM) and were produced using the millifluidic reactor, at total flow rate (TFR) = 1 ml/min and flow rate ratio (FRR, aqueous phase/ethanolic lipid solution) = 10. For the experimental conditions refer to **Table 5** (batch code #8).

Figure 43 shows the absorbance spectrum of Lipo/SNP (+4 °C and RT) and SNPs samples. The reason for the Lipo/SNP samples to show an increased curve towards 300 nm was the presence of liposomes in the sample. Unfortunately, peak values for the samples could not be observed due to the limitations of the equipment employed. However, it is important to note that the samples had a bluish appearance that supported the presence of SNPs. On the other hand, even though the peak value could not be observed, it could be inferred that the curves for Lipo/SNP samples confirmed the presence of SNPs, as the curve became relatively flat from ~700 nm to ~800 nm instead of decreasing.

Overall, the separation of unencapsulated SNPs was tested using the agglomeration approach, and the method was found inefficient. The size distribution plots showed that the smaller nanoparticles disappeared over time, but the size plots also showed the existence of large SNPs that remained in

the sample. This was confirmed with the absorbance spectrum of the SNPs performed 4 weeks after production. Considering these findings together, it could be concluded that the method should be further investigated for longer timescales, also in combination with TEM or cryo-TEM techniques, to demonstrate SNP encapsulation more rigorously.

3.3.5.4 Evaluation of SNP encapsulation in liposomes

In addition to testing the separation of unencapsulated SNPs using different methods, as discussed in the previous sections, the EE% of SNPs into liposomes was evaluated using the images and dimensional properties obtained by TEM and DLS, respectively. This quantification was carried out without applying a separation process to remove unencapsulated SNPs.

3.3.5.4.1 Quantification based on image analysis

The evaluation of SNP encapsulation in liposomes was performed using the images obtained by TEM, as presented below. The Lipo/SNPs were characterised just after production, without performing any separation step. For the experimental conditions, refer to **Table 5** (batch code #9). Selected representative images of a Lipo/SNP sample are shown in **Figure 44**.

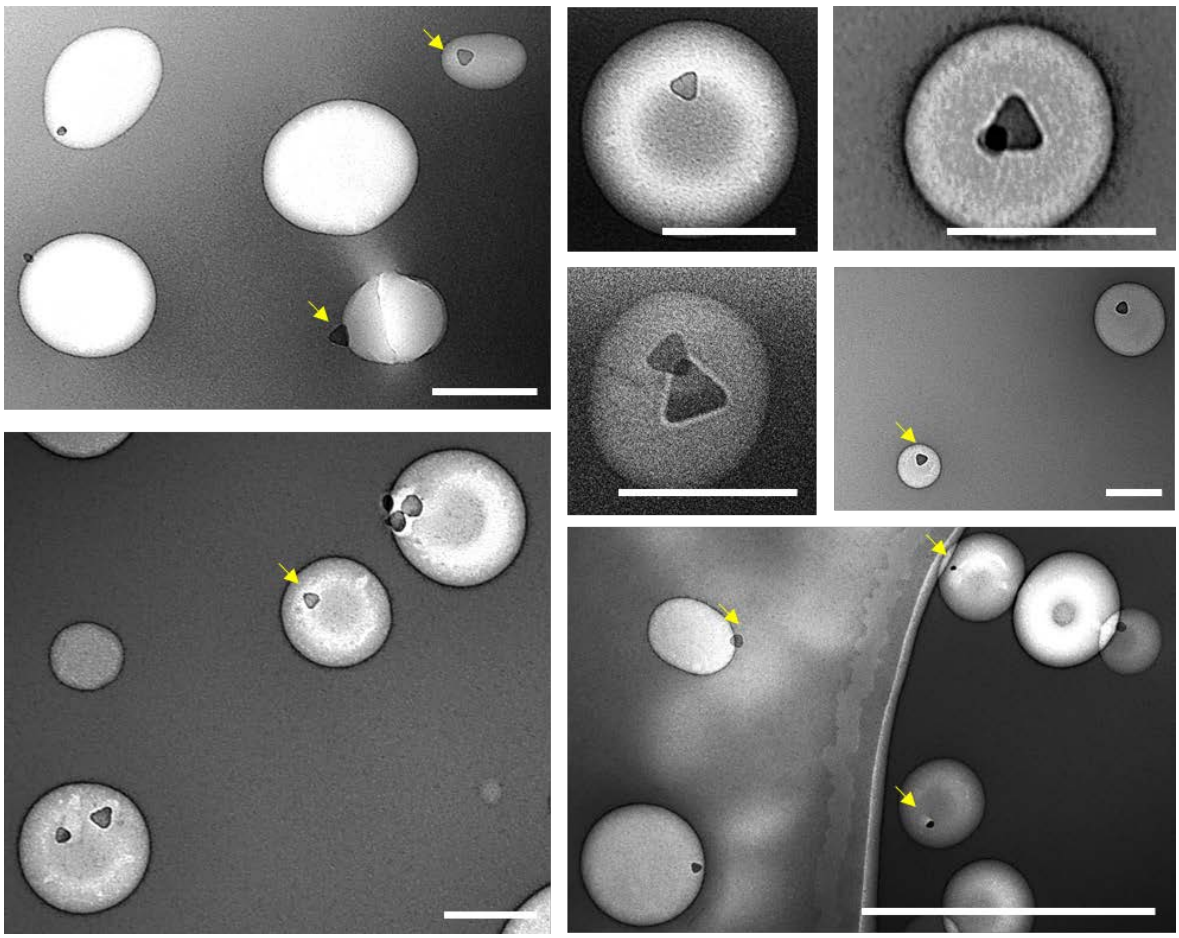

Figure 44 TEM images of Lipo/SNP samples produced using millifluidics-based production. Selected images belonged to the same sample. Liposomal samples comprised of

PC/Chol (28:12 mM) and were produced using the millifluidic reactor, at total flow rate (TFR) = 5 ml/min and flow rate ratio (FRR, aqueous phase/ethanolic lipid solution) = 10. For the experimental conditions, refer to **Table 5** (batch code #9). Bright circular structures and dark structures (mainly triangular shaped) represent liposomes and SNPs, respectively. The arrows point towards some of SNPs that were encapsulated within or associated with the liposomes.

Figure 44 shows selected images belonging to the same Lipo/SNP sample. SNPs were observed to associate with the membrane of the liposomes, but there were also cases where nanoparticles could be encapsulated inside the liposomes. The images could not provide precise information about whether the SNPs were on the surface, within the bilayer, or inside the core of liposomes. However, they could confirm that SNPs were interacting with liposomes in many cases. It is important to note that the samples were stained negatively for the imaging procedure, which may adversely affect the observation of free/unencapsulated SNPs and result in the observation of liposomes and encapsulated/associated SNPs only. Additionally, the EE% was calculated by manually counting the free SNPs and encapsulated/associated SNPs, and the result was found as 77.48%. However, the EE% was calculated based on the images that were specifically taken (see **Figure S1**) on a particular portion of the grid (see **Figure S2**). Also, it is important to note that, the liposomes that were not associated with SNPs were not counted (see **Eq. 2** above). Also, the associated staining procedure, and its 2D nature, were found to be the main limitations associated with the use of TEM for the evaluation of SNP encapsulation.

An additional experiment was thus performed for the demonstration of SNP encapsulation in liposomes. SNP/Lipo samples were prepared and embedded in resin; it was then cut into thin sections, which were subsequently imaged (**Figure 45**). For the experimental conditions, refer to **Table 5** (batch code #10).

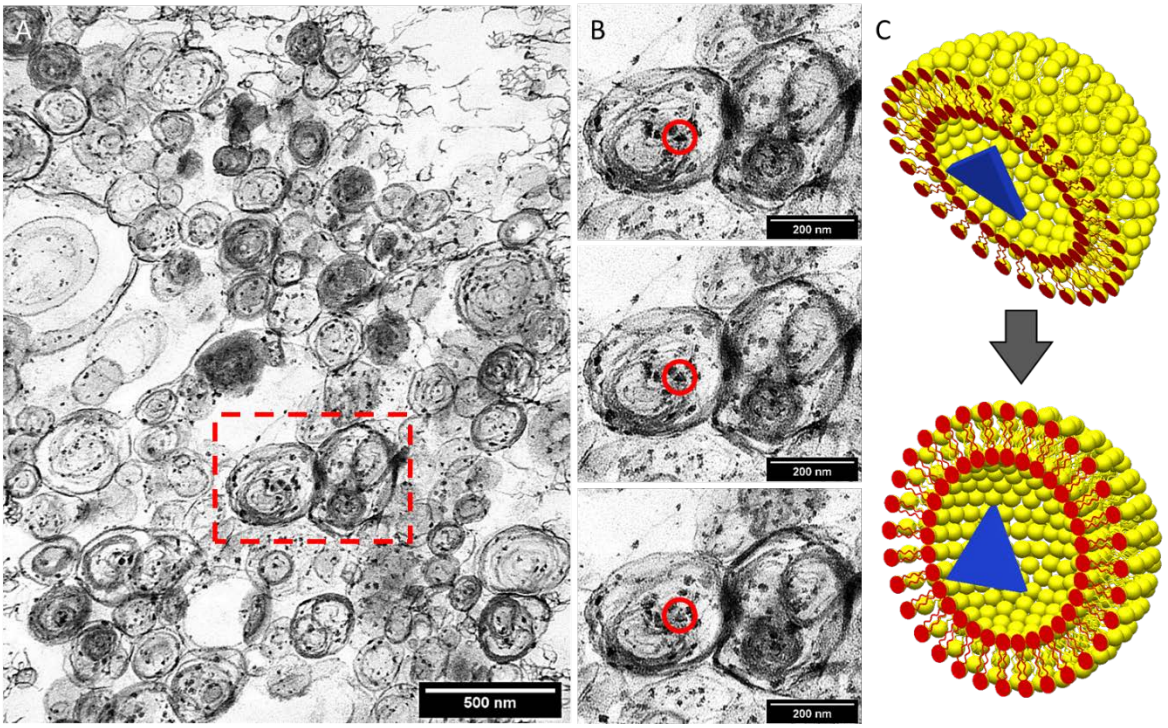

Figure 45 (A) TEM image of Lipo/SNP sample embedded in resin. (B) Images show a zoomed in view of the TEM image of a Lipo/SNP sample. Here, the images (from top to bottom) were collected by tilting the holder of the TEM machine (changing the angle of the holder). (C) The illustration shows how the triangular nanoparticles (SNPs) encapsulated in liposomes become more clearly visible when the angle of the imaging plane is tilted. Liposomal samples comprised of PC (100 mM) and were produced using the millifluidic reactor, at total flow rate (TFR) = 1 ml/min and flow rate ratio (FRR, aqueous phase/ethanolic lipid solution) = 25. For the experimental conditions refer to **Table 5** (batch code #10).

Figure 45A, B & **C** show images of embedded Lipo/SNP samples, a zoomed-in view of a selected region taken at different angles, and the illustration of SNP encapsulation in liposomes at different angles, respectively. In **Figure 45A** the liposomes could be observed as circular structures, along with darker materials mostly inside the liposome and in their proximity. The darker materials in the image were thought to be mostly AgNPs and a few residuals left from the sample preparation. For confirmation, a selected region was analysed specifically by taking the images with different angles, as shown in **Figure 45B.** The images taken from different angles were shown from top to bottom. In the images, an SNP trapped in a liposome is shown in a red circle. It was observed that the triangular structure of the SNP in the red circle could be easily detected, especially in the final image, as the upper edge of the triangular structure became more clear. This observation was also illustrated in **Figure 45C.** Considering the observation of SNPs inside the lipid bilayer within the evaluated section, which has a thickness around 800-900 Å, it was thought that SNP encapsulation in liposomes was demonstrated. Although it could be hypothesised that not all of the dark materials

in the image were AgNPs, the encapsulation of SNPs in liposomes appeared to be highly efficient. Also, it is important to note that the exact location of SNPs (i.e., either within the aqueous core, or within/associated with the liposome shell) could not be verified from these images. The technique was however found to be quite effective in enabling understanding of SNPs encapsulation in liposomes. Further research may include detailed characterisation of Lipo/SNPs prepared with various concentrations of SNPs or liposomes, that could potentially help in understanding the EE%.

3.3.5.4.2 Size distribution and zeta potential analysis

The encapsulation of SNPs in liposomes was also evaluated using zeta potential measurements along with size distribution plots. For liposomal dispersions, the zeta potential is an important indicator of the surface charge of the nanoparticle, and can provide information about the colloidal dispersions [218]. Here, the evaluation of SNPs encapsulation was made based on the overall resultant zeta potential value after liposomes mixed with SNPs. The Lipo/SNP samples were synthesized using positively and negatively charged lipids, and the resultant dispersions were characterized with DLS. The results were shown in **Figure 46** and **Figure 47**, respectively. For the experimental conditions, refer to **Table 5** (batch code #11 and #12).

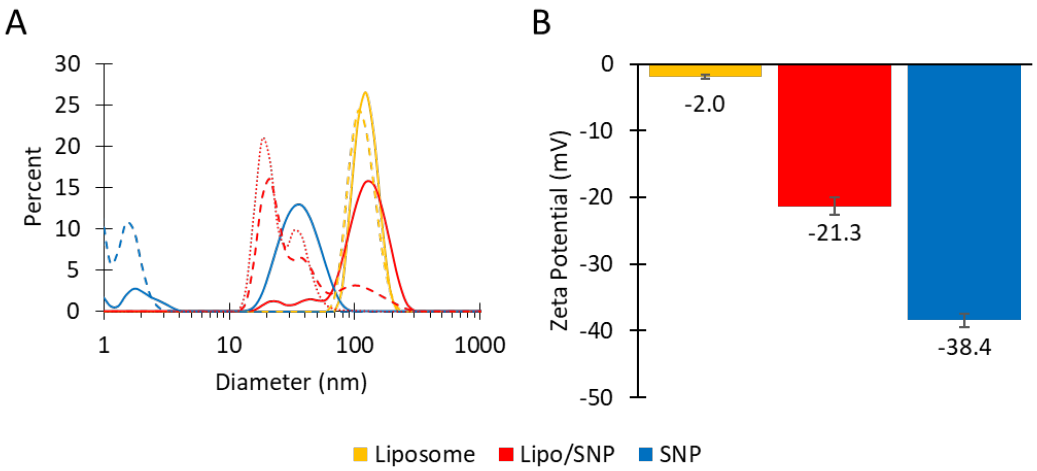

Figure 46 (A) Size distribution plots and (B) zeta potential values of liposome, SNP and Lipo/SNP samples. The solid, dashed, and dotted lines represent the size distributions for intensity, volume and number, respectively. Liposomal samples comprised of PC (16 mM) and were produced using the millifluidic reactor, at total flow rate (TFR) = 1 ml/min and flow rate ratio (FRR, aqueous phase/ethanolic lipid solution) = 10. For the experimental conditions, refer to **Table 5** (batch code #11).

Figure 46 shows the size distribution and zeta potential characteristics of SNPs along with liposomes and Lipo/SNPs that were synthesized using negatively charged lipids. In **Figure 46A** the size

distribution plots showed that the SNPs and the liposomes had peak values of 40 nm and 130 nm, respectively. According to the volume-based distributions, liposomes had a similar peak, while the peak value of SNPs dropped to ~1 nm. However, the sample of Lipo/SNP showed a peak value at ~150 nm, which was assumed to be an indicator of the encapsulation of SNPs in liposomes. Because, the peak value of SNP dispersion (~40 nm) was almost disappeared and the peak value of Lipo/SNPs was observed as almost same or higher than the peak value of liposomes despite to relatively higher amount of SNPs. On the other hand, the volume and number-based distribution of Lipo/SNP sample showed smaller peak values. This might be due to the greater amount of unencapsulated SNPs in the dispersion, compared to encapsulated SNPs. Considering the distribution graphs all together, it can be concluded that SNP encapsulation has been achieved to some extent.

Figure 46B shows that the average zeta potential values of liposomes and SNPs were -2 mV and -38.4 mV respectively. The lipids (PC) employed for the production of liposomes was neutral, resulting in the formation of liposomes having no net surface charge [218]. However, when the lipids were mixed with SNPs, the resulting Lipo/SNPs dispersion had a zeta potential value of -21.3 mV, suggesting that the liposomes had an interaction with SNPs. Additionally, the zeta potential distribution showed only one peak suggesting that there were no discrete particles in the dispersion (data not shown), thus further suggesting that liposomes and SNPs had some form of interaction. Therefore, based on these data, it was concluded that the encapsulation of SNPs was achieved to some extent. It is also important to note that similar to the approach used here, the use of zeta potential as an indicator for the interaction of colloidal systems has been demonstrated previously [219, 220].

The same experiment was performed by employing positively charged lipids to observe any possible interactions between SNPs and liposomes due to positive and negative interactions, and the results were shown in **Figure 47**.

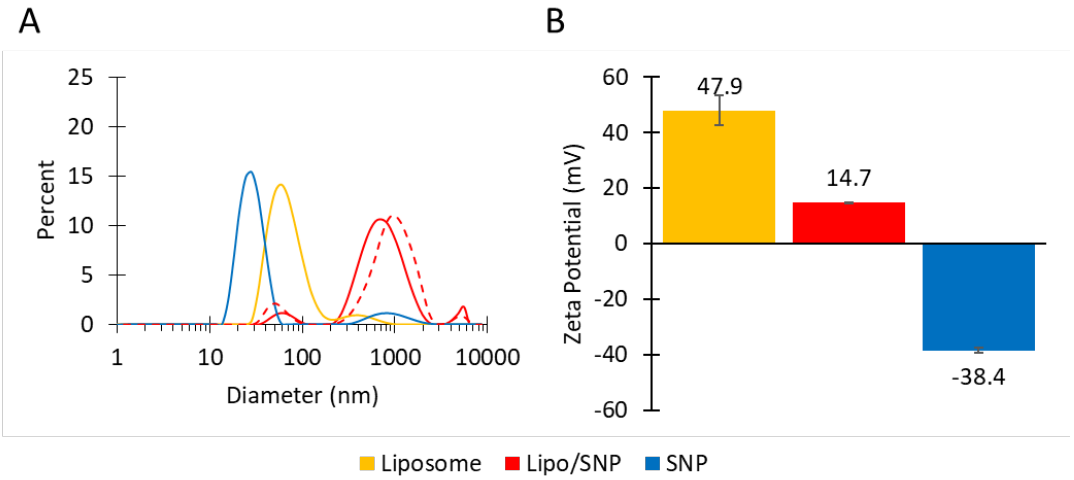

Figure 47 (A) Size distribution plots and (B) zeta potential values of liposome, SNP and Lipo/SNP samples. The solid, dashed and dotted lines represent the size distributions for intensity, volume and number, respectively. Liposomal samples comprised of DPPC/ODA/PEG-40 (14.4:1.6:0.01 mM) and were produced using the millifluidic reactor, at total flow rate (TFR) = 1 ml/min and flow rate ratio (FRR, aqueous phase/ethanolic lipid solution) = 3. For the experimental conditions, refer to **Table 5** (batch code #12).

Figure 47A shows the size distribution of liposome, SNP and Lipo/SNP samples. The peak values were observed at ~65, ~25 and at ~700 nm, respectively. It could be appreciated that the addition of SNPs to the liposomes caused a significant size increase, as shown in the size distribution of Lipo/SNPs. Also, the volume-based distribution of Lipo/SNPs was similar to intensity-based distribution, supporting the increase of the size upon addition of SNPs. One reason for the significant increase in size was thought to be the formation of structures that are relatively larger than liposomes, composed of liposomes surrounded by SNPs, giving a relatively high hydrodynamic radius. Another explanation could be the formation of lipid-SNP clusters. Additionally, another possibility that was also covering the peak at ~50 nm for number-based distribution of Lipo/SNPs, might be SNPs covered with lipids. Comparing to the size distribution of Lipo/SNPs that were formed using neutral lipids, the Lipo/SNP size here was much greater. This showed that the interaction of positively charged lipids with SNPs was enhanced in the presence of negatively charged lipids. Notably, the production method, which comprised the addition of SNPs to the dispersion after liposomes had formed, possibly affected the size distribution.

In **Figure 47B** the zeta potential values of liposome, SNPs and Lipo/SNPs were shown as 47.9, -38.4 and 17.4 mV respectively, which showed a similar trend as for the data shown in **Figure 46B**. The zeta potential graph of Lipo/SNPs had one peak, and the value of Lipo/SNPs was positive, showing

that an interaction between liposomes and SNPs occurred. In the literature, the interaction between positively and negatively charged materials was also demonstrated [221, 222]. As a supporting information, the positively charged liposomal dispersion (including SNPs and a fluorescent dye (rhodamine)) synthesized in millifluidic reactor, was imaged using TEM (see **Figure 54A**), and the interaction between SNPs and liposomes was demonstrated as explained here.

It is important to note that the zeta potential values between +30 and -30 mV are commonly considered as neutral and also unstable in the literature. Besides, the concentration of the sample, the pH of the dispersion and the size of the nanoparticle play an important role when measuring the zeta potential. In this study, the composition and pH of the samples were kept similar across samples, and attention was devoted to differences in zeta potential values when AgNPs were added to the samples. Also, when zeta potential values were negative or positive, the samples were generally accepted as negatively or positively charged, and evaluation of encapsulation was performed relying on that information. Overall, the analyses have provided valuable information for understanding the interaction between nanoparticles and liposomes; however, additional measurements are required, taking into account the concentration of the samples and the size of nanoparticles, to generate more reliable data on SNP encapsulation [216, 218, 219].

3.4 Conclusions

SNP loaded into liposomes can act as effective theranostic agents due to remarkable physico-chemical properties of SNPs; however, this system has not been produced nor characterised yet. Here, the encapsulation of SNPs in liposomes was performed using a continuous-flow millireactor, and confirmed with different characterization techniques including DLS, UV-Vis or TEM.

The separation of unloaded AgNPs was tested via different methods including centrifugation, gel filtration and agglomeration; because the free SNPs might not be preferable for some applications as they may potentially cause toxicity. The centrifugation method was found to be effective for SNSs, but would need further improvements for SNPs. The gel filtration technique suffered from some important limitations, as it may affect the shape of SNPs, although TEM images suggested that the method may be further improved. Separation based on the sedimentation of SNP aggregates demonstrated potential, although it would require further studies, particularly at longer timescales.

Analysis of DLS data was found an effective means to evaluate EE%, but it requires SNPs to have low size dispersity. TEM and UV-Vis methods were the most reliable ways of evaluating EE%, although it was observed that sample preparation could significantly affect the sample and accordingly the obtained images.

Overall, the SNP encapsulation in liposomes has been achieved in either microfluidics or batch production and could be demonstrated by imaging. A definite quantification of EE% would require different characterisation techniques or procedures that can provide separation of unentrapped materials or allow 3D imaging, such as Cryo-TEM.

Chapter 4 Photothermal Drug Release from Liposomes with Dual Encapsulation of Silver Nanoparticles and Model Drugs

4.1 Introduction

Surface plasmon resonance (SPR) refers to the excitation of electrons at the interface between the conductor and insulator part of the material triggered by light [98]. When excited by incident light at specific wavelengths, conduction electrons on the surface of metal undergo a collective resonant oscillation. With the light absorbed by the electrons in plasmonic metal nanoparticles, it can arise as local heat. Therefore, the photothermal property of plasmonic metal nanoparticles can be used for light-controlled drug delivery and also for tracking drugs in real-time to detect cancer tissues [99].

Silver nanoparticles (AgNPs), which have the SPR effect, have attracted considerable interest because of their simple synthesis and unique physiochemical especially optical properties [100]. AgNPs have been widely used in, e.g., molecular diagnostics, photonics, conductive inks, antimicrobial coatings, textiles, and biomedical devices [101, 102]. Optical properties of these nanoparticles are mainly shape and size dependent, and accordingly, the SPR depends on the composition, shape and size of the silver nanoparticles [103-105]. By varying the reaction conditions during AgNPs synthesis, e.g., by adding certain amounts of reagents including silver nitrate, trisodium citrate, hydrogen peroxide, sodium borohydride and water, and by controlling the mixing process, different shapes and sizes of AgNPs can be formed with resulting optical properties [106]. Spectral properties of a range of AgNPs have been demonstrated well in previous studies [98, 107].

By using the SPR property of plasmonic nanoparticles which can convert the photo energy into local heat, gold or silver and gold nanoparticles have been attractive for drug delivery applications to release the drug in a controllable manner. In principle, when plasmonic nanoparticles are encapsulated inside the drug carrier such as liposomes, the heat created by light irradiation can trigger the liposomes layer to phase transition [21, 97, 109].

Studies on fluorescent gold nanoclusters and doxorubicin dual-loaded liposomes have demonstrated intracellular fluorescent thermometry, photothermal drug release and tumour therapy [97]. The system operated as a light-triggered nanoswitch for controlled drug release. When the temperature was above the phase transition the membrane of the liposome underwent a phase change from gel to liquid crystalline state and released the drug. When the temperature

was under the phase transition temperature the membrane was reversed to a gel state and the drug retained in the liposome. Additionally, it was shown that the AgNPs were able to restrain the division of cancer cells and induce cell death [200]. Because of these cytotoxic effects, AgNPs are also the subject of research as anticancer agents.

Among AgNPs studied, triangular silver nanoprisms (SNPs) have attracted particular attention due to their remarkable features of SPR associated with the sharp tip morphology [19, 20]. It was shown that chitosan covered SNPs could act as phototherapeutic agents in cancer treatment, by triggering localized hyperthermia of tumours [206]. Also, the employment of SNPs as a tool for determining dissolved oxygen content due to their specific optical properties was demonstrated [223].

In this part of the PhD study, considering the remarkable properties of SNPs, with the aim of producing a novel drug delivery vehicle that can initiate the drug release based on photothermal properties, liposomes dual loaded with a model drug (rhodamine) and SNP were synthesized. A millireactor was used for continuous-flow production based on the development as presented in previous Chapters. The system was investigated for drug release performance under different liposomal compositions upon laser illumination under different conditions.

4.2 Materials and Methods

4.2.1 Materials

Ethanol (99.9%), HEPES (≥99.5%), rhodamine B (Rho, ≥95.0%), Triton™ X-100, dipalmitoylphosphatidylcholine (DPPC, >99.0%), octadecylamine (ODA, 99.0%, stearylamine), polyoxyethylene (40) stearate (PEG-40) and agarose were obtained from Sigma Aldrich (Gillingham, UK). PHOSPHOLIPON®90G (purified phosphatidylcholine, or PC, from soybean lecithin) was kindly provided as a gift by Phospholipid GmbH (Lipoid, Ludwigshafen, Germany). Silver nitrate (AgNO3 99%), tri-sodium citrate dihydrate (TSCD), polyvinylpirrolidone (PVP, average molecular weight AMw ≈ 29,000 gmol-1), hydrogen peroxide (H2O2, 30% by weight (wt-%)), and sodium borohydride (NaBH4, 99%), were obtained from Sigma Aldrich (Gillingham, UK) and used as purchased. All water employed was Milli-Q.

In the millifluidic reactor system, the syringe pumps (AL-1010) were purchased from World Precision Instruments (Hertfordshire, UK), and 20 mL BD-Plastipak syringes with luer lock connectors were obtained from Fisher Scientific (Loughborough, UK). Male luer lock rings, polytetrafluoroethylene (PTFE) tubing, and hot plate stirrer (UC152D) were supplied by Cole-

Parmer (St. Neots, UK). The tubing to connect the outlet port of the millireactor to the collection vial was 21.5 cm long (inner diameter: 0.5 mm; outer diameter: 1.6 mm) and was purchased from Cole-Parmer (St. Neots, UK).

4.2.2 Synthesis of liposomes

All lipids (PC, DPPC, ODA, and PEG-40) were dissolved in ethanol. In continuous-flow production of liposomal dispersions by solvent exchange mechanism, the ethanolic lipid solution and the aqueous phase (HEPES, 20 mM, pH 7.4) were injected via the two inlets into the millireactor main reaction channel. The millireactor was fabricated by following the previously reported protocol, combining micromilling with replica moulding (referred to as μMi-REM) [28, 34, 135]. A schematic of the experimental set-up for the production of liposomes using the millireactor is illustrated in **Figure 48.**

4.2.3 Synthesis of SNPs

For the batch synthesis of SNPs, 24 mL of solution containing TSCD (0.1 M, 0.375 mL), silver nitrate (AgNO3, 0.05 M, 0.05 mL), PVP (0.7 mM, 0.375 mL) and hydrogen peroxide (H2O2, 30 wt.%, 0.125 mL) was stirred vigorously at room temperature. After 7 minutes a freshly prepared solution of sodium borohydride (NaBH4, 25.00 mM, 1.00 mL) was rapidly injected. After about 30 minutes, the solution colour changed through yellow to orange-brown, then green-blue through to blue after a further 5 - 10 minutes. The batch synthesis of AgNPs was performed by Dr Domenico Andrea Cristaldi and Dr Harriet Kimpton.

4.2.4 Synthesis of liposomal dispersions including Rho with/without SNPs

Liposomal dispersions encapsulating only Rho, or Rho with SNPs were labelled as Lipo/Rho and Lipo/Rho/SNPs respectively. The aqueous phase was used as HEPES (20 mM, pH 7.4, with Rho) for Lipo/Rho samples. For the production of Lipo/Rho/SNP samples, HEPES solution (40 mM, pH 7.4, including Rho) was 1:1 v/v mixed with the SNP dispersion and used as the aqueous phase. For the production of Lipo/Rho+SNP samples, the SNPs was 1:1 v/v mixed with the synthesized and purified Lipo/Rho dispersion (40 mM, pH 7.4).

Here, the liposome formulations comprised PC, DPPC, ODA or PEG-40 considering the stability and the release properties of the lipid bilayer. Depending on the desired phase transition properties, PC or DPPC was used as the main component of the lipid bilayer. Cholesterol was not included in the composition of the liposomes considering the possible negative effects on the release efficiency from the bilayer [180, 224, 225]; instead, PEG-40 was used as the stabilizing agent [226]. Also, ODA

was included in some of the formulations for the evaluation of drug release from positively charged liposomes.

For continuous-flow production in the millireactor, experiments were conducted under various flow conditions, corresponding to variations in both flow rate ratio (FRR) and total flow rate (TFR). Herein, the FRR is defined as the ratio between the inlet volumetric flow rates of water and the ethanolic lipid solution, and TFR as the total volumetric flow rate (i.e., the sum of ethanol and water flow rates). Liposomal dispersions were produced either at room temperature (RT), or at 65 °C by placing the millireactor on a hot plate stirrer. In the latter case, the ethanolic lipid solution and the aqueous phase (in separate syringes) were placed in a beaker containing water at 65 °C, prior to injection in the millifluidic device. The detailed information of the millireactor fabrication and synthesis of liposomal dispersions (using millireactor or batch) is also presented in paragraphs **2.2.2** and **2.2.3,** respectively**.** The operational parameters and batch codes for the synthesized samples are given in **Table 6.**

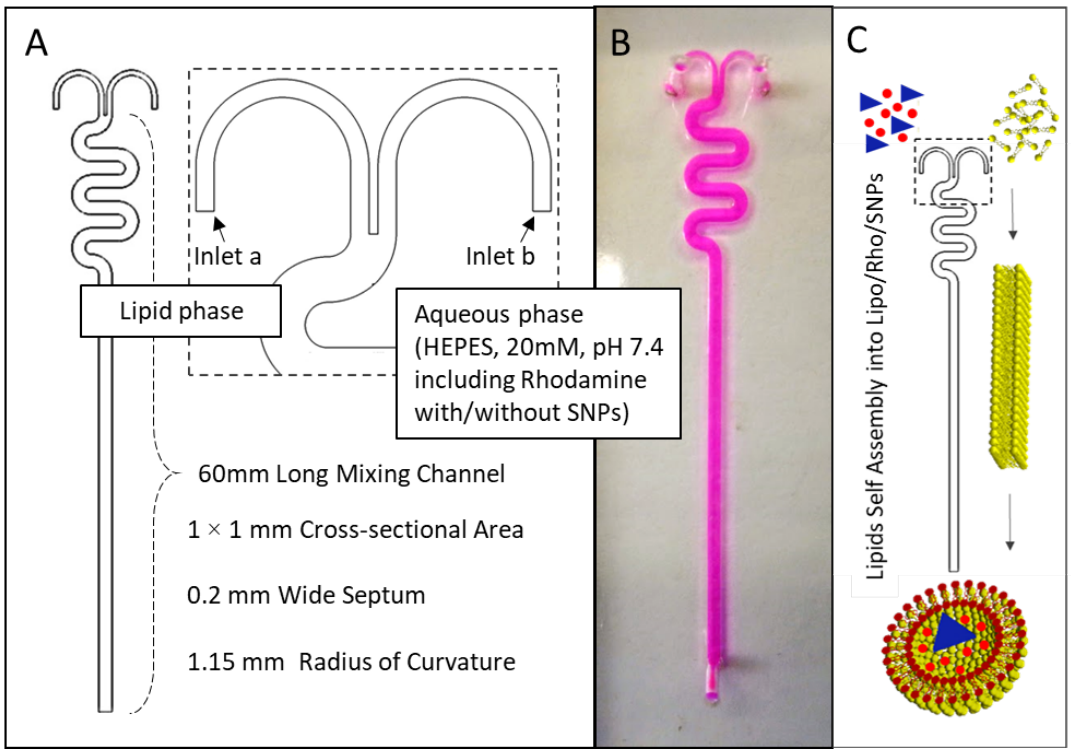

Figure 48 (A) Millireactor geometrical characteristics and device's inlet section with indication of the injected media, (B) top view photograph of the millireactor, and (C) schematic illustration of the experimental approach for the production of liposomal dispersions using the millireactor.

Table 6 The operational parameters and chemical formulations along with drug release.

Batch code[1]	Sample	Flow conditions	Lipid composition (mM)[2]				Rhodamine Concentration (mM)	EE%	Test Platform
		TFR:FRR	PC	DPPC	ODA	PEG-40			
#1	Liposomal dispersions with/without Rho or SNP	1:10	16	-	-	-	0.02975	-	Gel
#2		1:10	-	12.8	1.6	1.6		41.57	Gel, Channel
#3		1:10	12.8	-	1.6	1.6		5.31	Channel
#4		1:10	90	-	5	5		-	Channel
#5		1:10	100	-				68.43	Channel
#6		1:10	-	16	-	-		27.65 - 24.87[3]	Plate reader
#7		1:3	-	14.4	1.6	0.01		70.00	Plate Reader

The experimental conditions for liposomal dispersions are reported together with its corresponding fluidic parameters, chemical formulation, encapsulation efficiency (EE%) and the drug release test platform respectively. Flow rate ratio (FRR) is defined as the ratio between the inlet volumetric flow rates of water (or AgNP dispersion) and the ethanolic lipid solution, and TFR as the total volumetric flow rate (i.e. the sum of ethanol and water (or AgNP dispersion) flow rates). [1]Batch code given represents the number of the produced liposomal dispersion batch along with its fluidic parameters, chemical formulation, and the separation method. [2]Given parameters represent the amount of the phospholipid (phosphatidylcholine soybean (P90G) or dipalmitoylphosphatidylcholine (DPPC)), stabilizer (octadecylamine (ODA)), or polyoxyethylene (40) stearate (PEG-40) in the liposomal dispersions, reported in millimolar (mM) concentration. [3]Represents two liposomal dispersions as Lipo/Rho and Lipo/Rho/SNP, and accordingly the EE% was given for two samples, respectively.

4.2.5 Separation of unencapsulated Rho or SNPs

Separation of unencapsulated Rho was performed by using dialysis bags with 12KD. Dialysis Kit 12KD was obtained from Medicell Membranes Ltd (London, UK). The sample and dialysate volume was changed at either 2 mL or 300-400 mL, respectively. The dialysis was performed for 3 days long. The encapsulation efficiency (EE%) of Rho was calculated by using the formula below (**Eq.3**). The amount of unencapsulated Rho was obtained by measuring the absorbance and fluorescence intensity of the solution. The correlations between the measurement and the concentration are shown in **Figure 49A**. The correlation equations shown in the figures were used for the calculation of the amount of unencapsulated Rho in the dialysate when calculating the EE%.

$$EE\% = \frac{\text{Total amount of Rho} - \text{unencapsulated Rho}}{\text{Total amount of Rho}}\ x\ 100\% \qquad \textbf{(Eq. 3)}$$

The measurement of absorbance and fluorescence intensity was performed using a FLUOstar Omega plate reader from BMG LABTECH (Aylesbury, UK). The concentration curve plots of rhodamine shown below were based on absorbance and fluorescence intensity, respectively.

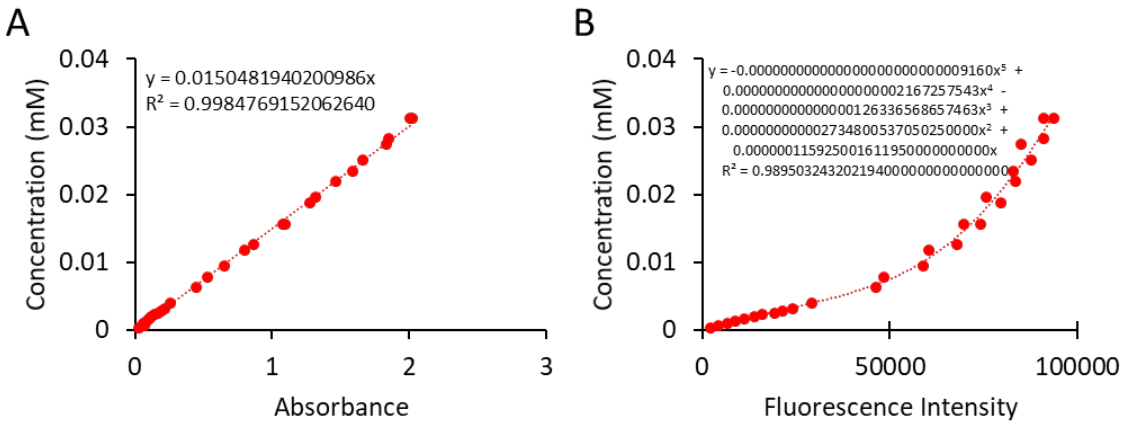

Figure 49 The concentration curve of Rho based on (A) absorbance and (B) fluorescence intensity.

However, the separation of unencapsulated SNPs was not performed as an efficient procedure could not be obtained, as discussed in the previous chapter. Therefore, experiments for drug release were performed by using dispersions including both encapsulated and unencapsulated SNPs in the dispersion.

The Rho was used here as a hydrophilic model drug to investigate drug release from different liposomal formulations. Additionally, PEG-40 was included in the liposome composition as a stabilizing agent. Besides, the drug release experiments were performed on the same day just after the separation process to decrease the effect of possible Rho leakage. Also, it must be noted that the obtained liposomal sample after separation of unencapsulated Rho was observed as having a bright pink colour, and there was no increase in fluorescence intensity levels after 3 days even if the sample was placed in complete fresh buffer. Based on the aforementioned considerations, it was believed that the leakage of Rho was at a negligible level during the experiments.

4.2.6 Characterization of liposomal dispersions with dual encapsulation

4.2.6.1 Size distribution and zeta potential measurements

The size distribution and zeta potential of the liposomal dispersions were characterised by Dynamic Light Scattering (DLS) technique, using a Zetasizer Nano ZS (Malvern Instruments Ltd., Malvern, UK). The measurements were performed at 25 °C, using polystyrene semi-micro (Fisherbrand™ FB55147, Fisher Scientific, Loughborough, UK) cuvettes and folded capillary cell (DTS1070, Malvern Instruments Ltd., Malvern, UK) type cuvettes, respectively. Samples used for size measurements had a volume of 1 mL (without dilution). Viscosity values used for DLS measurements were

calculated using the Zetasizer Software 7.12, by considering the effects of different FRRs or VRs on the fluid's viscosity (see paragraph **2.2.4.1**) [167].

Evaluations of the liposomal size distribution were carried out by considering the intensity-based distributions, as recommended in the ISO 13321 and ISO 22412 [168, 195]. Please refer to paragraph **3.2.6.1** for detailed information.

4.2.6.2 TEM imaging

The synthesized liposomal dispersions were imaged using transmission electron microscopy (TEM) technique; 5 µL of the sample was placed on a carbon-coated grid and allowed to adsorb for 30 s, and any excess amount was removed with a filter paper (Whatman). Samples including liposomes were negatively stained by adding 5 µL of 5% ammonium molybdate containing 1% trehalose on the grid (for 30 s), and the excess amount was again removed using a filter paper. TEM images were taken using the Tecnai T12 (FEI, Hillsboro, OR, USA). The characterization of SNP samples using TEM was performed following the same protocol, but without the negative staining step.

4.2.6.3 Theoretical calculation of drug release

Experiments to evaluate the drug release performance using a fluorescent microscope (EVOS M5000 Imaging System from Fisher Scientific, Loughborough, UK) were performed on agarose-made gel platforms. Agarose gels (%2 w/v) were prepared in HEPES (20 mM, pH 7.4). Prepared gel solution was poured in a mould (**Figure 50A & B**) having cylindrical holes. The resultant gel based platforms (**Figure 50C**) were in a form of cylinder (height: 45 mm, radius: 10 mm) containing spaces in the centre-top (height: 5 mm, radius: 3 mm). 15 µl of the sample (Lipo/Rho or Lipo/Rho/SNP) to be used for the drug release was placed in the space on the top-centre (**Figure 50D**). The gel based platform was imaged every minute for 10 minutes under a fluorescent microscope as shown in **Figure 51**. In the case of the illumination based experiment the gel based platform was illuminated with a laser module (50 mW, 650 nm, energy flux was calculated as 0.71 W/cm^2). Additionally, the same experiment was performed by placing the sample in the centre of the millifluidic channel under the fluorescent microscope, where the illumination was performed from side for different durations.

The drug release results are given in section 4.3.3, and the normalized data are given in section 6.2 for each experiment. The normalization was performed to observe the relative change compared to the baseline. The data were obtained by subtracting the initial value from the measured value for each measured value and dividing the obtained result by the initial value. This approach was used to observe whether there was an effect of illumination on drug release by setting the initial value to zero.

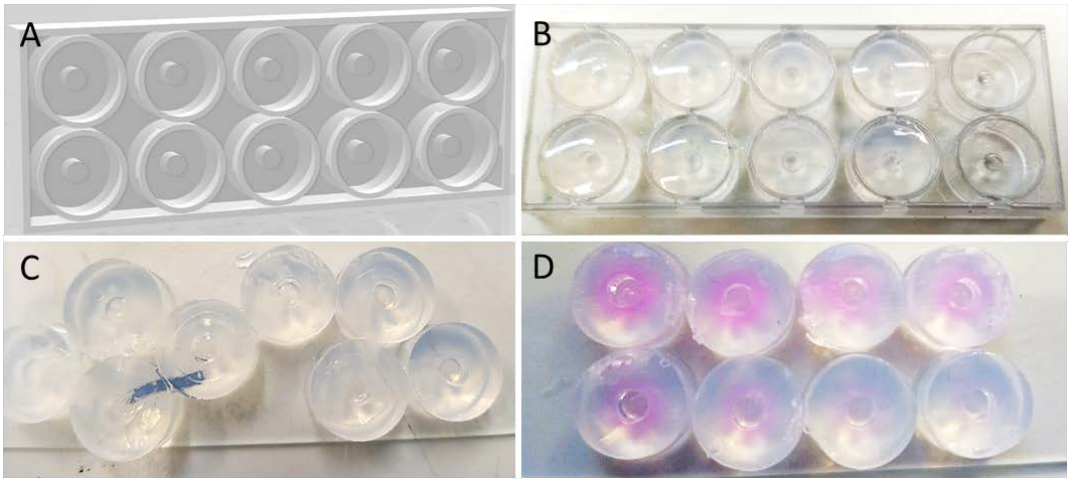

Figure 50 (A) The illustration of the mould used for the preparation of gel based platforms for drug delivery. The mould filled up with agarose gel (B), and after solidification the gel platforms were placed on a microscope slide (C). The relevant sample was placed on the space of the gel platform (D) and microscope slide placed under the fluorescent microscope for the experiment.

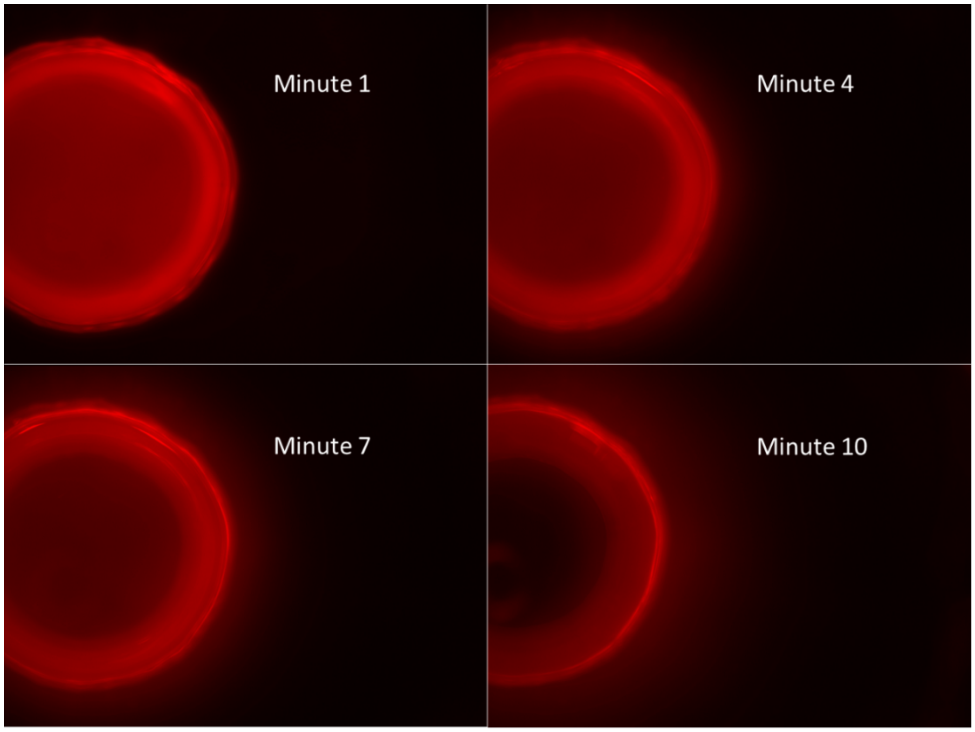

Figure 51 Representative images of gel based platform under illumination. The Lipo/Rho or Lipo/Rho/SNP sample was placed in the space on the top of the gel based platform. In the first image (Minute 1) the fluorescence image of the sample indicates no diffusion, i.e. not released, while the rhodamine diffusion as a result of release can be clearly seen in the final image (Minute 10).

Drug release performance was also evaluated by measuring the fluorescence of the samples using a plate reader (FLUOstar Omega plate reader from BMG LABTECH, Aylesbury, UK). The protocol was followed as reported previously [227], with minor modifications. 500 µL of Lipo/Rho or Lipo/Rho/SNP samples were mixed with 1500 µL of HEPES buffer. These dispersions were placed in a water bath at 42 °C. At different time points (0, 5, 15, and 20 minutes), 200 µL of the dispersions was withdrawn and placed in ice water. 50 µL of these samples were mixed with 150 µL of buffer, and measured for fluorescence using a plate reader. For the laser illumination test, 200 µL of the samples were placed in a 96 well-microplate (Fisher Scientific, Loughborough, UK) separately. The samples were illuminated with a laser from top, and 12.5 µL of the sample was withdrawn at different time points (0, 2.5, 5, and 10 minutes), and placed in ice water. Those samples were mixed with 187.5 µL of buffer separately and the florescence intensities were measured. The formula used for calculating the drug release efficiency (EE%) is shown below [227-229]. The total fluorescence intensity was measured after adding 0.1% Triton X-100.

$$EE\% = \frac{\text{fluoescence intensity at different time points} - \text{fluorescence intensity at minute 0}}{\text{Total fluorescence intensity} - \text{fluorescence intensity at minute 0}}\ x\ 100\% \qquad \textbf{(Eq. 4)}$$

4.3 Results and Discussion

4.3.1 Methodological Rationale

It was reported that DPPC based liposomes can go through a phase change at 42 °C [183], and the lipid layers may allow for the release of encapsulated material. Based on this information, it was hypothesized that DPPC liposomes encapsulating SNPs compared to those that did not encapsulate SNPs, would reach the phase transition temperature of 42 °C faster under a laser beam due to the SPR and resulting photothermal effect. For the evaluation of the hypothesis, the experiments were designed as follows.

Firstly, the liposomal dispersions with or without Rho and SNPs that were synthesized using neutral and positively charged lipids were characterized with DLS and TEM, for the evaluation of dimensional characteristics along with the encapsulation of SNPs. Secondly, the drug release experiments were performed by measuring the fluorescence change using either a plate reader, or a gel based platform under a fluorescent microscope after the illumination of the samples using a laser. The rationale behind applying positively charged liposomes was based on the potential interactions between negatively charged SNPs and positively liposomes, that could provide higher encapsulation of SNPs.

4.3.2 Dimensional properties of liposomal dispersions

The samples of Lipo/Rho and Lipo/Rho/SNP were synthesized using different lipid compositions and were characterised with DLS after the purification. The results of size distribution and zeta potential measurements are shown in **Figure 52**. For the experimental conditions please refer to **Table 6** (batch code #1).

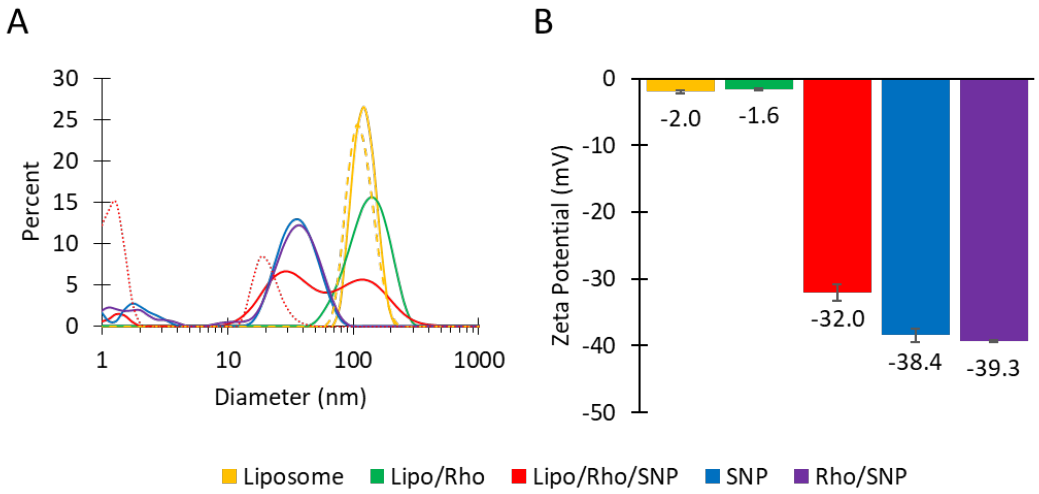

Figure 52 (A) Size distribution plots and (B) zeta potential values of negatively charged liposome, SNP and Lipo/SNP samples. The solid and dotted lines represent the size distributions for intensity and number respectively. Liposomal samples comprised of PC (16 mM) and were produced using the millifluidic reactor, at total flow rate (TFR) = 1 ml/min and flow rate ratio (FRR, aqueous phase/ethanolic lipid solution) = 10. For the experimental conditions please refer to **Table 6** (batch code #1).

As seen in **Figure 52A** the liposome and Lipo/Rho sample showed similar peak values at ~130 and 150 nm, respectively. However, Lipo/Rho/SNP sample showed two peaks with comparable heights at ~25 and 130 nm, which possibly indicating unencapsulated free SNPs and liposomes (interacted with SNPs), respectively. The zeta potential values (**Figure 52B**), showed that liposomes and Lipo/Rho samples were almost having zero surface charge, but the Lipo/Rho/SNP sample showed a value of -32 mV which was similar to the value of SNPs (-38.4 mV). The addition of Rho did not affect significantly the size distribution or the zeta potential values of the dispersions. These findings might indicate a possible adherence between liposomes and SNPs, resulted in a complex with higher zeta potential value in terms of stability. On the other hand, the existence of the second peak for Lipo/Rho/SNP sample at ~130 nm supported this assumption. Here, the interpretation was made on the hypothesis that, despite the high amount of SNPs, a peak that could be observed at ~120 nm was most likely the result of the incorporation of some of the SNPs with liposomes. The

encapsulation of SNPs in liposomes when using PC lipids was also confirmed with findings in paragraphs **3.2.6.2** and **3.2.6.3.**

As a different lipid composition, the characterization of the liposomal dispersions synthesized using positively charged lipids with DLS is shown in **Figure 53A**.

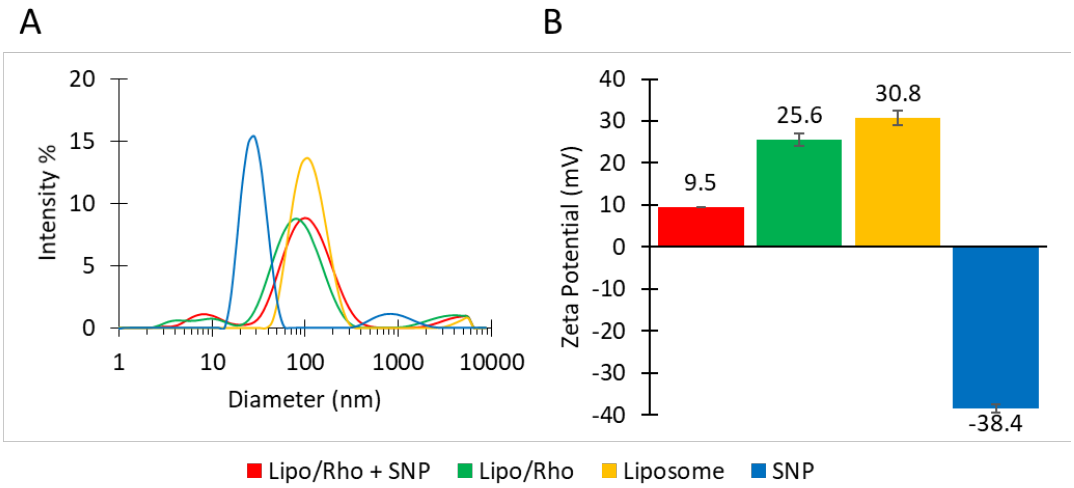

Figure 53 (A) Size distribution plots and (B) zeta potential values of negatively charged liposome, SNP and Lipo/SNP samples. The solid line and dotted line represent the size distributions for intensity and number respectively. Liposomal samples comprised of DPPC/ODA/PEG-40 (12.8:1.6:1.6 mM) and were produced using the millifluidic reactor, at total flow rate (TFR) = 1 ml/min and flow rate ratio (FRR, aqueous phase/ethanolic lipid solution) = 10. For the experimental conditions please refer to **Table 6** (batch code #2).

The peak heights of liposomes, Lipo/Rho and Lipo/Rho+SNP samples were around 90, 90 and 70 nm respectively, as shown in **Figure 53A**. Here, it must be noted that the SNPs were mixed with the Lipo/Rho sample after the purification. The assumption here for this approach was based on the potential interaction between the negatively charged SNPs and positively charged liposomes, as suggested in previous studies [222]. According to the size distribution plots, the addition of SNPs shifted the peak of Lipo/Rho and increased the diameter. However, there occurred a second peak at ~10 nm which was possibly indicating the unencapsulated free SNPs, in line with that observed in **Figure 52A**. One possible explanation for the increase could be that the addition or the attachment of the SNPs onto the liposome layer, resulting in a liposome vesicle surrounded by SNPs that would have relatively higher hydrodynamic radius. The addition of SNPs into Lipo/Rho sample also changed the zeta potential significantly. As can be seen in **Figure 53B**, the zeta potential value of Lipo/Rho (25.6 mV) decreased to 9.5 mV (Lipo/Rho+SNP sample) with the addition of SNPs, suggesting that a possible adherence between SNPs and liposomes.

Additionally, the Lipo/Rho+SNP sample, along with liposomes and SNPs were imaged by TEM, and the result are shown in **Figure 54.**

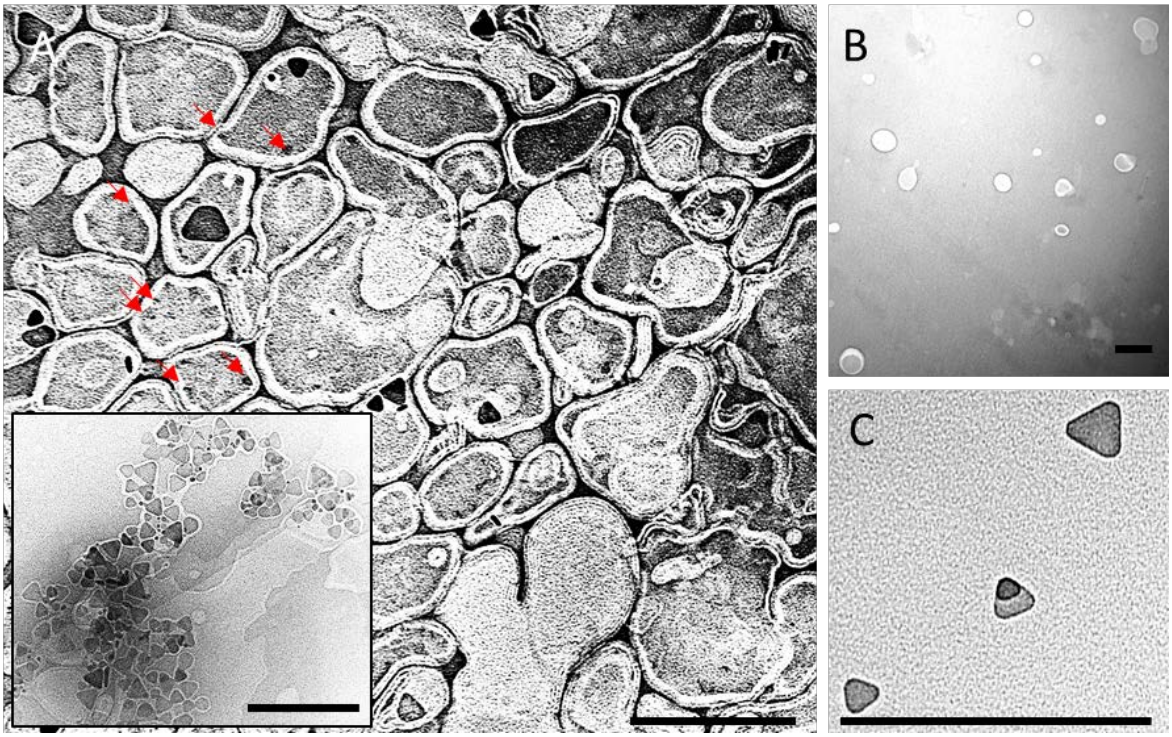

Figure 54 TEM images of (A) Lipo/Rho+SNP, (B) liposome and (C) SNP samples. Presented sections were selected from the different images of the same sample. Bright circular structures and dark structures (mainly triangular shaped) represent liposomes and SNPs, respectively. Liposomal samples comprised of DPPC/ODA/PEG-40 (12.8:1.6:1.6 mM) and were produced using the millifluidic reactor, at total flow rate (TFR) = 1 ml/min and flow rate ratio (FRR, aqueous phase/ethanolic lipid solution) = 10. For the experimental conditions please refer to **Table 6** (batch code #2). Arrows show the location of some AgNPs in the liposomes.

Figure 54A, B & C show the selected images belonging to the Lipo/Rho+SNP, liposome and SNP samples. The structures of liposomes and SNPs were observed as expected, being similar to the images obtained from different samples (see **Figure 23**, **Figure 44**). However, the structure of Lipo/Rho+SNP samples appeared to be interwoven between liposomes. Additionally, the structure of liposomes was observed as far from being round, and the layer of liposome size was observed as more pronounced compared to the images obtained for other samples.

The difference in layer could be related to the composition of the lipid mixture used in the synthesis. The unround shape of liposomes might be due to an error in the experimental procedure when preparing the sample for TEM process, or the location of SNPs. In **Figure 54A**, SNPs can be seen to be embedded in the walls of the liposome, as achieved with the highest contrast. Relatively small

darker structures were thought to be SNPs as some of them was also had triangular form. This finding supported the assumption of a potential interaction between the SNPs and the positively charged liposomes. The embedding of SNPs in liposomes could be the reason for the change in liposome shape, that needs further investigation with repetitive trials.

On the other hand, the inset showed that the interaction between SNPs and positively charged lipids also resulted in SNPs being covered by a lipid layer Furthermore, this interaction could cause the form of aggregates composed of lipid covered SNPs. Overall, the TEM image of Lipo/Rho+SNP sample confirmed the encapsulation of SNPs in liposomes.

4.3.3 Evaluation of drug release performance

The evaluation of drug release performance was carried out by using the agarose made gel platform. The experiment was performed by comparing the release of Rho in the gel for the liposomal dispersions of SNP loaded and Rho/SNP dual loaded, with or without the laser illumination. Presented data was also shown as rescaled to be able to compare the relative change to the baseline [230, 231] (**Figure S3A**), that was also referred to in discussion below. The first experiment was performed with a laser illumination from the top for 45 seconds for liposomal dispersions synthesized using PC lipids, and the results were shown in **Figure 55**.

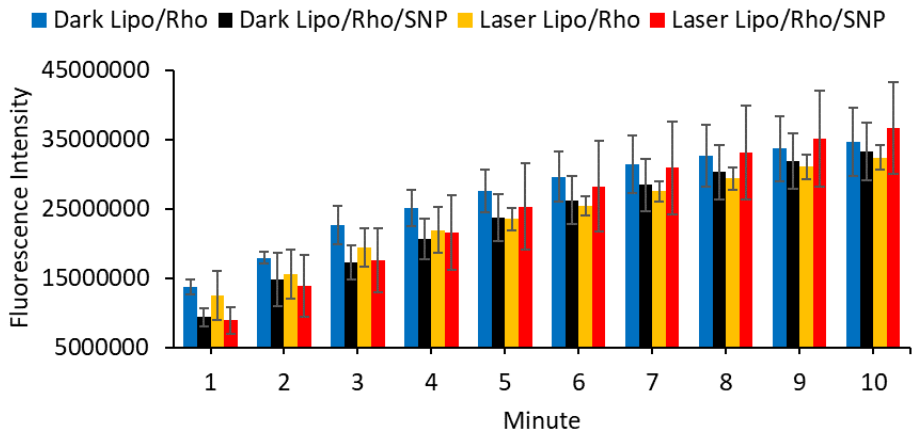

Figure 55 The fluorescence intensity change during drug release in an agarose gel based platform for 10 minutes. The laser illumination was performed for between 5 and 50 seconds, which was then followed by capturing image for each minute using a fluorescence microscope. Liposomal samples comprised of PC (16 mM) and were produced using the millifluidic reactor, at total flow rate (TFR) = 1 ml/min and flow rate ratio (FRR, aqueous phase/ethanolic lipid solution) = 10. For the experimental conditions please refer to **Table 6** (batch code #1).

Figure 55 shows the measured fluorescence intensity for 10 minutes for the samples. The Rho release over time showed that there was no statistically significant difference for different samples. This was expected as the lipid type used here (PC) had a phase of liquid crystalline at room temperature, so that the relatively faster drug release via illumination for samples including SNPs could not be observed. However, the normalized data showed that the increasing trend over time was relatively higher for Lipo/Rho/SNP samples ($p > 0.05$) (**Figure S3A**). This suggested that the existence of SNPs in the dispersion might have affected the release of Rho, or the fluorescence characteristics of Rho.

The second experiment was performed with the samples synthesized by using the positively charged lipids. Similarly to the previous experiment, the gel was illuminated from the top for 45 seconds and the fluorescent images of the gel under the fluorescent microscope was captured for 10 minutes. For this experiment, only the samples including SNPs were tested with or without illumination, the results were shown in **Figure 56**. For the experimental conditions please refer to **Table 6** (batch code #2).

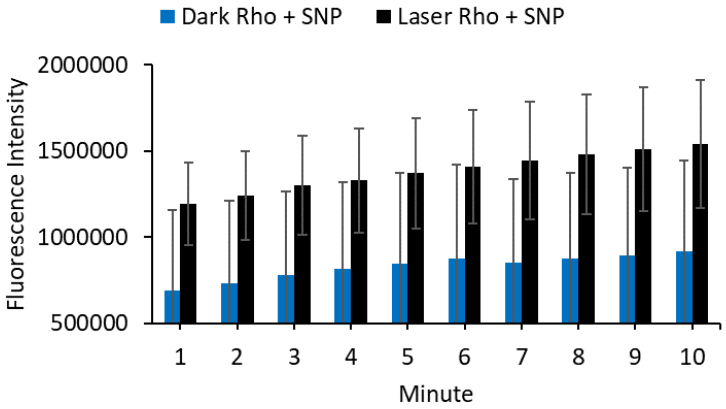

Figure 56 The fluorescence intensity change during drug release in an agarose gel based platform for 10 minutes. The laser illumination was performed for between 5 and 50 seconds, which was then followed by capturing image for each minute using a fluorescence microscope. Liposomal samples comprised of DPPC/ODA/PEG-40 (12.8:1.6:1.6 mM) and were produced using the millifluidic reactor, at total flow rate (TFR) = 1 ml/min and flow rate ratio (FRR, aqueous phase/ethanolic lipid solution) = 10. For the experimental conditions please refer to **Table 6** (batch code #2).

Figure 56 shows the measured fluorescence intensity of Rho release over time for 10 minutes for the samples of Lipo/Rho/SNP with or without laser illumination. It was observed that the fluorescence intensity for illuminated sample was much higher than the not illuminated one. However, the increase in trend was similar for both samples as seen in the normalized data ($p >$

0.05) (**Figure S3B)**. This showed that the initial release of Rho for the illuminated sample was much higher, that is, the Rho release occurred for the first minute during the illumination, and the measured fluorescence intensity for the first minute was higher. However, an increase in fluorescence over time in addition to the first burst release was not observed. One reason for that could be the phase transition from gel to crystalline upon illumination has occurred and accordingly, the burst release of Rho has been observed. However, when the illumination stopped after 45 seconds, the phase transition occurred from crystalline to gel and the liposome layers switched off so that the Rho release stopped. On the other hand, the reason why the burst release did not increase the measured fluorescence intensity over time remains unclear.

The final experiment for the drug release test using gel based platform was performed for liposomal dispersions synthesized using positively charged lipids similar to the previous experiment. Differently, the experiment was performed for samples of SNP loaded and Rho/SNP dual loaded, with or without the laser illumination, with illumination for 10 minutes, and the results were shown in **Figure 57**. For the experimental conditions please refer to **Table 6** (batch code #6).

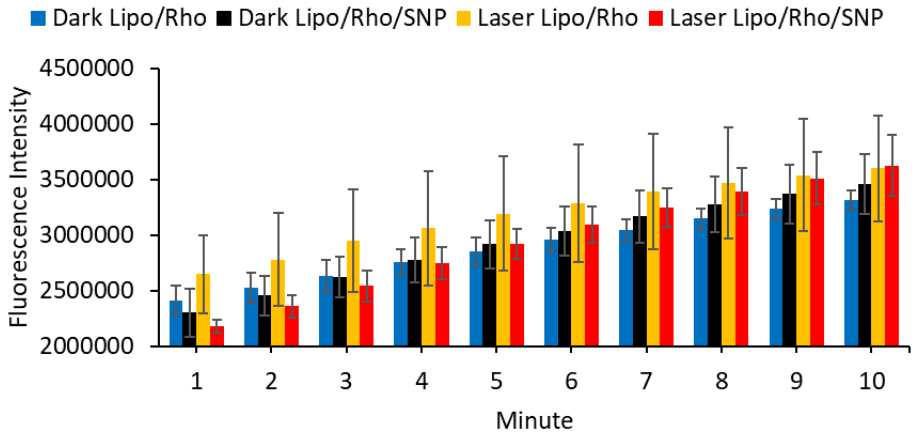

Figure 57 The fluorescence intensity change during drug release in an agarose gel based platform for 10 minutes. The laser illumination was performed for between 5 and 50 seconds, which was then followed by capturing an image for each minute using a fluorescence microscope. Liposomal samples comprised of DPPC (16 mM) and were produced using the millifluidic reactor, at total flow rate (TFR) = 1 ml/min and flow rate ratio (FRR, aqueous phase/ethanolic lipid solution) = 10. For the experimental conditions please refer to **Table 6** (batch code #6).

Figure 57 shows the fluorescence intensity over time for different liposomal dispersions in dark or under laser illumination for 10 minutes. The final fluorescence intensity over time was observed as not significantly different from each other. However, the trend in increase in normalized data for Lipo/Rho/SNP sample was observed as relatively higher compared to other samples (**Figure S3C)**. However, considering the previous observation, there was no significant increase observed for

illuminated Lipo/Rho/SNP sample comparing to the dark one ($p > 0.05$). However, the samples including SNPs was found to result in higher levels of Rho release.

Overall, a possible explanation for that could be the effect of SNP existence in liposomes causing drug release, considering the properties of Rho fluorescence under different temperatures. The temperature increase due to the SPR effect of SNPs caused the liposome layer to a phase change from gel to crystalline resulting in burst Rho release as seen in **Figure 56**, although the exact temperature was practically difficult to measure *in situ*. When the illumination stopped the phase of liposome layer changed into the gel and the Rho release stopped. A similar effect was not observed in **Figure 57**, because the temperature kept high during the test since the illumination was performed for 10 minutes, and this might have resulted in a miscalculation of the measured fluorescence intensity. The decrease in fluorescence levels of Rho when the temperature increased was shown in the literature [232]. The relatively higher trend in increase observed for the samples including SNPs also could be caused by the SNPs existence creating gaps in the liposome layers because of the edge tips arising from the triangular shape that could have increased the Rho escape. However, the mentioned explanations need to investigate with further repetitive experiments.

The drug release test also performed by placing the liposomal dispersions in the centre of millifluidic channel. The illumination was performed for different duration times and the images were captured for the Rho release under a fluorescent microscope. The results are shown in **Figure 58**. For the experimental conditions please refer to **Table 6** (batch code #2, #3, #4, #2, #3 and #5 for the plots respectively).

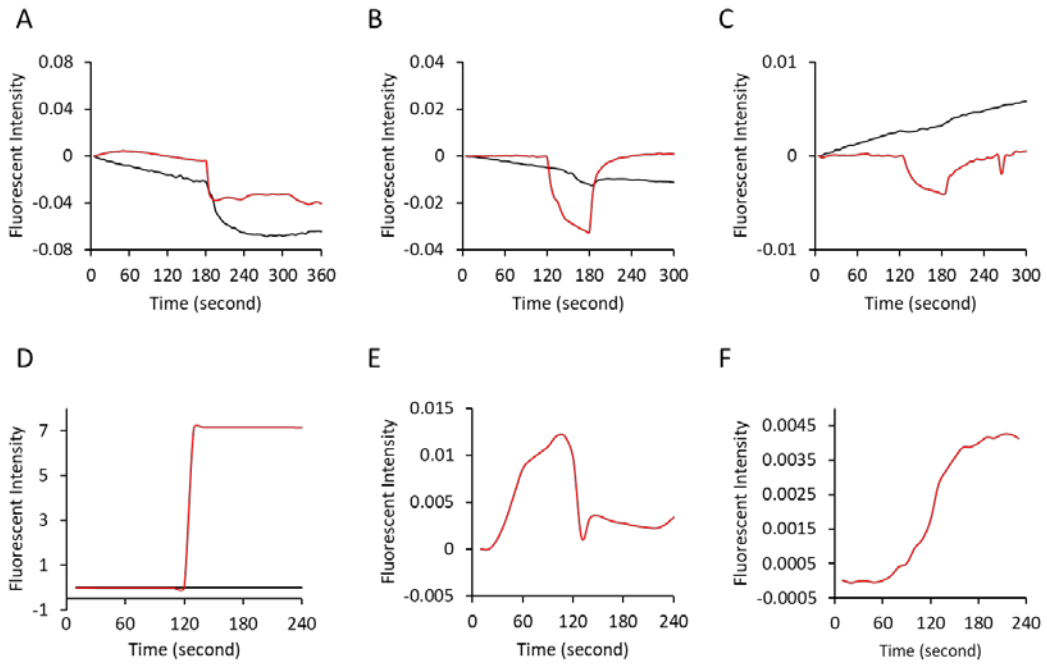

Figure 58 The normalized fluorescence intensity of drug release in a millifluidic channel over time. Liposomal samples comprised of DPPC/ODA/PEG-40 (12.8:1.6:1.6 mM), PC/ODA/PEG-40 (12.8:1.6:1.6 mM), PC/ODA/PEG-40 (90:5:5 mM), DPPC/ODA/PEG-40 (12.8:1.6:1.6 mM), PC/ODA/PEG-40 (12.8:1.6:1.6 mM), PC (100 mM) and were produced using the millifluidic reactor, at total flow rate (TFR) = 1 ml/min and flow rate ratio (FRR, aqueous phase/ethanolic lipid solution) = 10. For the experimental conditions please refer to **Table 6** (batch code #2, #3, #4, #2, #3 and #5 respectively). The red and black lines represent the samples of Lipo/Rho and Lipo/Rho/SNP.

Figure 58 shows the measured fluorescence intensity over time for different samples under different illumination parameters for samples of Lipo/Rho (red curves) and Lipo/Rho/SNP (black curves). The fluorescence intensity in **Figure 58A** was calculated from the images captured every 5 seconds for 6 minutes, where the illumination was performed for only 1 minute after 3 minutes passed. For the plots in **Figure 58B & C**, the measurement was performed for 5 minutes and images were captured every 5 seconds, where the illumination was performed for 1 minute, after two minutes passed. For the plots in **Figure 58D, E & C**, the images were captured every 10 seconds and the samples were illuminated for 2 minutes, after 2 minutes passed.

As shown in the figure, the measured fluorescent intensity after illumination was found as relatively higher in DPPC based liposomal dispersions including SNPs comparing to the ones that were not including SNPs (**Figure 58A & D**). However, in **Figure 58B & C,** following the illumination, an increase in Lipo/Rho/SNP sample and an increase in the Lipo/Rho sample were observed in terms of fluorescence levels, respectively. In **Figure 58E & F**, upon illumination, samples showed a

decrease and an increase in fluorescent levels, respectively. Overall, the inconsistent data, as described above, showed that the technique used was not effective in understanding drug release behaviour upon illumination, and therefore the technique was found not useful.

Finally, the drug release performance was tested by measuring the fluorescence intensity of the samples using a plate reader. The measurement was performed at 42 °C and upon laser illumination, for the DPPC based neutral samples of Lipo/Rho and Lipo/Rho/SNP. The results were shown in **Figure 59**. For the experimental conditions please refer to **Table 6** (batch code #7).

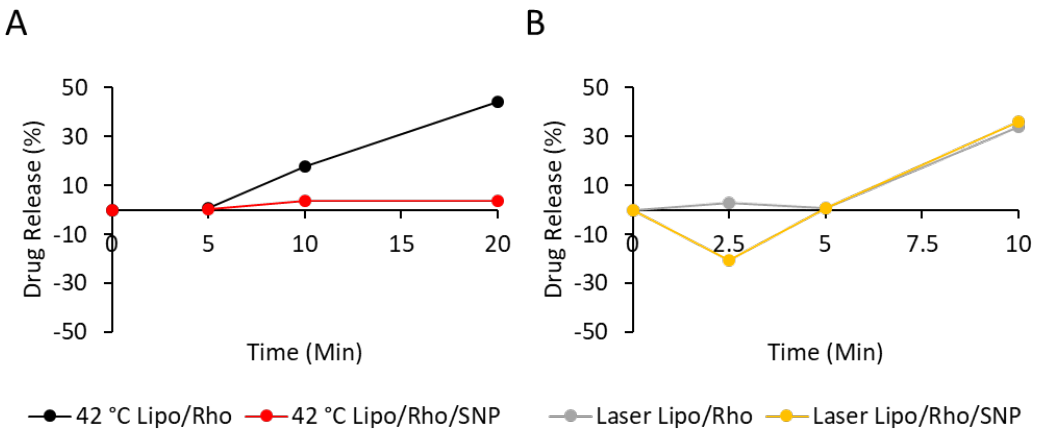

Figure 59 The release of Rho over time (A) at 42 °C and (B) upon laser illumination. Liposomal samples comprised of DPPC (16 mM) and were produced using the millifluidic reactor, at total flow rate (TFR) = 1 ml/min and flow rate ratio (FRR, aqueous phase/ethanolic lipid solution) = 10. For the experimental conditions please refer to **Table 6** (batch code #6).

Figure 59A & **B** shows the drug release for Lipo/Rho and Lipo/Rho/SNP samples at 42 °C and upon laser illumination respectively. At 42 °C, the Rho release was observed started after minute 5 and for Lipo/Rho/SNP and Lipo/Rho samples. At 20 minutes, the release of Rho was at ~50% for Lipo/Rho, but at the same duration, the release for Lipo/Rho/SNP was at ~3%. For the laser illumination, the release was at ~45% for both samples for 10 minutes' duration which was higher than observed at 42 °C. The Rho release in Lipo/Rho sample was observed as much higher comparing to Lipo/Rho/SNP sample at 42 °C; however, the Rho release was similar under laser illumination for both samples. The relatively lower release in Lipo/Rho/SNP sample must be investigated with further experiments. However, a possible explanation could be the blockage of fluorescence by SNPs, when the amount of Rho was low (i.e. EE%: ~25%) in the sample.

A further experiment was performed by positively charged DPPC based liposomes. Results were shown in **Figure 60**.

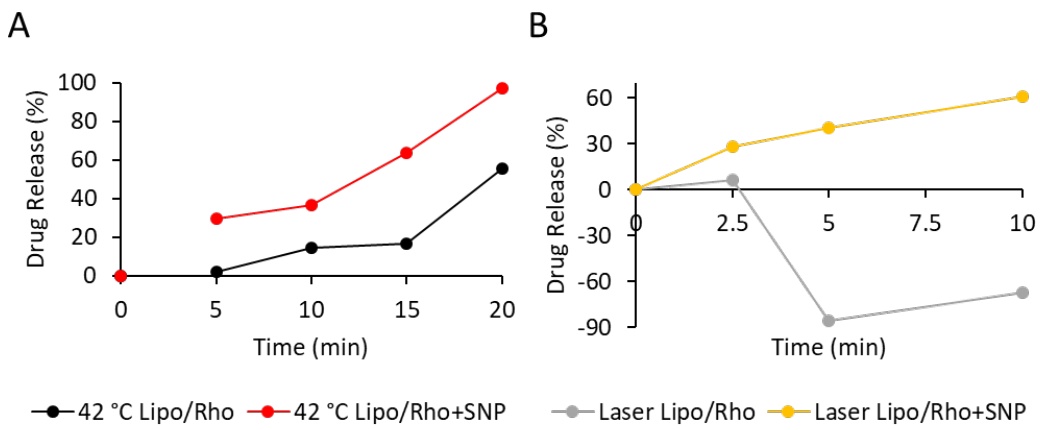

Figure 60 The release of Rho over time (A) at 42 °C and (B) upon laser illumination. Liposomal samples comprised of DPPC/ODA/PEG-40 (14.4:1.6:1.6 mM) and were produced using the millifluidic reactor, at total flow rate (TFR) = 1 ml/min and flow rate ratio (FRR, aqueous phase/ethanolic lipid solution) = 3. For the experimental conditions please refer to **Table 6** (batch code #7).

Figure 60A & **B** shows the drug release for Lipo/Rho and Lipo/Rho+SNP samples at 42 °C and upon laser illumination respectively. At 42 °C, the Rho release was observed starting at minute 5 and at minute 10 for Lipo/Rho+SNP and Lipo/Rho respectively. At 20 minutes, the release of Rho was almost completed for Lipo/Rho+SNP, but at the same duration, the release for Lipo/Rho was at ~60%. For the laser illumination, the release was at ~60% for the Lipo/Rho+SNP for 10 minutes' duration which was higher than that observed at 42 °C. Interestingly, the Rho release upon illumination for Lipo/Rho was calculated as negative, and the reason was unclear.

At 42 °C, the higher Rho release in Lipo/Rho/SNP was thought to be due to the small gaps in the liposome layers because of the edge tips of the encapsulated SNPs (**Figure 54**) leading to release of Rho. On the other hand, the relatively higher Rho release upon illumination observed in the Lipo/Rho+SNP sample supported the hypothesis that SNPs caused an increase in local temperature due to the SPR effect upon illumination, resulting in a gel-to-crystalline phase change of the liposome layers and, consequently, release of Rho.

Comparing to the previous findings (**Figure 59**), the release of Rho was almost similar in Lipo/Rho samples at 42 °C, however, there was no Rho release observed in neutral Lipo/Rho/SNP sample. A possible reason could be related to the EE%, that was much higher in the positively charged sample (70%), comparing to the neutral liposomal sample (~25%). The Rho release upon laser illumination relatively higher in positively charged Lipo/Rho/SNP sample, which could be related to the higher EE%, or the higher encapsulated amount of SNPs due to positive and negative interactions. On the

other hand, interestingly the Rho release was calculated negative for experiments (i.e. under laser illumination at minute 2.5 for neutral Lipo/Rho/SNP, and at minute 5 and 10 for Lipo/Rho samples). This result remained unclear, but could be related to the effect of laser illumination.

4.4 Conclusions

The light induced drug release in thermosensitive liposomes has been a commonly used attractive method for pharmaceutical and theranostic applications [6, 11, 233]. However, studies on the use of SNPs that are encapsulated in liposomes have been limited in the literature. Here, this approach was experimentally performed on rhodamine and SNP dual loaded liposomes under laser illumination.

The encapsulation was demonstrated based on the data from DLS and TEM. Positively charged liposomal dispersions were found as inclined to have SNPs encapsulated due to the positive and negative interactions. The drug release experiments were performed on a gel based platform, in a millifluidic channel and a microplate, using fluorescent microscope and plate reader. The experiments in millifluidic channel were found to be ineffective in understanding the behaviour. However, experiments using the gel based platform showed that the samples including SNPs could provide relatively higher release, suggesting that the hypothesis of SNPs effect on the phase change on liposome layers was plausible. Additionally, this behaviour was further confirmed with the experiments performed on a microplate. However, not all the results could be fully explained or interpreted.

Overall, the study here showed that the SNPs could be encapsulated in liposomes (especially when using positively charged lipids), and the drug release upon illumination was relatively higher in samples containing SNPs. It was thought that with further experiments, the behaviour of SNPs under the effect of liposome phase change and thus drug release could be well explained and demonstrated. Its success could lead to the achievement of a drug delivery vehicle potentially be used for theranostic applications.

Chapter 5 Overall Conclusion and Future Work

5.1 Key Findings

Considering the aim and objectives of the PhD project, it can be concluded that; (i) the synthesis of size-controllable empty liposomes, and the synthesis of liposomes encapsulating a model drug (rhodamine) and AgNPs (alone or together) has been achieved in a continuous-flow millireactor; and (ii) the drug release ability of these liposomal dispersions has been evaluated under illumination. The conclusions from the experimental results detailed in previous chapters can be summarised as below.

The ability of the continuous-flow millireactor to achieve tunable production of liposomes by varying key operational parameters was demonstrated (production rates of up to 16.7 mg/min). Moreover, the millireactor has proven to be suitable for the production of liposomes with a size (~100 nm; dispersity < 0.2) that is compatible with medicinal liposomal formulations, and this was demonstrated for a spectrum of different formulations that included cholesterol, charged moieties, and PEG-40. Also, the synthesis of liposomal dispersions encapsulating Rho and SNPs was successfully performed using the continuous-flow millireactor.

The synthesis of SNP loaded liposomes was performed successfully and characterised using TEM, UV-Vis and DLS. Separation of unencapsulated SNPs was found challenging, although they were tested using different techniques, including centrifugation, gel filtration, and agglomeration, due to difficulties, such as the relatively large size of the NP and its shape containing sharp ends and edges. However, the SNP encapsulation in liposomes has been achieved in millifluidics-based production and could be demonstrated by imaging.

Drug release tests suggested that the photothermal effect of SNPs was promising, however additional techniques need to be further employed to acquire additional results that can demonstrate the photothermal effect of SNPs on the release of drugs from liposomes. It was thought that with further experiments, the behaviour of SNPs under the effect of liposome phase change, and thus drug release could be well explained and demonstrated.

As a novelty, this study demonstrated the synthesis of SNP loaded liposomes, as a potential theranostic agent in a continuous-flow millireactor. Moreover, the drug release profiles of developed thermosensitive liposomes encapsulating model drugs and SNPs via a photothermal drug release mechanism assisted by SPR, has been characterised successfully.

5.2 Future directions

Future studies may focus on a number of different factors including mass production liposomal dispersions, encapsulation of AgNPs in liposomes with different lipid compositions, synthesis of AgNPs within the liposomes, purification of liposomal dispersions in millifluidic chip by using a dialysis membrane. Also, the drug release performance could be investigated using a different model drug (e.g. calcein) or a well-known chemotherapeutic agent (e.g. doxorubicin) instead of Rho. Moreover, the drug release performance could be tested on cell cultures. Additionally, detailed temperature analysis could be performed to achieve a better understanding of the photothermal effect of the liposomal system.

The mass production of liposomes using millifluidic reactors can provide the industrial translation of this technology, that can be employed in mass production of pharmaceutical products that can be used in therapies. This could potentially be achieved through parallelisation of multiple millireactors, development of hydraulic supply units of greater capacity, or the evaluation of millifluidic devices comprising even larger architectures.

The employment of different compositions of lipids, especially higher amount of positively charged lipids, in liposomal dispersions could help to obtain a dispersion including only SNP loaded liposomes. Also, in terms of production, increasing the TFR could provide higher mixing, and accordingly a higher EE%.

As a different approach, the synthesis of AgNPs within liposomes could be performed, which could provide a dispersion without unencapsulated SNPs without the need for an extra purification step. This approach was already tested and initial results were provided in paragraph Error! Reference source not found. in the supplementary information. Results have shown that the synthesis of AgNPs in liposomes could be performed, and the liposomes can be used as a nanoreactor.

It was thought that the local temperature increase has affected the fluorescence intensity of Rho. Employment of a different model drug or a chemotherapeutic that insensitive to temperature changes could provide more reliable results in understanding the drug release behaviour. Also, as a commonly used approach, the release performance could be tested on cell cultures. This could also provide additional information on how the liposomal dispersions will interact with the cell membranes.

Finally, a detailed analysis of local temperature increase could be performed using thermal analysis and SEM on specifically prepared samples of SNPs and liposomes including SNPs, to evaluate the

temperature increase on a single SNP. This would potentially enable quantifying the temperature increase associated with different exposure times, laser powers and wavelengths, which would in turn help designing the experiment more effectively.

Chapter 6 Supplementary Information

6.1 Images used for the calculation of EE%

The images shown below were used for the calculation of EE% of SNPs in liposomes.

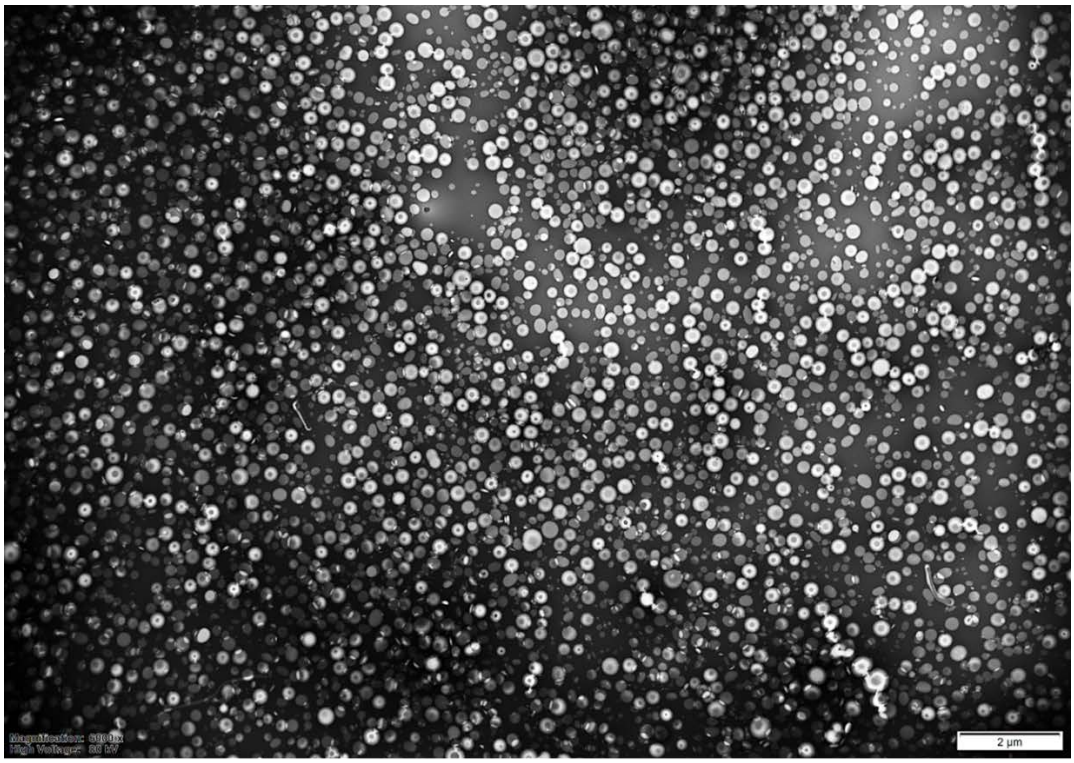

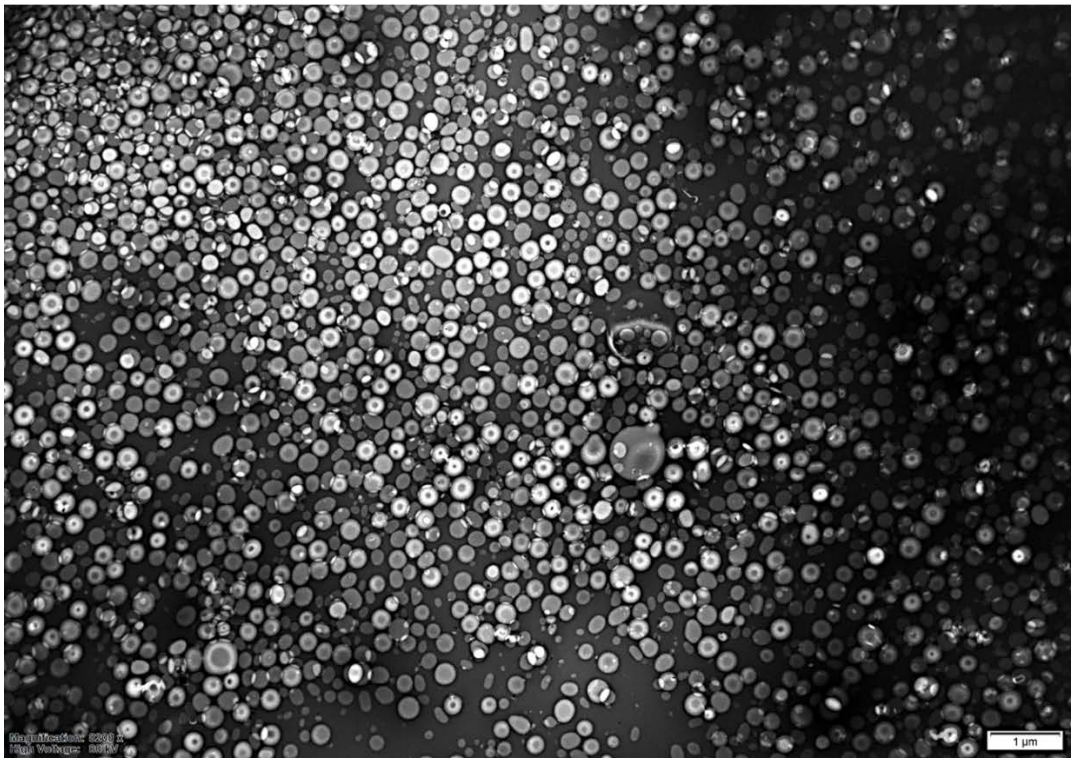

Figure S1 Raw TEM images of Lipo/SNP sample used for the calculation of encapsulation efficiency. Scale bars respectively: 2000 nm, 1000 nm.

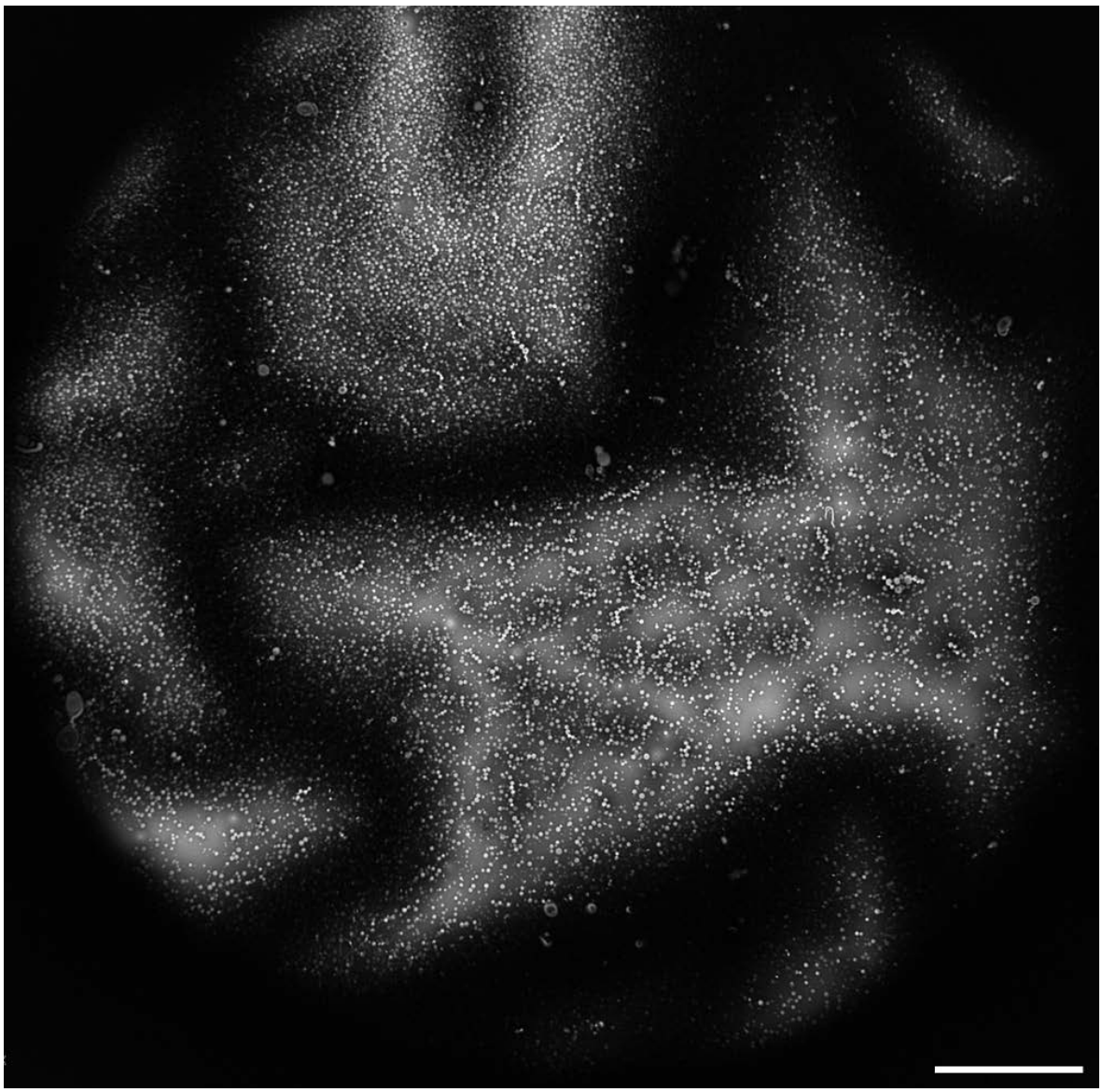

Figure S2 TEM image showing the selected section of the grid for the calculation of encapsulation efficiency. Scale bar: 10000 nm.

6.2 Rho Release upon Illumination

The normalized fluorescence intensity values observed for different samples of liposomal dispersions in drug release experiments were shown below in **Figure S3**.

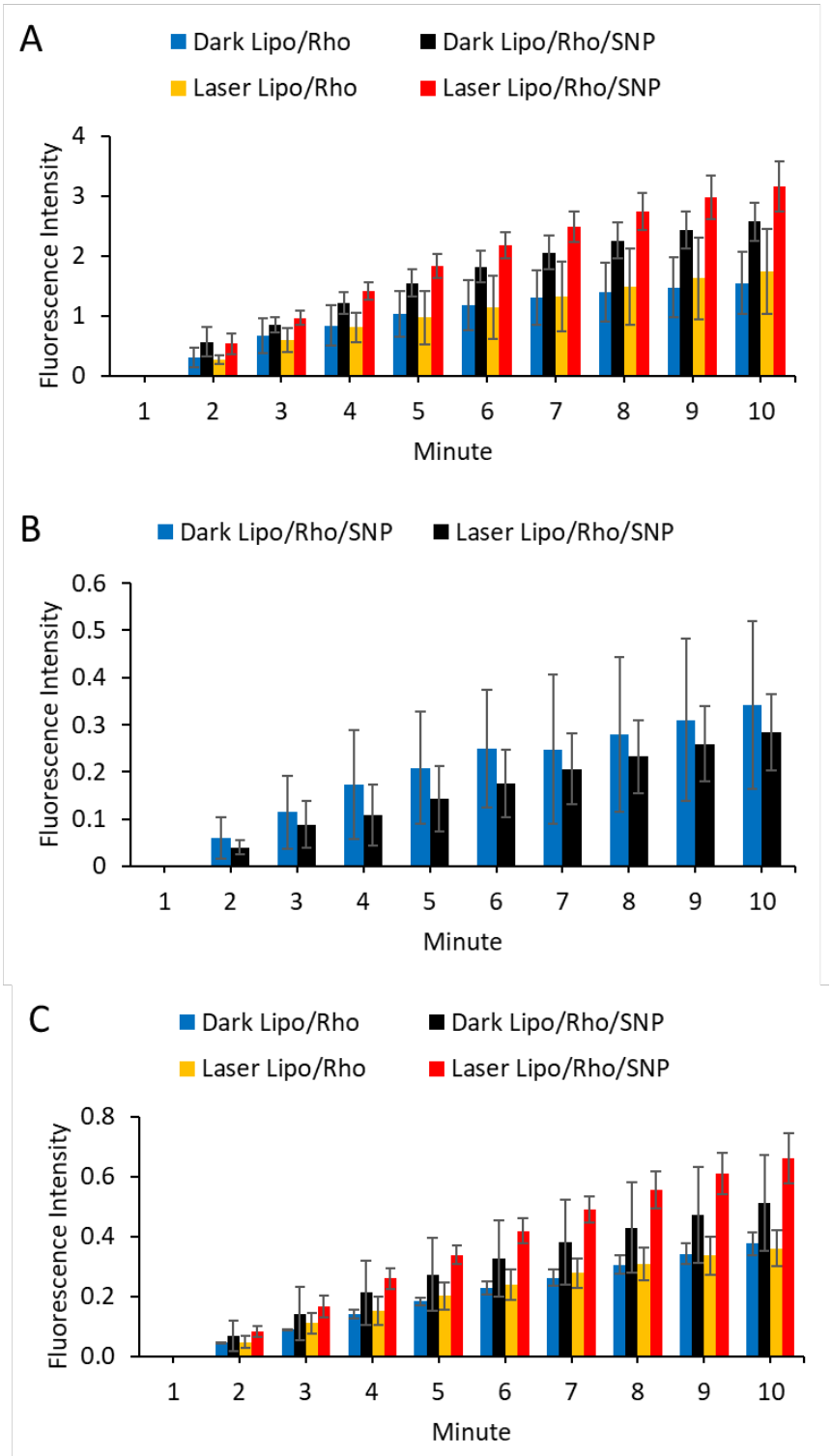

Figure S3 Normalized fluorescence intensity of the liposomal dispersions with or without laser illumination

6.3 Synthesis of SNSs in Liposomes

Because of the limitations in understanding the encapsulation in details due to the not complete separation of unencapsulated SNSs, it was performed to generate SNSs inside the liposome layers as a different approach. A different preparation method for the silver nanoparticles was followed for the generation of SNSs in the liposomes [234]. The procedure mentioned in the literature includes the addition of silver nitrate and an amino acid in a solution with proper amounts and illuminating the samples with Xenon light. It was demonstrated that mentioned method yields SNSs with a size around ranging from 15 to 30 nm [234].

Following the mentioned procedure in the literature [234], the dispersions of Lipo/AgNO3+Tryptone and AgNO3+Tryptone were prepared using Tryptone as an amino acid supplier. The experiment for liposomal dispersion was performed using millifluidic reactor with a TFR = 1 ml/min and FRR = 25, employing PC (100 mM) liposomes. After the illumination of the sample, colour change was observed in the vial to yellowish. Resultant samples were characterized only using TEM as shown in **Figure S4**.

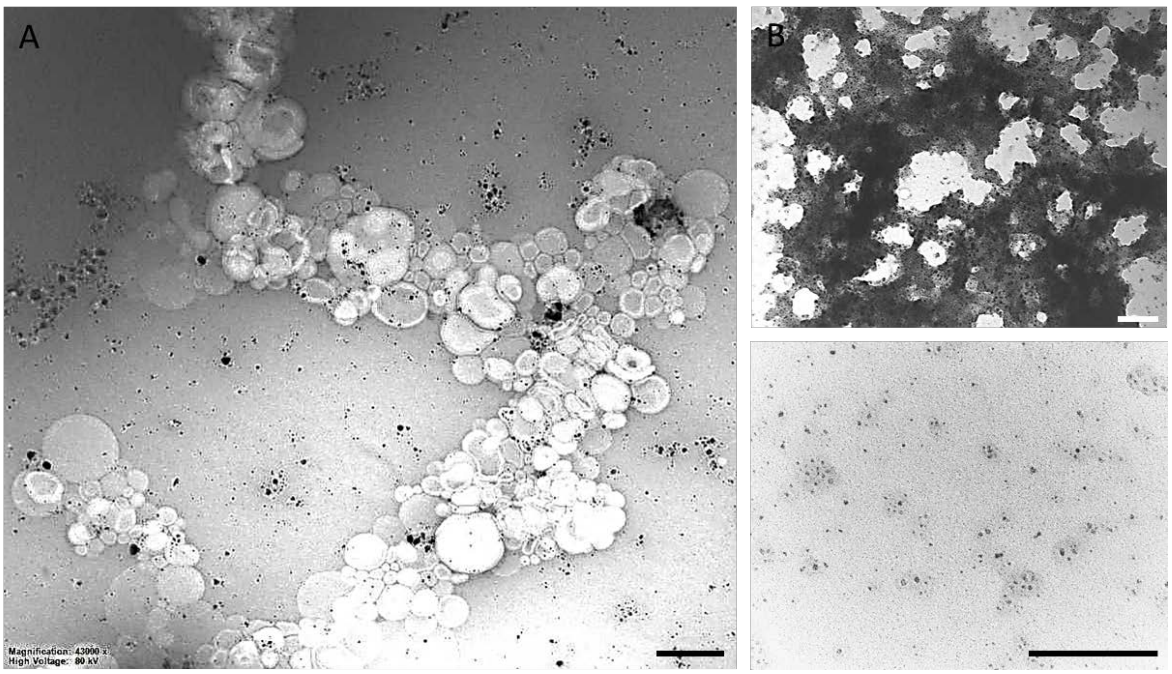

Figure S4 TEM images of (A) Lipo/SNS and (B) SNSs samples. Part (B) includes an additional image of the same sample with a higher magnification. Scale Bar: 200 nm.

Results showed that the production of silver nanospheres is achievable via illumination (**Figure S4**). Since the sample did not undergo any separation process to discharge the free SNSs, liposomes linked with SNSs (**Figure S4A**) and free SNSs (**Figure S4B**) both were observed. It was thought that some of the SNSs linked with liposomes were generated from silver nitrate and tryptone units which were inside the liposomes; which leads the given method to be investigated more with further

trials. This process is promising because the separation of free silver nitrate and tryptone from the liposomes is more applicable than the separation of free AgNPs from liposomes due to the smaller size of silver nitrate and amino acids.

Based on the aforementioned hypothesis, an additional experiment was performed with the separation of unencapsulated silver nitrate and tryptone units followed by illumination. This experiment was performed by using a laser in a shorter time (10 minutes) comparing to the previous experiment that was included the employment of an LED bulb for the illumination (5 hours). Initially, the dispersions of Lipo/AgNO3+Tryptone and AgNO3+Tryptone before and after illumination, were characterized with UV-Vis as shown in **Figure S5**, without performing separation process. The synthesis of liposomal dispersions was performed using ethanol injection technique (see paragraph **3.2.2**) with PC (16 mM).

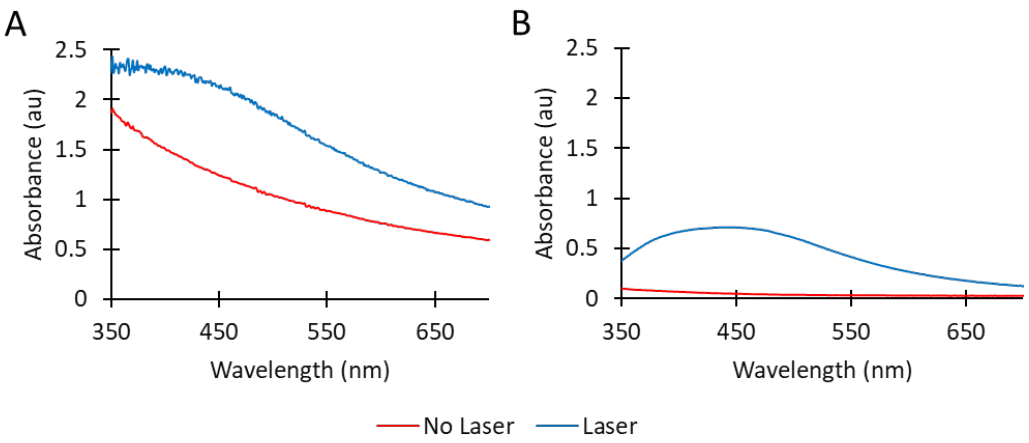

Figure S5 Absorbance spectrum of (A) Lipo/AgNO3+Tryptone and (B) AgNO3+Tryptone. The figure shows the comparison of samples with or without illumination with a laser.

The absorbance spectrum of the samples confirmed the production of Lipo/SNSs (**Figure S5A**) and SNSs (**Figure S5B**). The absorbance of AgNO3+Tryptone or Lipo/AgNO3+Tryptone did not show a peak before illumination. The reason for the increase in absorbance values towards 350 nm in **Figure S5A** was the existence of liposomes. However, the broad peak at ~430 nm as shown in **Figure S5A& B** after illumination demonstrated the production of Lipo/SNSs and SNSs by using a laser.

Following that, same experiment was performed including the separation process for Lipo/AgNO3+Tryptone sample before illumination. The samples of AgNO3+Tryptone and purified Lipo/AgNO3+Tryptone were imaged using TEM after illumination, and results were shown in **Figure S6**. The formation of SNSs only inside liposomes, was achieved after the separation process, indicating that the liposomes could work as a nanoreactor for SNS synthesis. Comparing to the

previous experiment (images of Lipo/SNS sample without the separation process **Figure S4A**) **,** there was a few free SNS observed during the TEM operation in the sample. The SNSs were observed mostly as encapsulated in liposomes. **Figure S6B & C** shows the synthesized SNSs in liposomes with a higher magnification, also confirms that the SNSs were synthesized inside liposomes, especially when comparing to the SNSs that were synthesized without liposomes in **Figure S6D.** The reason for the low amount of SNSs in liposomes could be that, the AgNO3 or Tryptone was tended be outside of the liposomes during the formation, so that after the separation of unencapsulated materials, the amount of simultaneously present AgNO3 and Tryptone in liposomes indeed was really low. Also, the duration for the illumination could be not enough because the liposome layers might have blocked the light which would enter inside the liposome and start the reaction for SNS synthesis.

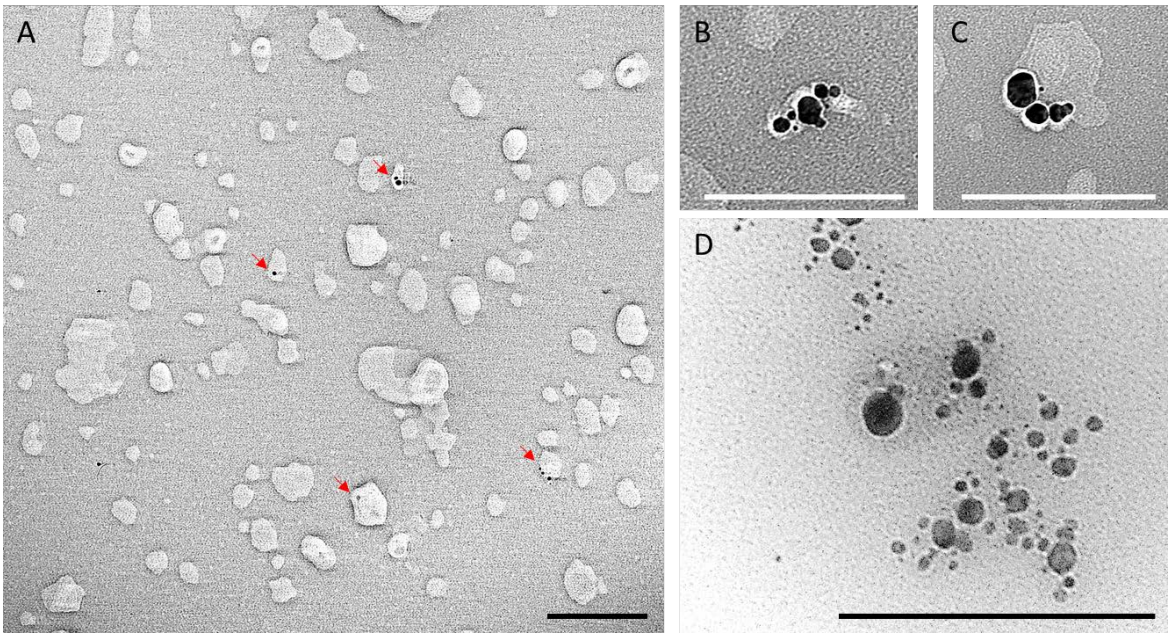

Figure S6 TEM images of (A), (B) & (C) purified and illuminated Lipo/SNS and (D) SNS samples. Part (B) & (C) shows the images of synthesized SNSs in liposomes with a higher magnification. Scale Bar: 200 nm. The arrows show the generated SNSs in liposomes.

Overall, the SNSs synthesis inside the liposomes via illumination was demonstrated. The TEM images have confirmed the AgNP presence in liposomes. However, the protocol must be improved to observe higher amount of encapsulated SNSs. Further experiments should focus on especially the amount of chemicals employed, or the duration time of illumination.

List of References

1. Dictionary., F.P.M. *disease*. 2007; Available from: http://medical-dictionary.thefreedictionary.com/disease.

2. Thomas A. M. Kramer, M., *Side Effects and Therapeutic Effects.* Medscape General Medicine., 2003.

3. Tamargo, J., J.-Y. Le Heuzey, and P. Mabo, *Narrow therapeutic index drugs: a clinical pharmacological consideration to flecainide.* European journal of clinical pharmacology, 2015. **71**(5): p. 549-567.

4. Education, S. *Drug Delivery Systems: Getting Drugs to Their Targets in a Controlled Manner*. 2016; Available from: https://www.nibib.nih.gov/science-education/science-topics/drug-delivery-systems-getting-drugs-their-targets-controlled-manner#1241.

5. De Jong, W.H. and P.J. Borm, *Drug delivery and nanoparticles: applications and hazards.* International journal of nanomedicine, 2008. **3**(2): p. 133.

6. Lajunen, T., et al., *Light induced cytosolic drug delivery from liposomes with gold nanoparticles.* Journal of Controlled Release, 2015. **203**: p. 85-98.

7. Hua, S. and S.Y. Wu, *The use of lipid-based nanocarriers for targeted pain therapies.* Frontiers in pharmacology, 2013. **4**: p. 143.

8. Çağdaş, M., A.D. Sezer, and S. Bucak, *Liposomes as potential drug carrier systems for drug delivery*, in *Application of nanotechnology in drug delivery*. 2014, InTech.

9. Chang, D.-K., et al., *Peptide-mediated liposomal Doxorubicin enhances drug delivery efficiency and therapeutic efficacy in animal models.* PLoS One, 2013. **8**(12): p. e83239.

10. Bulbake, U., et al., *Liposomal formulations in clinical use: an updated review.* Pharmaceutics, 2017. **9**(2): p. 12.

11. Spring, B.Q., et al., *A photoactivable multi-inhibitor nanoliposome for tumour control and simultaneous inhibition of treatment escape pathways.* Nature nanotechnology, 2016.

12. Escoffre, J.-M., et al., *Doxorubicin liposome-loaded microbubbles for contrast imaging and ultrasound-triggered drug delivery.* IEEE transactions on ultrasonics, ferroelectrics, and frequency control, 2013. **60**(1): p. 78-87.

13. Yan, F., et al., *Paclitaxel-liposome–microbubble complexes as ultrasound-triggered therapeutic drug delivery carriers.* Journal of Controlled Release, 2013. **166**(3): p. 246-255.

14. Sercombe, L., et al., *Advances and challenges of liposome assisted drug delivery.* Frontiers in pharmacology, 2015. **6**: p. 286.

15. Keat, C., et al., *Biosynthesis of nanoparticles and silver nanoparticles. Bioresources and Bioprocessing, 2 (1)*. 2015.

16. Mulvaney, S.P., et al., *Glass-coated, analyte-tagged nanoparticles: a new tagging system based on detection with surface-enhanced Raman scattering.* Langmuir, 2003. **19**(11): p. 4784-4790.

17. Doering, W.E., et al., *SERS as a foundation for nanoscale, optically detected biological labels.* Advanced Materials, 2007. **19**(20): p. 3100-3108.

18. Aygün, A., et al., *Biological synthesis of silver nanoparticles using Rheum ribes and evaluation of their anticarcinogenic and antimicrobial potential: A novel approach in phytonanotechnology.* Journal of Pharmaceutical and Biomedical Analysis, 2020. **179**: p. 113012.

19. Xu, X., et al., *Synthesis of triangular silver nanoprisms and studies on the interactions with human serum albumin.* Journal of molecular liquids, 2016. **220**: p. 14-20.

20. Xue, B., et al., *Towards high quality triangular silver nanoprisms: improved synthesis, six-tip based hot spots and ultra-high local surface plasmon resonance sensitivity.* Nanoscale, 2015. **7**(17): p. 8048-8057.

21. Carboni, M., *Silver nanoprisms embedded in a polymeric matrix for energy saving glazing*. 2014, University of Southampton.

22. Lopez, R.R., V. Nerguizian, and I. Stiharu, *Mass Production of Liposomes—Pushing Forward Next-Generation Therapies.* Substance ÉTS, 2018.

23. Gomez, F.A., *The future of microfluidic point-of-care diagnostic devices.* Bioanalysis, 2013. **5**(1): p. 1-3.

24. Hulme, J.P., et al., *Rapid prototyping for injection moulded integrated microfluidic devices and diffractive element arrays.* Lab on a Chip, 2002. **2**(4): p. 203-206.

25. Kitson, P.J., et al., *Configurable 3D-Printed millifluidic and microfluidic 'lab on a chip'reactionware devices.* Lab on a Chip, 2012. **12**(18): p. 3267-3271.

26. Sanchez-Salmeron, A., et al., *Recent development in micro-handling systems for micro-manufacturing.* Journal of materials processing technology, 2005. **167**(2-3): p. 499-507.

27. García-Manrique, P., et al., *Continuous flow production of size-controllable niosomes using a thermostatic microreactor.* Colloids and Surfaces B: Biointerfaces, 2019. **182**: p. 110378.

28. Cristaldi, D.A., et al., *Easy-to-perform and cost-effective fabrication of continuous-flow reactors and their application for nanomaterials synthesis.* New biotechnology, 2018. **47**: p. 1-7.

29. Lohse, S.E., et al., *A simple millifluidic benchtop reactor system for the high-throughput synthesis and functionalization of gold nanoparticles with different sizes and shapes.* ACS nano, 2013. **7**(5): p. 4135-4150.

30. Wang, L., et al., *Self-optimizing parallel millifluidic reactor for scaling nanoparticle synthesis.* Chemical Communications, 2020. **56**(26): p. 3745-3748.

31. Seaberg, J., et al., *A rapid millifluidic synthesis of tunable polymer-protein nanoparticles.* European Journal of Pharmaceutics and Biopharmaceutics, 2020.

32. Vikram, A., et al., *A Millifluidic Reactor System for Multistep Continuous Synthesis of InP/ZnSeS Nanoparticles.* ChemNanoMat, 2018. **4**(9): p. 943-953.

33. Carugo, D., et al., *Liposome production by microfluidics: potential and limiting factors.* Scientific reports, 2016. **6**: p. 25876.

34. Carugo, D., et al., *Facile and cost-effective production of microscale PDMS architectures using a combined micromilling-replica moulding (μMi-REM) technique.* Biomedical Microdevices, 2016. **18**(1): p. 4.

35. Siegel, R., et al., *Cancer treatment and survivorship statistics, 2012.* CA: a cancer journal for clinicians, 2012. **62**(4): p. 220-241.

36. Institute, N.C. *What is Cancer*. National Cancer Institute 2015; Available from: https://www.cancer.gov/about-cancer/understanding/what-is-cancer.

37. Falandry, C., et al., *Biology of cancer and aging: a complex association with cellular senescence.* Journal of Clinical Oncology, 2014. **32**(24): p. 2604-2610.

38. Kennedy, J.E., *High-intensity focused ultrasound in the treatment of solid tumours.* Nature reviews cancer, 2005. **5**(4): p. 321-327.

39. Enger, E., *Concepts in Biology'2007 Ed. 2007 Edition.* Rex Bookstore, Inc. isbn, 2012. **430727436**.

40. Brannon-Peppas, L. and J.O. Blanchette, *Nanoparticle and targeted systems for cancer therapy.* Advanced drug delivery reviews, 2012. **64**: p. 206-212.

41. Gabizon, A., et al., *Systemic administration of doxorubicin-containing liposomes in cancer patients: a phase I study.* European Journal of Cancer and Clinical Oncology, 1989. **25**(12): p. 1795-1803.

42. Tom, R.T., et al., *Ciprofloxacin-protected gold nanoparticles.* Langmuir, 2004. **20**(5): p. 1909-1914.

43. Rudokas, M., et al., *Liposome delivery systems for inhalation: a critical review highlighting formulation issues and anticancer applications.* Medical Principles and Practice, 2016. **25**(Suppl. 2): p. 60-72.

44. Hajos, F., et al., *Inhalable liposomal formulation for vasoactive intestinal peptide.* International journal of pharmaceutics, 2008. **357**(1-2): p. 286-294.

45. Liu, J., et al., *Solid lipid nanoparticles for pulmonary delivery of insulin.* International journal of pharmaceutics, 2008. **356**(1-2): p. 333-344.

46. Vieira, D.B. and L.F. Gamarra, *Getting into the brain: liposome-based strategies for effective drug delivery across the blood–brain barrier.* International journal of nanomedicine, 2016. **11**: p. 5381.

47. Helfand, W.H. and D.L. Cowen, *Evolution of pharmaceutical oral dosage forms.* Pharmacy in history, 1983. **25**(1): p. 3-18.

48. Park, K., *Controlled drug delivery systems: past forward and future back.* Journal of Controlled Release, 2014. **190**: p. 3-8.

49. Park, K., *Facing the truth about nanotechnology in drug delivery.* ACS nano, 2013. **7**(9): p. 7442-7447.

50. Safari, J. and Z. Zarnegar, *Advanced drug delivery systems: Nanotechnology of health design A review.* Journal of Saudi Chemical Society, 2014. **18**(2): p. 85-99.

51. Park, K., Y.H. Bae, and R.J. Mrsny, *The missing components today and the new treatments tomorrow*, in *Cancer Targeted Drug Delivery*. 2013, Springer. p. 689-707.

52. Initiative, N.N. *What is Nanotechnology?* ; Available from: https://www.nano.gov/nanotech-101/what/definition.

53. Nikalje, A., *Nanotechnology and its applications in medicine.* Med chem, 2015. **5**(2): p. 081-089.

54. Erickson, H.P., *Size and shape of protein molecules at the nanometer level determined by sedimentation, gel filtration, and electron microscopy.* Biological procedures online, 2009. **11**(1): p. 32.

55. Bangham, A., M.M. Standish, and J.C. Watkins, *Diffusion of univalent ions across the lamellae of swollen phospholipids.* Journal of molecular biology, 1965. **13**(1): p. 238-IN27.

56. Marty, J., *Nanoparticles-a new colloidal drug delivery system.* Pharm. Acta Helv., 1978. **53**: p. 17-23.

57. Forssen, E.A. and Z. Tökès, *Use of anionic liposomes for the reduction of chronic doxorubicin-induced cardiotoxicity.* Proceedings of the National Academy of Sciences, 1981. **78**(3): p. 1873-1877.

58. Weissig, V., T.K. Pettinger, and N. Murdock, *Nanopharmaceuticals (part 1): products on the market.* International journal of nanomedicine, 2014. **9**: p. 4357.

59. Bharali, D.J. and S.A. Mousa, *Emerging nanomedicines for early cancer detection and improved treatment: current perspective and future promise.* Pharmacology & therapeutics, 2010. **128**(2): p. 324-335.

60. Farokhzad, O.C. and R. Langer, *Impact of nanotechnology on drug delivery.* ACS nano, 2009. **3**(1): p. 16-20.

61. Salata, O.V., *Applications of nanoparticles in biology and medicine.* Journal of nanobiotechnology, 2004. **2**(1): p. 3.

62. Gürsoy, A., E. Kut, and S. Özkırımlı, *Co-encapsulation of isoniazid and rifampicin in liposomes and characterization of liposomes by derivative spectroscopy.* International journal of pharmaceutics, 2004. **271**(1-2): p. 115-123.

63. Hofheinz, R.-D., et al., *Liposomal encapsulated anti-cancer drugs.* Anti-cancer drugs, 2005. **16**(7): p. 691-707.

64. Barenholz, Y.C., *Doxil®—the first FDA-approved nano-drug: lessons learned.* Journal of controlled release, 2012. **160**(2): p. 117-134.

65. Sharma, A. and U.S. Sharma, *Liposomes in drug delivery: progress and limitations.* International journal of pharmaceutics, 1997. **154**(2): p. 123-140.

66. Shaheen, S.M., et al., *Liposome as a carrier for advanced drug delivery.* Pak J Biol Sci, 2006. **9**(6): p. 1181-1191.

67. Akbarzadeh, A., et al., *Liposome: classification, preparation, and applications.* Nanoscale research letters, 2013. **8**(1): p. 102.

68. Etheridge, M.L., et al., *The big picture on nanomedicine: the state of investigational and approved nanomedicine products.* Nanomedicine, 2013. **9**(1): p. 1-14.

69. Kibria, G., et al., *The effect of liposomal size on the targeted delivery of doxorubicin to Integrin αvβ3-expressing tumor endothelial cells.* Biomaterials, 2013. **34**(22): p. 5617-5627.

70. Papahadjopoulos, D., et al., *Sterically stabilized liposomes: improvements in pharmacokinetics and antitumor therapeutic efficacy.* Proceedings of the National Academy of Sciences, 1991. **88**(24): p. 11460-11464.

71. Marcucci, F. and F. Lefoulon, *Active targeting with particulate drug carriers in tumor therapy: fundamentals and recent progress.* Drug discovery today, 2004. **9**(5): p. 219-228.

72. Hope, M., et al., *Production of large unilamellar vesicles by a rapid extrusion procedure. Characterization of size distribution, trapped volume and ability to maintain a membrane potential.* Biochimica et Biophysica Acta (BBA)-Biomembranes, 1985. **812**(1): p. 55-65.

73. Huang, C.-H., *Phosphatidylcholine vesicles. Formation and physical characteristics.* Biochemistry, 1969. **8**(1): p. 344-352.

74. Zhigaltsev, I.V., et al., *Bottom-up design and synthesis of limit size lipid nanoparticle systems with aqueous and triglyceride cores using millisecond microfluidic mixing.* Langmuir, 2012. **28**(7): p. 3633-3640.

75. Gregoriadis, G. and B. Ryman, *Liposomes as carriers of enzymes or drugs: a new approach to the treatment of storage diseases.* Biochemical Journal, 1971. **124**(5): p. 58P.

76. Gregoriadis, G., *Drug entrapment in liposomes.* Febs Letters, 1973. **36**(3): p. 292-296.

77. KOBAYASHI, T., S. TSUKAGOSHI, and Y. SAKURAI, *Enhancement of the cancer chemotherapeutic effect of cytosine arabinoside entrapped in liposomes on mouse leukemia L-1210.* GANN Japanese Journal of Cancer Research, 1975. **66**(6): p. 719-720.

78. Lopez-Berestein, G., et al., *Liposomal amphotericin B for the treatment of systemic fungal infections in patients with cancer: a preliminary study.* Journal of Infectious Diseases, 1985. **151**(4): p. 704-710.

79. Ishida, T., H. Harashima, and H. Kiwada, *Liposome clearance.* Bioscience reports, 2002. **22**(2): p. 197-224.

80. Abuchowski, A., et al., *Effect of covalent attachment of polyethylene glycol on immunogenicity and circulating life of bovine liver catalase.* Journal of Biological Chemistry, 1977. **252**(11): p. 3582-3586.

81. Torchilin, V., et al., *Targeted accumulation of polyethylene glycol-coated immunoliposomes in infarcted rabbit myocardium.* The FASEB journal, 1992. **6**(9): p. 2716-2719.

82. Northfelt, D.W., et al., *Doxorubicin Encapsulated in Liposomes Containing Surface-Bound Polyethylene Glycol: Pharmacokinetics, Tumor Localization, and Safety in Patients with AIDS-Related Kaposi's Sarcoma.* The Journal of Clinical Pharmacology, 1996. **36**(1): p. 55-63.

83. Dams, E.T., et al., *Accelerated blood clearance and altered biodistribution of repeated injections of sterically stabilized liposomes.* Journal of Pharmacology and Experimental Therapeutics, 2000. **292**(3): p. 1071-1079.

84. Pinheiro, M., et al., *Liposomes as drug delivery systems for the treatment of TB.* Nanomedicine, 2011. **6**(8): p. 1413-1428.

85. Accardo, A. and G. Morelli, *Review peptide-targeted liposomes for selective drug delivery: Advantages and problematic issues.* Peptide Science, 2015. **104**(5): p. 462-479.

86. Noble, G.T., et al., *Ligand-targeted liposome design: challenges and fundamental considerations.* Trends in biotechnology, 2014. **32**(1): p. 32-45.

87. Hua, S., *Targeting sites of inflammation: intercellular adhesion molecule-1 as a target for novel inflammatory therapies.* Frontiers in pharmacology, 2013. **4**: p. 127.

88. Lasic, D.D., *Liposomes: from physics to applications*. 1993: Elsevier Science Ltd.

89. Wang, X., et al., *Advances of cancer therapy by nanotechnology.* Cancer research and treatment: official journal of Korean Cancer Association, 2009. **41**(1): p. 1.

90. Gregoriadis, G., *Engineering liposomes for drug delivery: progress and problems.* Trends in biotechnology, 1995. **13**(12): p. 527-537.

91. Schmitt, C.J., et al., *Replacement of conventional doxorubicin by pegylated liposomal doxorubicin is a safe and effective alternative in the treatment of non-Hodgkin's lymphoma patients with cardiac risk factors.* Annals of hematology, 2012. **91**(3): p. 391-397.

92. Lasic, D., *Doxorubicin in sterically stabilized liposomes (vol 380, pg 562, 1996).* Nature, 1996. **381**(6583): p. 630-630.

93. Gabizon, A., et al., *Clinical studies of liposome-encapsulated doxorubicin.* Acta Oncologica, 1994. **33**(7): p. 779-786.

94. Xing, M., et al., *Efficacy and cardiotoxicity of liposomal doxorubicin-based chemotherapy in advanced breast cancer: a meta-analysis of ten randomized controlled trials.* PLoS One, 2015. **10**(7): p. e0133569.

95. Smolin, G., et al., *Idoxuridine-liposome therapy for herpes simplex keratitis.* American journal of ophthalmology, 1981. **91**(2): p. 220-225.

96. Wang, T.-Y., et al., *Ultrasound and microbubble guided drug delivery: mechanistic understanding and clinical implications.* Current pharmaceutical biotechnology, 2013. **14**(8): p. 743-752.

97. Gui, R., et al., *Intracellular fluorescent thermometry and photothermal-triggered drug release developed from gold nanoclusters and doxorubicin dual-loaded liposomes.* Chemical Communications, 2014. **50**(13): p. 1546-1548.

98. Mahmudin, L., et al., *Optical properties of silver nanoparticles for surface plasmon resonance (SPR)-based biosensor applications.* J. Mod. Phys., 2015. **6**.

99. Noguez, C., *Surface plasmons on metal nanoparticles: the influence of shape and physical environment.* The Journal of Physical Chemistry C, 2007. **111**(10): p. 3806-3819.

100. Orbaek, A.W., M.M. McHale, and A.R. Barron, *Synthesis and characterization of silver nanoparticles for an undergraduate laboratory.* Journal of Chemical Education, 2014. **92**(2): p. 339-344.

101. Lubick, N., *Nanosilver toxicity: ions, nanoparticles or both?* 2008, ACS Publications.

102. Li, W.-R., et al., *Antibacterial activity and mechanism of silver nanoparticles on Escherichia coli.* Applied microbiology and biotechnology, 2010. **85**(4): p. 1115-1122.

103. Link, S., Z.L. Wang, and M. El-Sayed, *Alloy formation of gold− silver nanoparticles and the dependence of the plasmon absorption on their composition.* The Journal of Physical Chemistry B, 1999. **103**(18): p. 3529-3533.

104. Cobley, C.M., et al., *Shape-controlled synthesis of silver nanoparticles for plasmonic and sensing applications.* Plasmonics, 2009. **4**(2): p. 171-179.

105. Haynes, C.L. and R.P. Van Duyne, *Nanosphere lithography: a versatile nanofabrication tool for studies of size-dependent nanoparticle optics*. 2001, ACS Publications.

106. Panzarasa, G., *Just What Is It That Makes Silver Nanoprisms so Different, so Appealing?* Journal of Chemical Education, 2015. **92**(11): p. 1918-1923.

107. Sherry, L.J., et al., *Localized surface plasmon resonance spectroscopy of single silver triangular nanoprisms.* Nano letters, 2006. **6**(9): p. 2060-2065.

108. nanoComposix. *Silver Nanoparticles: Optical Properties*. 2020; Available from: https://nanocomposix.com/pages/silver-nanoparticles-optical-properties.

109. Skrabalak, S.E., et al., *Gold nanocages: synthesis, properties, and applications.* Accounts of chemical research, 2008. **41**(12): p. 1587-1595.

110. Jesorka, A. and O. Orwar, *Liposomes: technologies and analytical applications.* Annu. Rev. Anal. Chem., 2008. **1**: p. 801-832.

111. Patil, Y.P. and S. Jadhav, *Novel methods for liposome preparation.* Chemistry and physics of lipids, 2014. **177**: p. 8-18.

112. New, R.R., *Preparation of liposomes.* Liposomes: a practical approach., 1990: p. 33-104.

113. Pons, M., M. Foradada, and J. Estelrich, *Liposomes obtained by the ethanol injection method.* International journal of pharmaceutics, 1993. **95**(1-3): p. 51-56.

114. Dixon, R.A. and R.A. Gonzales, *Plant cell culture: a practical approach*. 1994: IRL press.

115. Szoka, F. and D. Papahadjopoulos, *Procedure for preparation of liposomes with large internal aqueous space and high capture by reverse-phase evaporation.* Proceedings of the national academy of sciences, 1978. **75**(9): p. 4194-4198.

116. Mayer, L.D., et al., *Characterization of liposomal systems containing doxorubicin entrapped in response to pH gradients.* Biochimica et Biophysica Acta (BBA)-Biomembranes, 1990. **1025**(2): p. 143-151.

117. Aliabadi, H.M., et al., *Encapsulation of hydrophobic drugs in polymeric micelles through co-solvent evaporation: the effect of solvent composition on micellar properties and drug loading.* International journal of pharmaceutics, 2007. **329**(1-2): p. 158-165.

118. Whitesides, G.M., *The origins and the future of microfluidics.* Nature, 2006. **442**(7101): p. 368-373.

119. Kirby, B.J., *Micro-and nanoscale fluid mechanics: transport in microfluidic devices*. 2010: Cambridge University Press.

120. Khan, I.U., et al., *Production of nanoparticle drug delivery systems with microfluidics tools.* Expert opinion on drug delivery, 2015. **12**(4): p. 547-562.

121. Bhatia, S.N. and D.E. Ingber, *Microfluidic organs-on-chips.* Nature biotechnology, 2014. **32**(8): p. 760-772.

122. Jahn, A., et al., *Preparation of nanoparticles by continuous-flow microfluidics.* Journal of Nanoparticle Research, 2008. **10**(6): p. 925-934.

123. Chatterjee, D., et al., *Droplet-based microfluidics with nonaqueous solvents and solutions.* Lab on a Chip, 2006. **6**(2): p. 199-206.

124. Schabas, G., et al., *Controlled self-assembly of quantum dots and block copolymers in a microfluidic device.* Langmuir, 2008. **24**(3): p. 637-643.

125. Cottam, B.F., S. Krishnadasan, and M.S. Shaffer, *Accelerated synthesis of titanium oxide nanostructures using microfluidic chips.* Lab on a Chip, 2007. **7**(2): p. 167-169.

126. Karnik, R., et al., *Microfluidic platform for controlled synthesis of polymeric nanoparticles.* Nano letters, 2008. **8**(9): p. 2906-2912.

127. Jahn, A., et al., *Controlled vesicle self-assembly in microfluidic channels with hydrodynamic focusing.* Journal of the American Chemical Society, 2004. **126**(9): p. 2674-2675.

128. Batchelor, G.K., *An introduction to fluid dynamics*. 2000: Cambridge university press.

129. Yu, B., R.J. Lee, and L.J. Lee, *Microfluidic methods for production of liposomes.* Methods in enzymology, 2009. **465**: p. 129-141.

130. Avila, K., et al., *The onset of turbulence in pipe flow.* Science, 2011. **333**(6039): p. 192-196.

131. Menon, E.S., *Fluid flow in pipes.* Transmission Pipeline Calculations and Simulations Manual, 2015: p. 149-234.

132. Nguyen, N.-T., et al., *Design, fabrication and characterization of drug delivery systems based on lab-on-a-chip technology.* Advanced drug delivery reviews, 2013. **65**(11-12): p. 1403-1419.

133. Xu, J., et al., *Controllable microfluidic production of drug-loaded PLGA nanoparticles using partially water-miscible mixed solvent microdroplets as a precursor.* Scientific Reports, 2017. **7**(1): p. 4794.

134. Chen, Z., et al., *High Throughput Nanoliposome Formation Using 3D Printed Microfluidic Flow Focusing Chips.* Advanced Materials Technologies, 2019. **4**(6): p. 1800511.

135. Yanar, F., et al., *Continuous-Flow Production of Liposomes with a Millireactor under Varying Fluidic Conditions.* Pharmaceutics, 2020. **12**(11): p. 1001.

136. Lasic, D., et al., *Transmembrane gradient driven phase transitions within vesicles: lessons for drug delivery.* Biochimica et Biophysica Acta (BBA)-Biomembranes, 1995. **1239**(2): p. 145-156.

137. Torchilin, V. and V. Weissig, *Liposomes: a practical approach*. 2003: Oxford University Press.

138. Ho, R.J., B.T. Rouse, and L. Huang, *Target-sensitive immunoliposomes: preparation and characterization.* Biochemistry, 1986. **25**(19): p. 5500-5506.

139. Grabielle-Madelmont, C., S. Lesieur, and M. Ollivon, *Characterization of loaded liposomes by size exclusion chromatography.* Journal of biochemical and biophysical methods, 2003. **56**(1-3): p. 189-217.

140. Jain, N.K., *Controlled and novel drug delivery*. 1997: CBS publishers & distributors.

141. Bartosova, L. and J. Bajgar, *Transdermal drug delivery in vitro using diffusion cells.* Current medicinal chemistry, 2012. **19**(27): p. 4671-4677.

142. Organization, W.H. *The top 10 causes of death*. January.2017; Available from: http://www.who.int/mediacentre/factsheets/fs310/en/.

143. Trotti, A., et al. *CTCAE v3. 0: development of a comprehensive grading system for the adverse effects of cancer treatment*. in *Seminars in radiation oncology*. 2003. Elsevier.

144. Cans, A.-S., et al., *Artificial cells: unique insights into exocytosis using liposomes and lipid nanotubes.* Proceedings of the National Academy of Sciences, 2003. **100**(2): p. 400-404.

145. Ahmed, K.S., et al., *Liposome: Composition, characterisation, preparation, and recent innovation in clinical applications.* Journal of drug targeting, 2019. **27**(7): p. 742-761.

146. Bozzuto, G. and A. Molinari, *Liposomes as nanomedical devices.* International journal of nanomedicine, 2015. **10**: p. 975.

147. Hay, R., *Liposomal amphotericin B, AmBisome.* Journal of Infection, 1994. **28**: p. 35-43.

148. Harashima, H. and H. Kiwada, *Liposomal targeting and drug delivery: kinetic consideration.* Advanced drug delivery reviews, 1996. **19**(3): p. 425-444.

149. Šentjurc, M., K. Vrhovnik, and J. Kristl, *Liposomes as a topical delivery system: the role of size on transport studied by the EPR imaging method.* Journal of controlled release, 1999. **59**(1): p. 87-97.

150. Danaei, M., et al., *Impact of particle size and polydispersity index on the clinical applications of lipidic nanocarrier systems.* Pharmaceutics, 2018. **10**(2): p. 57.

151. Nagayasu, A., K. Uchiyama, and H. Kiwada, *The size of liposomes: a factor which affects their targeting efficiency to tumors and therapeutic activity of liposomal antitumor drugs.* Advanced drug delivery reviews, 1999. **40**(1-2): p. 75-87.

152. Bahari, L.A.S. and H. Hamishehkar, *The impact of variables on particle size of solid lipid nanoparticles and nanostructured lipid carriers; a comparative literature review.* Advanced pharmaceutical bulletin, 2016. **6**(2): p. 143.

153. Maherani, B. and O. Wattraint, *Liposomal structure: A comparative study on light scattering and chromatography techniques.* Journal of Dispersion Science and Technology, 2017. **38**(11): p. 1633-1639.

154. Bera, B., *Nanoporous silicon prepared by vapour phase strain etch and sacrificial technique.* International Journal of Computer Applications, 2015. **975**: p. 8887.

155. Shaker, S., A.R. Gardouh, and M.M. Ghorab, *Factors affecting liposomes particle size prepared by ethanol injection method.* Research in pharmaceutical sciences, 2017. **12**(5): p. 346.

156. Kulkarni, V. and C. Shaw, *Chapter 4—Formulating creams, gels, lotions, and suspensions.* Essential Chemistry for Formulators of Semisolid and Liquid Dosages; Kulkarni, VS, Shaw, C., Eds, 2016: p. 29-41.

157. Capretto, L., et al., *Continuous-flow production of polymeric micelles in microreactors: experimental and computational analysis.* Journal of colloid and interface science, 2011. **357**(1): p. 243-251.

158. Maherani, B., et al., *Liposomes: a review of manufacturing techniques and targeting strategies.* Current nanoscience, 2011. **7**(3): p. 436-452.

159. Kurakazu, T. and S. Takeuchi. *Generation of lipid vesicles using microfluidic T-junctions with pneumatic valves*. in *2010 IEEE 23rd International Conference on Micro Electro Mechanical Systems (MEMS)*. 2010. IEEE.

160. Davies, R.T., D. Kim, and J. Park, *Formation of liposomes using a 3D flow focusing microfluidic device with spatially patterned wettability by corona discharge.* Journal of Micromechanics and Microengineering, 2012. **22**(5): p. 055003.

161. Tan, Y.-C., K. Longmuir, and A. Lee. *Microfluidic Liposome Generation from Monodisperse Droplet Emulsion-Towards the Realization of Artificial Cells*. in *Summer Bioengineering Conference, Florida*. 2003.

162. Laouini, A., et al., *Preparation of liposomes: A novel application of microengineered membranes–From laboratory scale to large scale.* Colloids and surfaces B: biointerfaces, 2013. **112**: p. 272-278.

163. Pham, T.T., et al., *Liposome and niosome preparation using a membrane contactor for scale-up.* Colloids and surfaces B: biointerfaces, 2012. **94**: p. 15-21.

164. Charcosset, C., et al., *Preparation of liposomes at large scale using the ethanol injection method: Effect of scale-up and injection devices.* Chemical engineering research and design, 2015. **94**: p. 508-515.

165. Elhissi, A., D. Phoenix, and W. Ahmed, *Some approaches to large-scale manufacturing of liposomes*, in *Emerging Nanotechnologies for Manufacturing*. 2015, Elsevier. p. 402-417.

166. Wagner, A. and K. Vorauer-Uhl, *Liposome technology for industrial purposes.* Journal of drug delivery, 2011. **2011**.

167. Hills, E.E., et al., *Diffusion coefficients in ethanol and in water at 298 K: Linear free energy relationships.* Fluid Phase Equilibria, 2011. **303**(1): p. 45-55.

168. Instruments, M., *Dynamic light scattering common terms defined.* Inform White Paper.[Google Scholar], 2011.

169. Kastner, E., et al., *Microfluidic-controlled manufacture of liposomes for the solubilisation of a poorly water soluble drug.* International journal of pharmaceutics, 2015. **485**(1-2): p. 122-130.

170. Hashmi, A. and J. Xu, *On the quantification of mixing in microfluidics.* Journal of laboratory automation, 2014. **19**(5): p. 488-491.

171. Jahn, A., et al., *Microfluidic directed formation of liposomes of controlled size.* Langmuir, 2007. **23**(11): p. 6289-6293.

172. Jahn, A., et al., *Microfluidic mixing and the formation of nanoscale lipid vesicles.* ACS nano, 2010. **4**(4): p. 2077-2087.

173. Kimura, N., et al., *Development of the iLiNP device: fine tuning the lipid nanoparticle size within 10 nm for drug delivery.* ACS omega, 2018. **3**(5): p. 5044-5051.

174. Lee, J., et al., *High-throughput nanoscale lipid vesicle synthesis in a semicircular contraction-expansion array microchannel.* BioChip Journal, 2013. **7**(3): p. 210-217.

175. Sedighi, M., et al., *Rapid optimization of liposome characteristics using a combined microfluidics and design-of-experiment approach.* Drug delivery and translational research, 2019. **9**(1): p. 404-413.

176. Zizzari, A., et al., *Continuous-Flow Production of Injectable Liposomes via a Microfluidic Approach.* Materials, 2017. **10**(12): p. 1411.

177. Pradhan, P., et al., *A facile microfluidic method for production of liposomes.* Anticancer research, 2008. **28**(2A): p. 943-947.

178. Jovanović, A.A., et al., *Comparative Effects of Cholesterol and β-Sitosterol on the Liposome Membrane Characteristics.* European journal of lipid science and technology, 2018. **120**(9): p. 1800039.

179. Lee, S.-C., et al., *The effect of cholesterol in the liposome bilayer on the stabilization of incorporated retinol.* Journal of liposome research, 2005. **15**(3-4): p. 157-166.

180. Briuglia, M.-L., et al., *Influence of cholesterol on liposome stability and on in vitro drug release.* Drug delivery and translational research, 2015. **5**(3): p. 231-242.

181. Nele, V., et al., *Effect of formulation method, lipid composition, and PEGylation on vesicle lamellarity: a small-angle neutron scattering study.* Langmuir, 2019. **35**(18): p. 6064-6074.

182. Li, J., et al., *A review on phospholipids and their main applications in drug delivery systems.* Asian journal of pharmaceutical sciences, 2015. **10**(2): p. 81-98.

183. Tagami, T., M.J. Ernsting, and S.-D. Li, *Optimization of a novel and improved thermosensitive liposome formulated with DPPC and a Brij surfactant using a robust in vitro system.* Journal of controlled release, 2011. **154**(3): p. 290-297.

184. Rajendran, V., et al., *Stearylamine liposomal delivery of monensin in combination with free artemisinin eliminates blood stages of Plasmodium falciparum in culture and P. berghei infection in murine malaria.* Antimicrobial Agents and Chemotherapy, 2016. **60**(3): p. 1304-1318.

185. Kotouček, J., et al., *preparation of nanoliposomes by microfluidic mixing in herring-bone channel and the role of membrane fluidity in liposomes formation.* Scientific reports, 2020. **10**(1): p. 1-11.

186. Has, C., S.M. Phapal, and P. Sunthar, *Rapid single-step formation of liposomes by flow assisted stationary phase interdiffusion.* Chemistry and physics of lipids, 2018. **212**: p. 144-151.

187. Forbes, N., et al., *Rapid and scale-independent microfluidic manufacture of liposomes entrapping protein incorporating in-line purification and at-line size monitoring.* International journal of pharmaceutics, 2019. **556**: p. 68-81.

188. Rawicz, W., et al., *Effect of chain length and unsaturation on elasticity of lipid bilayers.* Biophysical journal, 2000. **79**(1): p. 328-339.

189. Jiang, F.Y., Y. Bouret, and J.T. Kindt, *Molecular dynamics simulations of the lipid bilayer edge.* Biophysical journal, 2004. **87**(1): p. 182-192.

190. Nakamura, K., et al., *Comparative studies of polyethylene glycol-modified liposomes prepared using different PEG-modification methods.* Biochimica et Biophysica Acta (BBA)-Biomembranes, 2012. **1818**(11): p. 2801-2807.

191. Chibowski, E. and A. Szcześ, *Zeta potential and surface charge of DPPC and DOPC liposomes in the presence of PLC enzyme.* Adsorption, 2016. **22**(4-6): p. 755-765.

192. Villasmil-Sánchez, S., et al., *Positively and negatively charged liposomes as carriers for transdermal delivery of sumatriptan: in vitro characterization.* Drug development and industrial pharmacy, 2010. **36**(6): p. 666-675.

193. Ruozi, B., et al., *AFM, ESEM, TEM, and CLSM in liposomal characterization: a comparative study.* International journal of nanomedicine, 2011. **6**: p. 557.

194. Regev, O., et al., *Dynamic light scattering and cryogenic transmission electron microscopy investigations on metallo-supramolecular aqueous micelles: evidence of secondary aggregation.* Colloid and Polymer Science, 2004. **282**(4): p. 407-411.

195. Composix, N., *Nano Composix's Guide To Dynamic Light Scattering Measurement and Analysis.* NanoComposix, San Diego, Calif, USA, 2012.

196. Zook, J.M. and W.N. Vreeland, *Effects of temperature, acyl chain length, and flow-rate ratio on liposome formation and size in a microfluidic hydrodynamic focusing device.* Soft matter, 2010. **6**(6): p. 1352-1360.

197. Calderón-Jiménez, B., et al., *Silver nanoparticles: technological advances, societal impacts, and metrological challenges.* Frontiers in chemistry, 2017. **5**: p. 6.

198. Simbine, E.O., et al., *Application of silver nanoparticles in food packages: a review.* Food Science and Technology, 2019. **39**(4): p. 793-802.

199. Zhang, F., et al., *Application of silver nanoparticles to cotton fabric as an antibacterial textile finish.* Fibers and Polymers, 2009. **10**(4): p. 496-501.

200. Zhang, X.-F., et al., *Silver nanoparticles: synthesis, characterization, properties, applications, and therapeutic approaches.* International journal of molecular sciences, 2016. **17**(9): p. 1534.

201. Das, C.A., et al., *Antibacterial activity of silver nanoparticles (biosynthesis): A short review on recent advances.* Biocatalysis and Agricultural Biotechnology, 2020: p. 101593.

202. Sriram, M.I., et al., *Size-based cytotoxicity of silver nanoparticles in bovine retinal endothelial cells.* Nanoscience Methods, 2012. **1**(1): p. 56-77.

203. Stoehr, L.C., et al., *Shape matters: effects of silver nanospheres and wires on human alveolar epithelial cells.* Particle and fibre toxicology, 2011. **8**(1): p. 36.

204. Kulkarni, A.P., et al., *Plasmon-enhanced charge carrier generation in organic photovoltaic films using silver nanoprisms.* Nano letters, 2010. **10**(4): p. 1501-1505.

205. Ciou, S.-H., et al., *SERS enhancement factors studies of silver nanoprism and spherical nanoparticle colloids in the presence of bromide ions.* The Journal of Physical Chemistry C, 2009. **113**(22): p. 9520-9525.

206. Boca, S.C., et al., *Chitosan-coated triangular silver nanoparticles as a novel class of biocompatible, highly effective photothermal transducers for in vitro cancer cell therapy.* Cancer letters, 2011. **311**(2): p. 131-140.

207. Gao, C., et al., *Highly stable silver nanoplates for surface plasmon resonance biosensing.* Angewandte Chemie International Edition, 2012. **51**(23): p. 5629-5633.

208. Xue, Y., et al., *Acute toxic effects and gender-related biokinetics of silver nanoparticles following an intravenous injection in mice.* Journal of Applied Toxicology, 2012. **32**(11): p. 890-899.

209. Yusuf, A., et al., *Liposomal encapsulation of silver nanoparticles enhances cytotoxicity and causes induction of reactive oxygen species-independent apoptosis.* Journal of Applied Toxicology, 2018. **38**(5): p. 616-627.

210. Yusuf, A. and A. Casey, *Evaluation of silver nanoparticle encapsulation in DPPC-based liposome by different methods for enhanced cytotoxicity.* International Journal of Polymeric Materials and Polymeric Biomaterials, 2020. **69**(13): p. 860-871.

211. Gabizon, A., et al., *Liposomes as in vivo carriers of adriamycin: reduced cardiac uptake and preserved antitumor activity in mice.* Cancer Research, 1982. **42**(11): p. 4734-4739.

212. Malam, Y., M. Loizidou, and A.M. Seifalian, *Liposomes and nanoparticles: nanosized vehicles for drug delivery in cancer.* Trends in pharmacological sciences, 2009. **30**(11): p. 592-599.

213. Stetefeld, J., S.A. McKenna, and T.R. Patel, *Dynamic light scattering: a practical guide and applications in biomedical sciences.* Biophysical reviews, 2016. **8**(4): p. 409-427.

214. Zmijan, R., et al., *In situ microspectroscopic monitoring within a microfluidic reactor.* RSC Advances, 2014. **4**(28): p. 14569-14572.

215. Ruysschaert, T., et al., *Liposome retention in size exclusion chromatography.* BMC biotechnology, 2005. **5**(1): p. 1-13.

216. Instruments, M., *Zeta potential: An Introduction in 30 minutes.* Zetasizer Nano Serles Tech. Note. MRK654, 2011. **1**(2): p. 1-6.

217. Wang, H., et al., *Mechanisms of PVP in the preparation of silver nanoparticles.* Materials Chemistry and Physics, 2005. **94**(2-3): p. 449-453.

218. Clogston, J.D. and A.K. Patri, *Zeta potential measurement*, in *Characterization of nanoparticles intended for drug delivery*. 2011, Springer. p. 63-70.

219. Honary, S. and F. Zahir, *Effect of zeta potential on the properties of nano-drug delivery systems-a review (Part 1).* Tropical Journal of Pharmaceutical Research, 2013. **12**(2): p. 255-264.

220. Vogel, R., et al., *High-resolution single particle zeta potential characterisation of biological nanoparticles using tunable resistive pulse sensing.* Scientific reports, 2017. **7**(1): p. 1-13.

221. Muñoz Javier, A., et al., *Combined atomic force microscopy and optical microscopy measurements as a method to investigate particle uptake by cells.* Small, 2006. **2**(3): p. 394-400.

222. Bangham, A., *Liposomes: the Babraham connection.* Chemistry and physics of lipids, 1993. **64**(1-3): p. 275-285.

223. Zuo, Y., et al., *Silver Nanoprism Enhanced Colorimetry for Precise Detection of Dissolved Oxygen.* Micromachines, 2020. **11**(4): p. 383.

224. Liang, L.P.T.H.J., T.W. Chung, and Y.Y.H.D.Z. Liu, *Liposomes incorporated with cholesterol for drug release triggered by magnetic field.* Journal of medical and biological Engineering, 2007. **27**(1): p. 29-34.

225. Jovanović, A., et al., *Influence of cholesterol on liposomal membrane fluidity, liposome size and zeta potential*. 2017.

226. Owen, J., et al., *The Role of PEG-40-stearate in the Production, Morphology, and Stability of Microbubbles.* Langmuir, 2018. **35**(31): p. 10014-10024.

227. Cheung, C.C., et al., *Microfluidic Production of Lysolipid-Containing Temperature-Sensitive Liposomes.* Journal of Visualized Experiments: Jove, 2020(157).

228. Deng, W., et al., *Controlled gene and drug release from a liposomal delivery platform triggered by X-ray radiation.* Nature communications, 2018. **9**(1): p. 2713.

229. Thomas, C.E., A. Ehrhardt, and M.A. Kay, *Progress and problems with the use of viral vectors for gene therapy.* Nature Reviews Genetics, 2003. **4**(5): p. 346-358.

230. Postma, M., et al., *Uniform cAMP stimulation of Dictyostelium cells induces localized patches of signal transduction and pseudopodia.* Molecular biology of the cell, 2003. **14**(12): p. 5019-5027.

231. Reinhard, N.R., et al., *The balance between Gαi-Cdc42/Rac and Gα12/13-RhoA pathways determines endothelial barrier regulation by sphingosine-1-phosphate.* Molecular biology of the cell, 2017. **28**(23): p. 3371-3382.

232. Kubin, R.F. and A.N. Fletcher, *Fluorescence quantum yields of some rhodamine dyes.* Journal of Luminescence, 1982. **27**(4): p. 455-462.

233. Leung, S.J. and M. Romanowski, *Light-activated content release from liposomes.* Theranostics, 2012. **2**(10): p. 1020-1036.

234. de Matos, R.A. and L.C. Courrol, *Biocompatible silver nanoparticles prepared with amino acids and a green method.* Amino acids, 2017. **49**(2): p. 379-388.